Volume 29, Number 6
December, 1970

SOVIET ATOMIC ENERGY

АТОМНАЯ ЭНЕРГИЯ
(ATOMNAYA ÉNERGIYA)

TRANSLATED FROM RUSSIAN

c/b CONSULTANTS BUREAU, NEW YORK

SOVIET ATOMIC ENERGY

Soviet Atomic Energy is a cover-to-cover translation of *Atomnaya Énergiya*, a publication of the Academy of Sciences of the USSR.

An arrangement with Mezhdunarodnaya Kniga, the Soviet book export agency, makes available both advance copies of the Russian journal and original glossy photographs and artwork. This serves to decrease the necessary time lag between publication of the original and publication of the translation and helps to improve the quality of the latter. The translation began with the first issue of the Russian journal.

Consultants Bureau journals appear about six months after the publication of the original Russian issue. For bibliographic accuracy, the English issue published by Consultants Bureau carries the same number and date as the original Russian from which it was translated. For example, a Russian issue published in December will appear in a Consultants Bureau English translation about the following June, but the translation issue will carry the December date. When ordering any volume or particular issue of a Consultants Bureau journal, please specify the date and, where applicable, the volume and issue numbers of the original Russian. The material you will receive will be a translation of that Russian volume or issue.

Subscription
$67.50 per volume (6 Issues)
2 volumes per year
(Add $5 for orders outside the United States and Canada.)

Single Issue: $30
Single Article: $15

CONSULTANTS BUREAU, NEW YORK AND LONDON

227 West 17th Street
New York, New York 10011

Davis House
8 Scrubs Lane
Harlesden, NW10 6SE
England

Second-class postage paid at Jamaica, New York 11431.

SOVIET ATOMIC ENERGY

A translation of *Atomnaya Énergiya*

Volume 29, Number 6 December, 1970

CONTENTS

CONTENTS

(continued)

The Russian press date (podpisano k pechati) of this issue was 11/16/1970. Publication therefore did not occur prior to this date, but must be assumed to have taken place reasonably soon thereafter.

ON THE SIXTIETH BIRTHDAY OF BORIS SERGEEVICH DZHELEPOV, CORRESPONDING MEMBER OF THE ACADEMY OF SCIENCES OF THE USSR

The Editorial Staff of Atomnaya Énergiya congratulate Boris Sergeevich Dzhelepov on his sixtieth birthday and wish him health and s successful continuation of his scientific and organixational activities on behalf of nuclear physics in the Soviet Union.

Translated from Atomnaya Énergiya, Vol. 29, No. 6, December, 1970.

TURBULENT HEAT AND MASS EXCHANGE

M. D. Millionshchikov

UDC 523.542

Turbulent heat and mass exchange in layers close to a wall has been studied by many authors [1, 3]. This problem has become especially important since it was discovered that the usual approach would not explain the observed heat and mass exchange for values of Prandtl's number P (the ratio of the molecular coefficient of kinematic viscosity to the thermal conductivity $\nu/\varkappa$) much larger than unity.

Some materials for which these processes have been experimentally investigated have Prandtl numbers of order 3000 or more. Deissler [1] analyzed experimental data for a wide range of values of P (0.5-3000), and developed a special theory of heat and mass exchange which, with the appropriate choice of certain constants, yields results in good agreement with experimental results in this range.

Deissler considers the laminar sublayer to be a region of interaction between molecular and turbulent exchange characterized by the distance from the wall and the kinematic viscosity. A logarithmic profile is used in the region of developing turbulence, and in this way a better quantitative description of the velocity profile is obtained than when a linear profile is used in the laminar sublayer and a purely logarithmic profile.

However this method does not yield a theory for the dependence of heat and mass transfer on Prandtl's number including small values.

Deissler also described the variation of Nusselt's number for large Prandtl numbers by taking it to be proportional to the Prandtl number raised to the power 1/4.

Another position was taken concerning heat and mass exchange by L. D. Landau and V. G. Levich [2]. Their theory agrees with that of P. L. Kapitsa [4, 5], in that they consider that there are stable liquid-motion waves in layers close to a wall. The thermal conduction is very low in the viscous layer for large Prandtl numbers, and so the turbulent pulsations in this layer lead to turbulent transfer comparable to molecular transfer at distances from the wall considerably smaller than the thickness of the hydrodynamic laminar sublayer. Hence the thickness of the thermal (or diffusion) laminar sublayer, i.e., the layer in which turbulent exchange may be neglected, is in general a function of the molecular thermal conductivity. The very general assumptions of the theory can be stated as follows:

1) The longitudinal component of the pulsation velocity u' varies like the mean velocity, i.e., it is proportional to the distance from the wall;

2) the pulsation frequency is independent of the distance from the wall;

3) the correlation between the transverse velocity component and the transverse transfer scale is independent of the distance from the wall.

Under these assumptions, the longitudinal velocity pulsations satisfy the relation [2]

$$u' \sim v_* \frac{y}{\delta_0},$$

where v_* is the dynamic velocity and δ_0 is the thickness of the hydrodynamic laminar sublayer.

The transverse velocity component corresponding to heat and mass transfer, estimated from the continuity condition for the flow has, in the layer close to the wall, the order

$$v' \sim v_* \left(\frac{y}{\delta_0}\right)^2.$$

Translated from Atomnaya Énergiya, Vol. 29, No. 6, pp. 411-426, December, 1970. Original article submitted August 28, 1970.

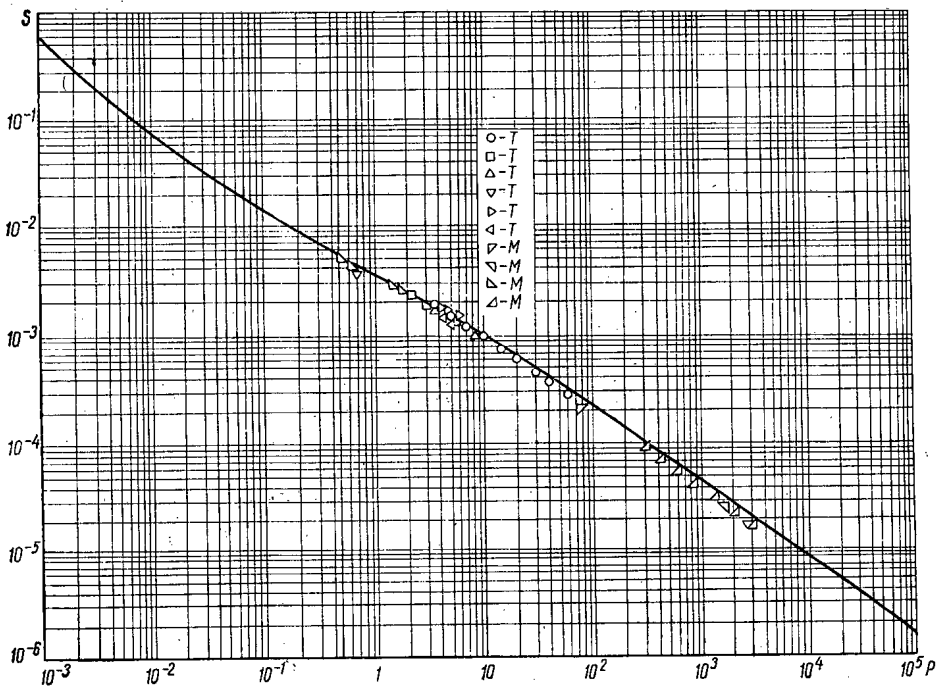

Fig. 1. The Stanton number S vs the Prandtl number P for the Reynolds number R = 10,000.

The transfer path in the transverse direction is proportional to v', i.e., it depends on y in the same way as the transverse velocity component and is proportional to y^2/δ_0.

The transverse heat transfer is proportional to the product of the transverse velocity component and the mean transverse transfer path:

$$\chi_T \sim v_* \delta_0 \left(\frac{y}{\delta_0}\right)^4,$$

where χ_T is the turbulent thermal conductivity.

Determination of δ_0 from the relation

$$\nu \sim v_* \delta_0,$$

yields

$$\chi_T = \text{const}\, \nu \left(\frac{y}{\delta_0}\right)^4.$$

Now taking the distance $y = \delta_0'$ from the wall as the thickness for which the turbulent thermal conductivity is of the order χ (the molecular thermal conductivity), we obtain V. G. Levich's formula

$$\delta_0' = c\delta_0 P^{-1/4}. \tag{1}$$

This relation directly yields the limit formula for the thermal conductivity law for large P [2], which is confirmed by Deissler's experimental data. No limit formula can be obtained for small or intermediate values of P.

Before turning to new constructions, we recall that, for P = 1, the laminar and thermal layers have the same thickness. We thus set c = 1 in (1), i.e., we have

$$\delta_0' = \delta_0 P^{-1/4} \quad \text{for} \quad P \gg 1. \tag{2}$$

For Prandtl numbers smaller than unity, both the tangential turbulent stresses and the turbulent transfer of heat and mass are negligibly small within the limit δ_0 of the laminar sublayer.

Hence, for P > 1, the value of δ_0', which is the distance from the wall at which turbulent heat and mass transfer begin, is equal to the thickness δ_0 of the hydrodynamic laminar sublayer:

$$\delta_0' = \delta_0 \quad \text{for} \quad P < 1. \tag{2'}$$

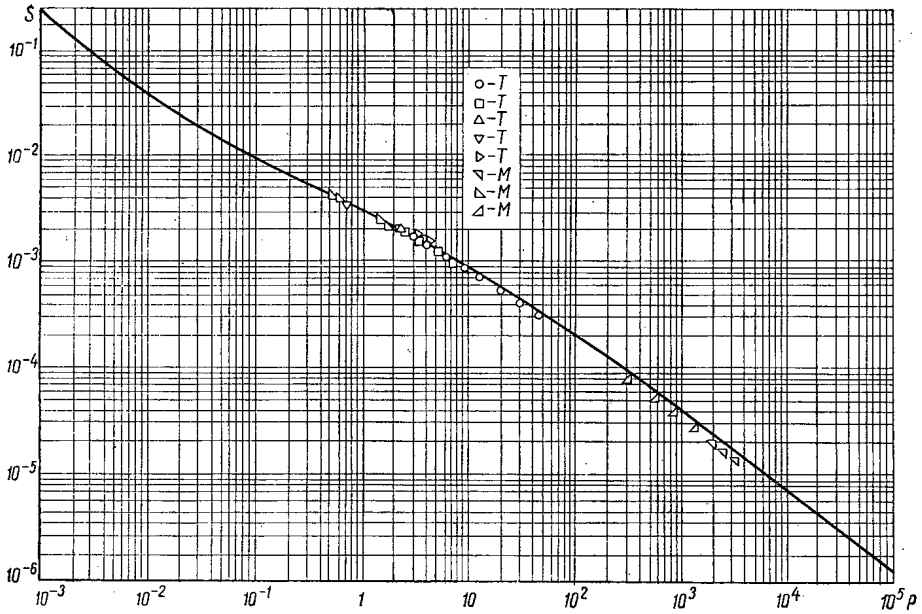

Fig. 2. The Stanton number S vs the Prandtl number P for the Reynolds number R = 25,000.

It should be noted that the constant in (1) which is taken to be unity is the only experimental quantity obtained from thermal measurements used in the following reasoning.

The investigation in [6, 9] of turbulent flow in a tube and the resistance laws shows that the superpostion of molecular viscosity and the various forms of turbulent viscosity leads to a very accurate description of the behavior of the velocity and the resistance coefficients, not only for strongly developed turbulence but also for the range of Reynolds numbers in which the influence of molecular viscosity may not be neglected. This fact is a basis for assuming that the use of the superposition principle for molecular and turbulent exchange might also yield useful results in connection with problems concerning heat exchange and mass exchange.

These two problems are completely analogous, and for the sake of definiteness we consider the heat-exchange problem and then, by changing notation, we obtain the corresponding results for the mass-exchange problem.

Let q be the heat flux towards a plane wall, and let the flow be parallel to the wall with velocity u(y).

Then

$$q = -(\varkappa + \rho c_p \varepsilon_T)\frac{dT}{dy}, \tag{3}$$

where T is the absolute temperature, T = T(y); $\varkappa = \rho c_p \chi$ is the molecular thermal conductivity; ε_T is the coefficient of turbulent mass exchange; and c_p is the specific heat at constant pressure.

According to Reynolds' hypothesis

$$\varepsilon_T = \nu_T,$$

where ν_T is the kinematic turbulent viscosity.

Generalizing Reynolds hypothesis, we have†

$$\varepsilon_T = a' v_* (y - \delta_0').$$

Our generalization lies in the fact that the thickness δ_0' of the thermal laminar layer is not in general equal to the thickness δ_0 of the laminar sublayer for the velocity field, and the quantity a' is defined as follows:

$$a' = \text{const} = a \quad \text{for} \quad y > \delta_0';$$
$$a' = 0 \quad \text{for} \quad y \leqslant \delta_0'.$$

†cf. [6, 7].

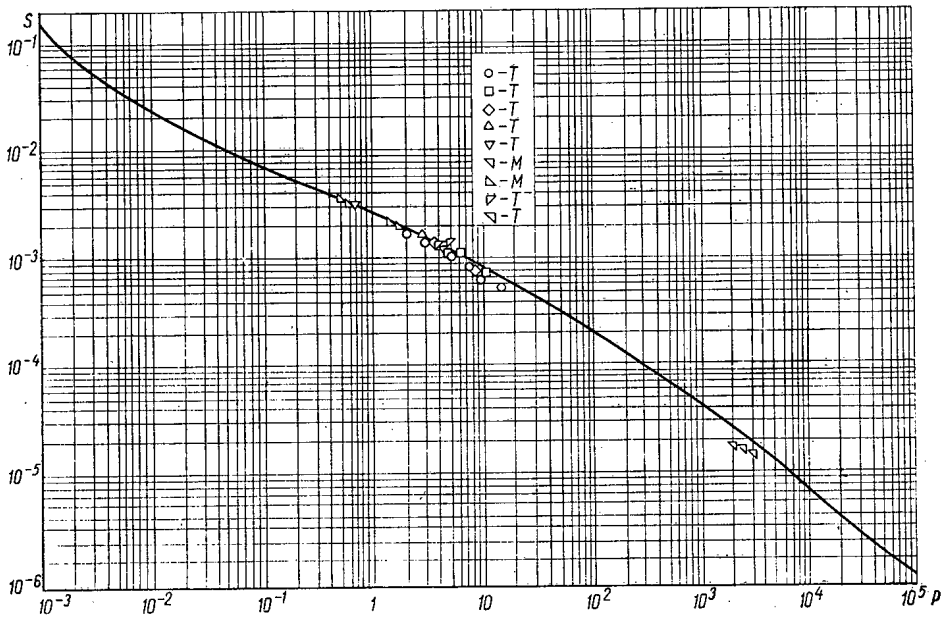

Fig. 3. The Stanton number S vs the Prandtl number P for the Reynolds number R = 50,000.

By integrating (3) we obtain a relation determining the temperature distribution:

$$\frac{\Delta\tilde{T}}{\beta}=\frac{1}{a'}\ln[1+a'P(\eta-\delta')]+\delta'P, \tag{4}$$

where

$$\beta=\frac{q}{\rho c_p T_0 v_*};\ \eta=\frac{yv_*}{\nu};\ T_0=T(0);$$
$$\delta=\frac{\delta_0 v_*}{\nu};\ \delta'=\frac{\delta_0' v_*}{\nu};\ \Delta\tilde{T}=1-\frac{\tilde{T}}{T_0}.$$

Relation (4) is analogous in form to the relation

$$\frac{u}{v_*}=\frac{1}{a}\ln[1+a(\eta-\delta)]+\delta \tag{5}$$

for the velocity distribution [6].

Relations (4) and (5) coincide if P = 1 and $\delta' = \delta$.

The quantities δ and a were determined in [6] from experimental data obtained by the measurement of velocities in the layer close to a wall or in tubes. We have good agreement with hydrodynamic experimental results for $\delta = 7.8$ and $a = 0.39$.

If we use (2), we find that (4) implies

$$\frac{\Delta\tilde{T}}{\beta}=\frac{1}{a}\ln[1+Pa(\eta-\delta\cdot P^{-1/4})]+\delta\cdot P^{3/4}. \tag{6}$$

This relation yields temperature distributions as functions of η and P.

For $a = 0.39$ and $\delta = 7.8$ (the values derived from hydraulic measurements), temperature profiles were calculated and comparisons were made with the experimental results in [1, 10, 11].

Unfortunately we have at our disposal only velocity-profile measurements for Prandtl numbers close to unity. The temperature profile obtained from (6) gives a good description of the whole range of distances from the wall.

For Prandtl numbers differing considerably from unity, i.e., for $0.5 < P < 3000$, the law for heat exchange has been investigated experimentally [1] from the point of view of the dependence of Stanton's number on Prandtl's number.

Stanton's number S is defined by the equation

$$S^{-1} = \frac{u_{\text{mean}}}{v_*} \cdot \frac{\tilde{T}_{\text{mean}}}{\beta}. \tag{7}$$

Experimental results are usually processed by taking an average weighted by the flow in a given section, i.e., by using the formula

$$\frac{\Delta\tilde{T}_{\text{mean}}}{\beta} = \frac{\int_0^{\eta_0} \frac{\Delta\tilde{T}}{\beta} \cdot \frac{u}{v_*} (\eta_0 - \eta)\, d\eta}{\int_0^{\eta_0} \frac{u}{v_*} (\eta_0 - \eta)\, d\eta}, \tag{8}$$

which is equivalent to defining S by the relation

$$S^{-1} = \frac{2}{\eta_0^2} \int_0^{\eta_0} \frac{\Delta\tilde{T}}{\beta} \cdot \frac{u}{v_*} (\eta_0 - \eta)\, d\eta,$$

where $\eta_0 = rv_*/\nu$ and r is the tube radius.

Relations (5) and (6) can be used explicitly to estimate the difference between the average given by (8) and the simple mean given by the formula

$$\frac{\Delta\tilde{T}'_{\text{mean}}}{\beta} = \frac{2}{\eta_0^2} \int_0^{\eta_0} \frac{\Delta\tilde{T}}{\beta} (\eta_0 - \eta)\, d\eta. \tag{9}$$

For P = 1 we have

$$\Delta\tilde{T}_{\text{mean}} \approx \Delta\tilde{T}'_{\text{mean}} \left[1 + \frac{5}{4a^2} \left(\frac{\beta}{\Delta\tilde{T}'_{\text{mean}}}\right)^2\right]. \tag{10}$$

For sufficiently large values of $\Delta\tilde{T}_{\text{mean}}/\beta$, the second term in (10) is small and we may take

$$\Delta\tilde{T}_{\text{mean}} = \Delta\tilde{T}'_{\text{mean}} \tag{11}$$

with a high degree of accuracy.

For large Prandtl numbers, the exact value of $\Delta\tilde{T}_{\text{mean}}$ in the heat-exchange law is of no great importance, and errors in its value may be ignored. Hence in our calculations we may use temperatures given by (9).

On the other hand averages obtained from (8) must be retained in the calculation of the heat balance, since errors in the calculation of the longitudinally transported flow are all retained in the calculations of the thermal balance.

Using the above facts concerning the average, and the relation

$$\frac{u_{\text{mean}}}{v_*} = \frac{2}{\eta_0^2} \int_0^{\eta_0} \frac{1}{a} \{\ln[1 + a(\eta - \delta)] + \delta\} (\eta_0 - \eta)\, d\eta = \sqrt{\frac{8}{\lambda}}, \tag{12}$$

where λ is the resistance, we have

$$\frac{\Delta\tilde{T}_{\text{mean}}}{\beta P} = \delta_1 - \frac{\delta_1^2}{\eta_0} + \frac{1}{3} \cdot \frac{\delta_1^3}{\eta_0^2} + \frac{2}{a_1^2 \eta_0} \left[1 + \frac{a_1\delta_1 - 1}{a_1\eta_0}\right] \left[\alpha(\ln\alpha - 1) + 1\right] + \frac{2}{a_1^3\eta_0^2} \left[\frac{\alpha^2}{2} \left(\ln\alpha - \frac{1}{2}\right) + \frac{1}{4}\right], \tag{13}$$

where $a_1 = aP$, $\delta_1 = \delta \cdot P^{-1/4}$, $\alpha = 1 + a_1(\eta_0 - \delta_1)$, $\eta_0 = rv_*/\nu$, and r is the tube radius, or we can use the approximation

$$\frac{\Delta\tilde{T}_{\text{mean}}}{\beta} = \sqrt{\frac{8}{\lambda}} + (P^{3/4} - 1)\,\delta + \frac{1}{a} \ln P + \varepsilon, \tag{13'}$$

where ε is small.

Hence for large Prandtl numbers we have the very accurate relation

$$S^{-1} = \frac{8}{\lambda} \left\{1 + \sqrt{\frac{\lambda}{8}} \left[(P^{3/4} - 1)\,\delta + \frac{1}{a} \ln P\right]\right\}. \tag{14}$$

It follows that for the Nusselt number $N = S \cdot R \cdot P$ we have

$$N^{-1} = \frac{8}{\lambda R \cdot P}\left\{1 + \sqrt{\frac{\lambda}{8}}\left[(P^{3/4} - 1)\delta + \frac{1}{a}\ln P\right]\right\}. \quad (15)$$

For Prandtl numbers smaller than unity (in this case $\delta_0' = \delta_0$), we have the following accurate relation

$$S^{-1} = \sqrt{\frac{8}{\lambda}}\left\{\frac{1}{a}\ln[1 + aP(\eta - \delta)] + \delta\right\}. \quad (16)$$

Figures 1-3 show curves obtained from values of S calculated from (14) for the values $a = 0.39$ and $\delta = 7.8$ obtained from hydrodynamic experiments and the corresponding values of λ given in [6].

Conversion of the above results to apply to diffusion problems is carried out by replacing the thermal conductivity χ by the diffusion coefficient D and the temperature T by the concentration C of the diffusing material.

The points marked in the diagrams are experimental values concerning heat and mass exchange (T and M) given by Deissler [1].

The accuracy of values of S and N obtained from (14), (15), and (16) depends on the accuracy of δ, and can be increased by improving the accuracy of determination of δ and the accuracy of the thermal measurements.

Calculated and experimental results can be considered to coincide within the contemporary accuracy possible in hydraulic and thermal measurements.

We note in conclusion that, by using the superposition of molecular and turbulent viscosity and the concept of a laminar sublayer whose thickness for hydrodynamic considerations is different from its thickness for heat and mass exchange, we have obtained a description of turbulent heat and mass exchange valid for a wide range of Prandtl numbers. Good quantitative agreement is obtained with experimental data over a wide range of Prandtl numbers without using any constants which must be determined from thermal measurements except the constant c = 1, used in (1). There is no need to consider the interaction between molecular and turbulent exchange or to use interpolation formulas requiring the determination of extra coefficients by experiment.

The author wishes to thank I. S. Kudryavtseva for her help in connection with the computations.

LITERATURE CITED

1. R. Deissler, NACA Report 1210 (1954).
2. V. G. Levich, Physicochemical Hydromechanics [in Russian], Nauka, Moscow (1962).
3. L. G. Loitsyanskii, Proceedings of the All-Union Congress on Theoretical and Applied Mechanics [in Russian], Izd-vo AN SSSR, Moscow–Leningrad (1962).
4. P. L. Kapitsa, "Wave flow of thin layers of a viscous liquid. I. Free flow. II. Flow accompanied by a gas flow and heat flux," Zh. Eksp. Teor. Fiz., 18, No. 1 (1948).
5. P. L. Kapitsa and S. P. Kapitsa, Zh. Éksp. Teor. Fiz., 19, No. 2 (1949).
6. M. D. Millionshchikov, Turbulent Flow in the Boundary Layer and in Tubes [in Russian], Nauka, Moscow (1969).
7. M. D. Millionshchikov, Atomnaya Énergiya, 28, 206 (1970).
8. M. D. Millionshchikov, Atomnaya Énergiya, 28, 317 (1970).
9. M. D. Millionshchikov, Atomnaya Énergiya, 29, 16 (1970).
10. B. Pinkel, Trans. ASME, 76, No. 2 (1954).
11. R. Deissler, Trans. ASME, 76, No. 1 (1954).

SPECIAL ASPECTS OF THE DEFORMATION OF URANIUM SUBJECTED TO TENSILE STRAIN AT A CONSTANT VELOCITY

A. I. Voloshchuk, V. F. Zelenskii, Yu. F. Konotop, and Yu. T. Miroshnichenko

UDC 621.039.543.4:621.039.544.57

The accelerated swelling of uranium under the influence of irradiation at 400 to 500°C is associated with the effects of stresses arising from radiation growth. Independently of the actual mechanism responsible for the formation of large pores [1, 2], the swelling is ultimately determined by the manner in which the stresses relax under specific irradiation conditions. The mechanism underlying the deformation of uranium is of particular interest [3-6].

In this paper we shall consider the results of a study of the deformation (strain) characteristics and the structure of deformed uranium samples of reactor purity (~0.3 wt.% of impurities) and also a uranium-base alloy containing an additional 0.5 wt.% of beryllium oxide.

RESULTS

Properties of Samples under Tensile Strain. We studied cylindrical rupture-test samples with a working part 15 mm long and a diameter of 3 mm. The samples were prepared from bars quenched from the β-phase after technological processing.

Judging from the strain curves (Fig. 1) the rate of strain hardening of the uranium alloy was the same as that of the uranium at 360°C, indicating that the conditions governing the blocking of sliding dislocations by tangled dislocations and well-dispersed particles were the same in the two cases. Deformation takes place mainly by way of the transverse slipping of screw dislocations. As the temperature increases, individual dislocations are thermally activated and are able to move by way of diffusion creeping. As a result of this, the system of intersecting dislocations enters into an unstable state, and softening of the material

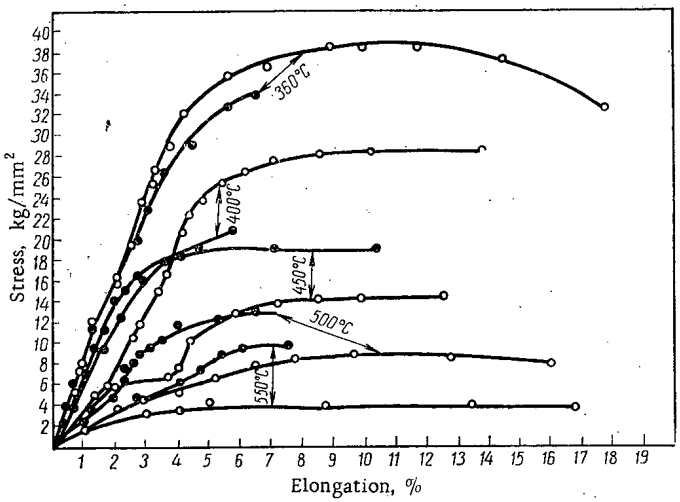

Fig. 1. Strain curves of uranium (○) and the alloy (●). Deformation at various temperatures at a rate of $6 \cdot 10^{-3}$ h^{-1}.

Translated from Atomnaya Énergiya, Vol. 29, No. 6, pp. 416-422, December, 1970. Original article submitted December 19, 1969; revision submitted May 4, 1970.

takes place. When the dislocations are blocked by dispersed particles, the creeping of individual dislocations has little effect on the deformation mechanism as a whole, and the softening of the dispersion-hardened materials occurs at higher temperatures. It follows from the strain curves that a considerable reduction in the rate of strain hardening of uranium sets in at temperatures of over 360°C. For the alloy containing beryllium oxide, raising the temperature from 360 to 450°C has little effect on the rate of strain hardening, the strain mechanism presumably remaining the same. Softening of the alloy occurs at temperatures of over 450°C; the rate of hardening of the alloy at 500 to 550°C is very similar to that of uranium at 450 to 500°C, suggesting that the mechanisms underlying the deformation of uranium and its alloy at the corresponding temperatures are analogous.

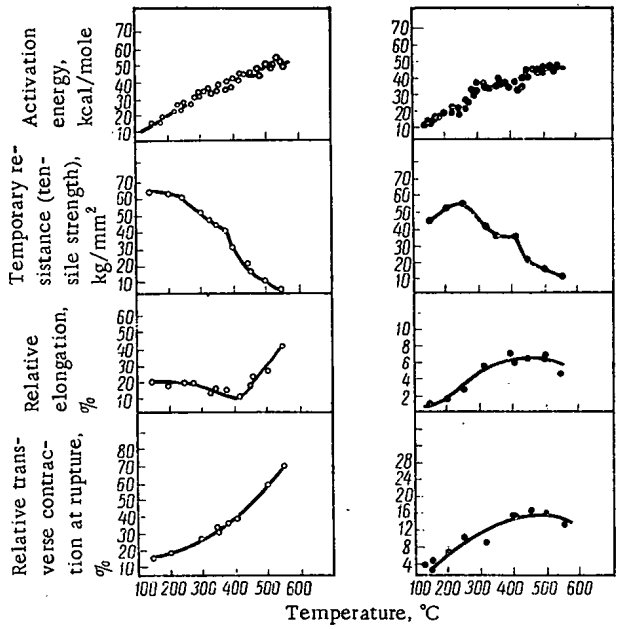

Fig. 2. Temperature dependence of the creep activation energy and the stress/strain characteristics of uranium and the U – BeO alloy (○ and ● respectively).

These results are in good agreement with earlier conclusions based on a study of the temperature dependence of the activation energy of creep [6], and are also supported by metallographic analysis.

Figure 2 illustrates the temperature dependence of the parameters characterizing some of the mechanical properties of uranium and the uranium alloy containing 0.5% beryllium oxide.

At temperatures of under 400°C, the alloy has lower strength characteristics than the unalloyed uranium. The relative elongation of the uranium has a minimum close to 400°C, coinciding with a region of softening associated with a change in the deformation mechanism. In the case of the alloy, the rise in ductility with temperature becomes less rapid in the neighborhood of these temperatures.

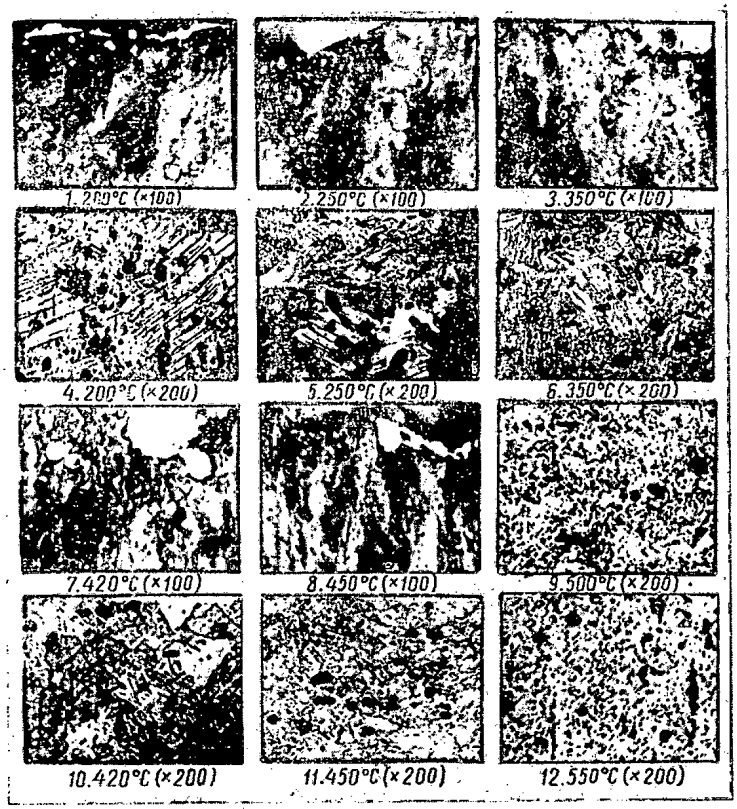

Fig. 3. Structure of ruptured uranium samples in the zone of maximum deformation.

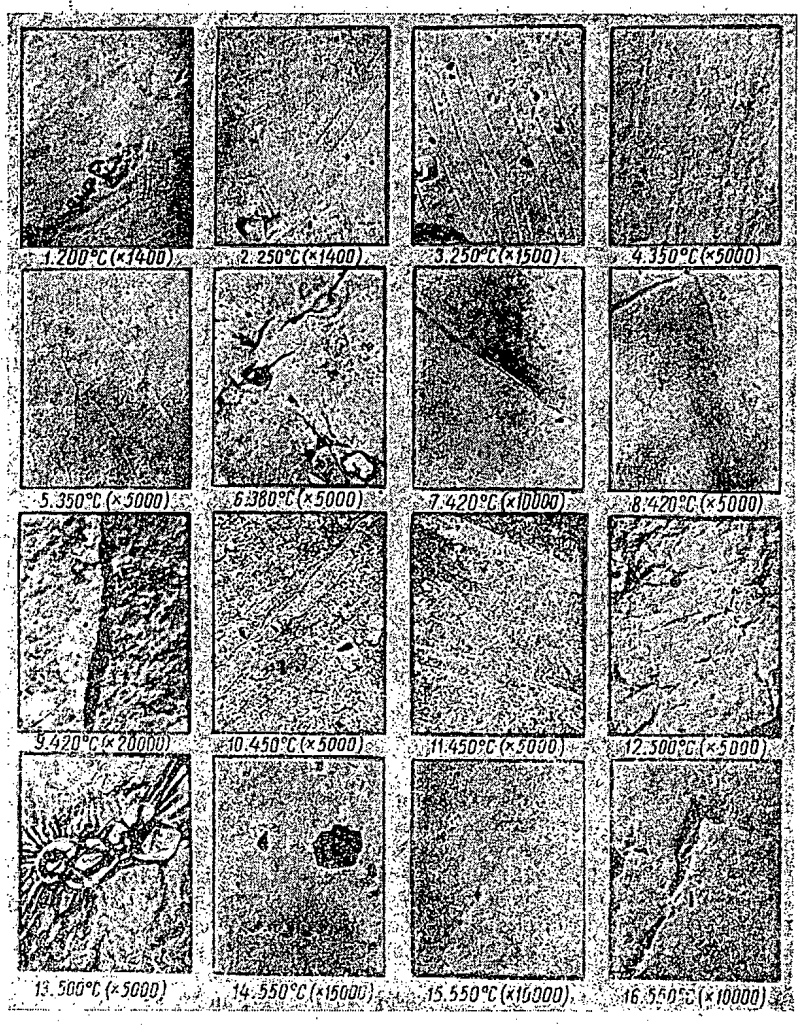

Fig. 4. Development of deformation processes in uranium.

Structure of Deformed Samples. The structure of the materials in question was studied in the zone of maximum deformation of samples ruptured at various temperatures by subjecting to a constant strain rate of $6 \cdot 10^{-3}\ h^{-1}$. The plane of the microsection was parallel to the elongation axis.

As the temperature rises, so does the degree of deformation of the grain, this being particularly noticeable at 450°C (Fig. 3, 8). A study of the development of slip lines, the behavior of the grain boundaries, and other structural characteristics yields the following conclusions. Up to temperatures of 400 to 420°C, deformation in the grains is effected by twinning or slipping. Starting from 420°C, in some regions intersecting slip systems appear; these indicate the activation of earlier-blocked slip directions. At 450°C there is a considerable refinement of the structure, and etch pits develop, these constituting the result of polygonization processes. A particularly high etch-pit density occurs in samples deformed at 500°C. At 550°C it would appear that a thermally-activated coarsening of the polygonized structure occurs, and the etch-pit density falls.

Electron-microscope analysis gives a more detailed picture of the mechanism underlying the deformation of the samples.

Deformation by twinning or simple slip takes place mainly between 200 and 250°C (Fig. 4, 1-3). On subjecting to deformation between 320 and 350°C, the samples develop characteristic transverse slip lines (Fig. 4, 4 and 5). At 380 to 420°C (region of minimum elongation) cracks are formed around particles and cavities along the grain boundaries (Fig. 4, 6 to 9). In the temperature range in which the creep activation energy is close to the activation energy of self-diffusion, migration of the grain boundaries and slip lines occurs, confirming the diffusion character of the deformation (see Fig. 4, 10 and 11). Samples ruptured at 500°C have a well-expressed polygonization structure. Considerable stress concentrations occur near the particles during the deformation process, leading, in individual cases, to the formation of cavities (Fig. 4,

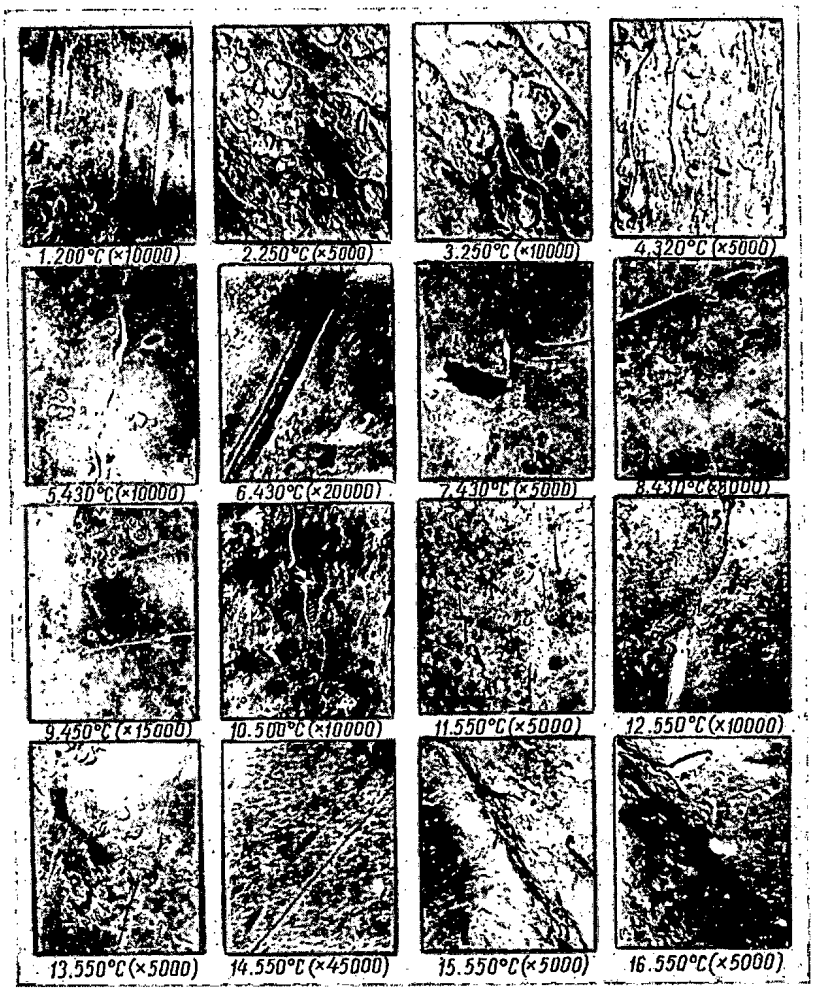

Fig. 5. Development of deformation processes in a U – 0.5% BeO alloy.

13). It is interesting to note that the cavities are formed, not exactly on the particle/matrix interface, but at some distance from the particles. In the samples deformed at 550°C, pores of diffusion origin develop (see Fig. 4, 14 and 15). In view of the high mobility of the subsidiary boundaries, the latter may sweep the dislocation tangles along during their motion and carry them toward obstacles of a more stable nature (particles or grain boundaries). As a result of this, pores of diffusion origin are formed at these obstacles; these may later grow as a result of the inflow of vacancies, accelerated by the applied stresses.

Together with the pores of a diffusion character, cavities of a mechanical origin are also found at this temperature (Fig. 4, 16).

In view of the high density of the second-phase particles, a metallographic analysis of the structural details of uranium–beryllium alloys is practically impossible. Structural analysis of deformed samples of the uranium–beryllium oxide alloy was therefore confined to electron-microscope observations (Fig. 5). Twins only appear in the samples ruptured at 200°C. Twinning is retarded by the beryllium oxide particles, and the individual twins are of small dimensions (Fig. 5, 1). Simple slip is retarded close to the particles in the early stages of loading, and the deformation develops principally by way of the "squeezing" of the dislocations between the particles in accordance with the Orowan mechanism (Fig. 5, 2 and 3). Transverse slip is to be seen between 320 and 550°C (see Fig. 5, 4, 8 to 11). Only at 550°C do we find slipping along grain boundaries, and a fan-like propagation of dislocations, constituting a result of creep processes (Fig. 5, 11 and 12). Cracks and cavities of mechanical origin appear at 430°C (Fig. 5, 7); these are usually associated with the grain boundaries and not the particles of beryllium oxide, even in the zones with high stress concentrations (Fig. 5, 15 and 16). Small cavities of mechanical (but not diffusion) origin were observed in the slip lines at 550°C (Fig. 5, 11, 13, and 14).

DISCUSSION OF RESULTS

The conditions governing the rupture of materials subjected to tensile tests differ considerably from those encountered as a result of the stresses arising from irradiation. In the first case, the deformation takes place as a result of the action of a concentrated load applied to the sample as a whole; in the second case, sources of stress are distributed uniformly throughout the whole sample. In tensile tests, the stress in the sample increases until the yield stress in the weakest section is exceeded. Subsequently the principal deformation (strain) occurs solely in the zone associated with this section, and in a low-ductility material rupture follows rapidly. In materials of high ductility, having the capacity to heal the defects arising under the influence of the load, higher strength characteristics may be achieved under these conditions.

In the case of a uniform distribution of stress sources, local cracks have a less severe effect on the deformation of the sample as a whole, and the character of sample rupture differs considerably from that associated with tensile tests. It is thus essential to be very cautious in drawing analogies between the results of strength and radiation tests. In interpreting the results of strength (tensile) tests, the main factor to be considered is not that of comparing the absolute values of the temporary resistance or time to rupture (failure), but that of considering the mechanisms of deformation under various conditions more deeply.

The results here obtained confirm the existence of at least three mechanisms of uranium deformation at high temperatures: transverse slip, creeping, and the migration of polygonal boundaries. This agrees with Holmes investigation [5] based on the analysis of published uranium creep data. It is also interesting to note that the observed temperature ranges, corresponding to the various mechanisms of uranium deformation, coincide with the stages of the temperature dependence of radiation growth established by Buckley [7]. This may be regarded as a confirmation of the generality of the mechanisms underlying the phenomena of radiation growth and the conditions of stress relaxation in uranium.

The activation of the diffusion processes in uranium (starting from temperatures of 380 to 400°C) leads to a change in the deformation mechanism, a certain reduction in the relative elongation, and a considerable softening of the samples on subjecting to tensile strain at low deformation rates. The latter fact is associated with the formation of a considerable number of cracks along the grain boundaries and around included particles. Although the mechanism of deformation by transverse slip remains operative to higher temperatures in the alloy containing beryllium oxide (440°C, see Fig. 1), the cavities at the grain boundaries, the reduction in the rate of increase of ductility with temperature, and the reduction in the temporary resistance (tensile strength) occur at practically the same temperatures, 420 to 430°C. Evidently the main reason for the formation of cavities in this temperature range is associated with special aspects of the development of the diffusion processes.

It is well known that diffusion occurs more intensively along grain boundaries, dislocations, and other structural disruptions. It may reasonably be considered that the cavities are formed at a stage of thermal activation at which a considerable softening takes place close to the grain boundaries or other surfaces of phase separation, as a result of a substantial acceleration of the diffusion processes. The supply of material through the grain to heal the damaged regions, however, is insufficiently rapid. At higher temperatures the diffusion contribution increases, and no cavities appear at the grain boundaries, or else they only appear rarely at points of maximum stress concentration. The hardening of the grain boundaries by well-dispersed particles slightly retards the onset of cavity formation; however, since the diffusion parameters remain practically unaltered, the effect of the hardening phase is comparatively slight.

At 550°C a new form of porosity appears, due to the intensive activation of three-dimensional diffusion. Whereas the dispersed particles have only a slight effect on the temperature of formation of mechanical cavities, they greatly retard the onset of the development of diffusion-type porosity. All the particles, and not simply those lying along the grain boundaries, have an effect on the pore growth. The mechanism of this effect may be twofold: the blocking of moving dislocations and subsidiary boundaries, and a redistribution in the flow of individual vacancies. In the latter case the vacancies may condense in a large number of dispersed particles, without the creation of appreciable porosity.

One further interesting fact should be emphasized. Cracks appear around included particles in uranium samples containing only a small number of inclusions. Yet in an alloy with a very high density of beryllium oxide particles no such cracks are to be found, even in places with considerable stress concentrations. For a low density of comparatively large particles, each such particle constitutes a barrier against a large number of moving dislocations. Since the stresses arising at the surface of a particle are proportional to

the number of dislocations present, their magnitude may prove sufficient for the formation of considerable cracks. In the case of a high density of particles and comparable degrees of deformation, the latter may become distributed among the particles in such a manner that individual disruptions in each particle will not necessarily lead to crack formation.

We may thus express the following views as to the possible mechanism underlying the swelling of uranium. The rupture of uranium as a result of the formation of cracks of mechanical origin under irradiation may occur in a narrow temperature range around 400°C. By hardening the grain boundaries, this range may be shifted in the high-temperature direction. In view of the activation of diffusion mobility within the grain, the conditions for the formation of cracks will then be less favorable, and the accelerated swelling associated with crack formation may cease. For high rates of irradiation, when the radiation-growth stresses remain operative up to temperatures of 450 to 550°C, another form of accelerated uranium swelling should appear; this is the formation of spherical pores of diffusion origin at the grain boundaries and other surfaces of phase separation at temperatures above 500°C. It follows from the foregoing analysis that dispersed particles may substantially reduce the rate of formation of such pores.

LITERATURE CITED

1. M. Speight and G. Greenwood, J. Nucl. Materials, 16, 327 (1965).
2. J. Harrison, J. Nucl. Materials, 23, 139-153 (1967).
3. D. Taplin, J. Austral. Inst. Metals, 12, 32-44 (1967).
4. P. Grenier and P. Lacombe, J. Nucl. Materials, 22, No. 3, 241-256 (1967).
5. J. Holmes, Trans. Amer. Soc. Metals, 59, No. T-1 (1966).
6. V. E. Ivanov, Atomnaya Énergiya, 29, 178 (1970).
7. S. Buckley, AERE-R, 5262 (1966).

SUBBARRIER NEUTRON FISSION OF Pu^{238} (E/T)

S. B. Ermagambetov and G. N. Smirenkin

UDC 539.173.4

As with most even–even nuclei, the cross section σ_f for fast-neutron fission of Pu^{238} has a "threshold" nature, and, as shown in [1], it is in rather good agreement with the monotonic exponential dependence of the fission width at a few hundred kiloelectron volts:

$$\Gamma_f(E_n) \sim P(E_n) = \left[1+\exp\left(2\pi\,\frac{E_f-B_n-E_n}{\hbar\omega}\right)\right]^{-1},$$

where P, E_f, and $\hbar\omega$ are the penetrability, height, and buckling parameter of the fission barrier. However, the magnitude of $\Gamma_f(0) \approx$ 30-50 MeV, obtained in that study by extrapolating the fission width to $E_n = 0$, is somewhat larger than the thermal value Γ_f^T, which is about 1 MeV, which is easily estimated from the radiation width $\Gamma_\gamma \approx 30$ MeV and the fission and absorption cross sections (which are 18 and 615 barns respectively [2]). In 1965 data was published [3] for the experimental upper estimates of the fission widths Γ_{fr} for the first three resonances of the reaction Pu^{238} + n; these are shown in Table 1. They indicated a further strong difference between Γ_{fr} and $\Gamma_f(0)$. Some more recent measurements [4], also shown in Table 1, indicate a rather large fissility of Pu^{238} by s-neutrons. The average fission width $\bar{\Gamma}_{fr}$ determined from the first ten resonances was about 5 MeV, which is much larger than the value obtained by James [3], but as usual, much smaller than the value of $\Gamma_f(0)$ found in [1].

The ratio $\Gamma_{fr}/\Gamma_f(0) \ll 1$ is realized in many nuclei and has been interpreted in terms of the two-humped fission barrier picture [5] as a consequence of the intermediate structure in the cross sections in the resonance region of the neutron energies [6]. The origin of this structure lies in the presence of quasistationary levels in the second well (between the humps). This interpretation permits significant deviations of Γ_{fr} from the average value in the interval between the levels, without the total suppression of the s-waves as is often assumed when discussing the large difference between Γ_{fr} and $\Gamma_f(0)$. These consequences of the two-humped barrier model are underscored by the results for the distribution of the fission widths in (n, f) reactions in Pu^{240} and Np^{237} [6], for which the ratio $\Gamma_{fr}/\bar{\Gamma}_{fr}$ varies over a rather large range.

The available information concerning resonance neutron fission of Pu^{238} is insufficient and, as the above shows, very contradictory. However, the question of the role of s-waves in the fission of Pu^{238} can be solved in another way: one can study σ_f in the high energy region where the individual resonances are not resolved, but where the s-wave makes the dominant contribution to the cross section for forming a compound nucleus. We have made such measurements on an electrostatic generator using Pu^{238} as a target. The preliminary results of that study have been published elsewhere [7]. This paper will present some more accurate data and the results of a more detailed analysis.

TABLE 1. Fission Widths (MeV) for Pu^{238} in the Epithermal Energy Range of the Neutrons

Neutron resonance energy, eV	Data and reference	
	[3]	[4]
2,9	0,083	1,2
10,1	0,196	6,8
18,7	0,202	1,6

The measurements were performed using the comparative method. U^{235} was used as a standard. Glass detectors were used to record the fission fragments. The neutron source was the reaction T(p, n). As a rule, a number of pairs of fissionable layers and detectors were irradiated at once. The detectors were situated at various angles ranging from 0 to 150° with respect to the proton beam. The Pu^{238} used was practically isotopically pure (99.8%), so that the fission of impurities was not included. The relative behavior of σ_f for Pu^{238}, as corrected for the background of spontaneous fission and

Translated from Atomnaya Énergiya, Vol. 29, No. 6, pp. 422-424, December, 1970. Original article submitted May 11, 1970.

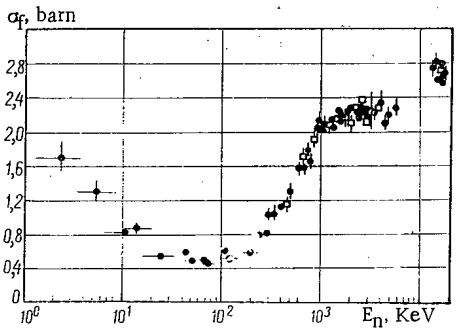

Fig. 1

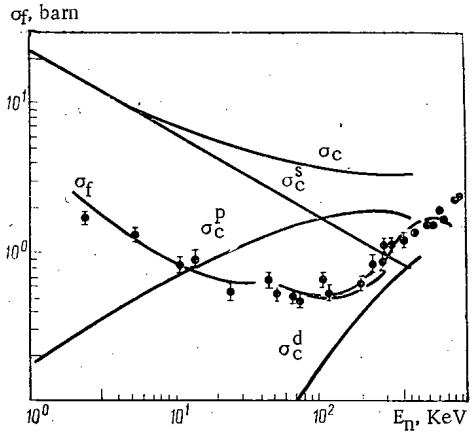

Fig. 2

Fig. 1. Pu^{238} fission cross section σ_f as a function of the neutron energy E_n: □) [9]; ▲) [10]; ●) present work and [8].

Fig. 2. Comparison of the experimental and calculated results: σ_c and $\sigma_c^{(l)}$ are respectively the cross sections for forming a compound nucleus and its partial components for s-, p-, and d-neutrons. The solid curve for σ_f is computed from Eqs. (1-3); the dotted line is calculated with all the allowed states $K \leq 7/2$ included.

TABLE 2. Measured Cross Sections σ_f for Fission of Pu^{238}

E_n, KeV	σ_f (Pu^{238}), barn	E_n, KeV	σ_f (Pu^{238}), barn
2,4±1,3	1,70±0,18	420±15	1,14±0,05
5,5±2,5	1,30±0,12	635±25	1,60±0,06
11,3±6,0	0,83±0,06	680±25	1,60±0,06
14,4±5,0	0,88±0,07	770±25	1,67±0,07
25,5±10	0,55±0,04	910±10	2,06±0,08
46,4±20	0,62±0,04	1080±20	2,11±0,08
53±6	0,52±0,03	1210±20	2,13±0,08
70±7	0,50±0,03	1330±20	2,08±0,08
78±10	0,47±0,02	1430±25	2,20±0,10
110±7	0,62±0,03	1500±20	2,15±0,07
120±10	0,53±0,03	1650±20	2,20±0,10
200±20	0,60±0,03	1800±20	2,18±0,10
250±5	0,80±0,04	2000±20	2,30±0,10
290±20	0,84±0,04	2260±20	2,25±0,09
305±10	1,05±0,05	2400±20	2,22±0,09
350±8	1,06±0,04		

the fission due to epicadmium neutrons and the neutrons scattered in the target, was normalized to the values which we obtained earlier [8]. The measured values of σ_f for Pu^{238} are shown in Table 2 and the reference values of σ_f for U^{235} were taken from [9]. Figure 1 shows the good agreement between the data for σ_f for Pu^{238} from our work and the values in [8-10]. The data in the range $0.1 \lesssim E_n \lesssim 1.5$ MeV from [1, 2] is 20-30% higher on the average, but the relative behavior of σ_f is very close to that shown in Fig. 1.

We have recently become aware of a work [11] which is an experimental study in the 1-10 keV energy range which used a nuclear explosion as a source of neutrons [12]. The results of these measurements revealed a resonant structure with resonance widths of about 0.1-0.2 keV and separations averaging about 1 keV. In [11] this structure was related to the quasistationary states in the second well of the fissible nucleus Pu^{239}. The energy resolution of our measurements has nearly smoothed out this structure, but the data from both experiments agree quite satisfactorily (if the values in [12] are averaged over the interval $2\Delta E_n$ shown in Table 1).

In addition to the experimental data for σ_f of Pu^{238}, Fig. 2 shows the cross section σ_c for forming a compound nucleus, together with its partial components $\sigma_c^{(l)}$ for s-, p-, and d-neutrons. Even without a detailed analysis it can be seen by comparing the characteristics shown that the s-neutron fission of Pu^{238} plays an important role. The energy dependence of the fission cross section for Pu^{238} for neutron energies less than 50 keV does not differ qualitatively from the behavior of $\sigma_f(E)$ for U^{233}, U^{235}, and Pu^{239}, and other isotopes which are easily split by slow neutrons [2].

In order to obtain a qualitative comparison of the probability of splitting Pu^{238} by s- and p-neutrons, we have calculated the fission cross sections using the static theory of Hauser and Feshbach

$$\sigma_f = \frac{\pi\lambda^2}{2} \sum_{J,K,\pi} (2J+1)\, T_l^J \frac{P_{K\pi}}{\sum\limits_{K' \leq J} P_{K'\pi} + \sum\limits_{l',j',\nu} T_{l'}^{j'}(E_n - E_\nu) + \frac{2\pi}{D_J}\Gamma_\gamma} \qquad (2)$$

under the assumption that the penetrability is the same for s- and p-neutrons; i.e.,

$$P_{JK\pi} = P_{K\pi} = P_{1/2+} = P_{1/2-} = P_{3/2-}, \quad (3)$$

K is the projection of the angular momentum J of the compound nucleus on the symmetry axis, λ is the neutron wavelength, T_l^J are the penetrability coefficients for neutrons with orbital momenta l [13], $\pi = (-1)^l$, $j' = l' \pm 1/2$, E_ν are the levels of the target nucleus, $D_J = (2D_{1/2})/2J + 1$ is the distance between levels of the compound nucleus with spin J ($D_{1/2} = 10$ eV), $\Gamma_\gamma = 30$ MeV is the radiation width. The solid line for $\sigma_f(E_n)$ in Fig. 2 was computed using Eqs. (1-3) and these parameters: $E_f = 0.5$ MeV, $\hbar\omega/2\pi = 0.115$ MeV, $P(0) = 10^{-2}$, $\Gamma_f(0) = 15$ MeV. This last quantity is only three times greater than the estimate of $\bar{\Gamma}_{fr}$ in [13]. The dotted line shows the results of a calculation in which the assumption of Eq. (3) is extended to the allowable angular momentum state $K \leq 7/2$ of both parities.

Keeping in mind the narrow interval over which the widths of the separate resonances Γ_{fr} were averaged in [4], the complicated structure in $\sigma_f(E_n)$ due to the quasistationary states in the second well, and the approximate nature of our original premises in this analysis, one cannot take the difference between $\bar{\Gamma}_{fr}$ and $\Gamma_f(0)$ too seriously. The results of this experiment do not indicate any kind of prohibition on the s-neutron fission of Pu^{238}. This conclusion is also confirmed by an analysis of the cross sections and angular anisotropies in the reactions $Pu^{239}(\gamma, f)$ and $Pu^{238}(n, f)$ in [14].

We wish to thank M. K. Golubeva for scanning the glass detectors.

LITERATURE CITED

1. P. E. Vorotnikov et al., Yadernaya Fizika, 3, 479 (1966).
2. Neutron Cross Sections. BNL-325, 2nd Ed. Suppl. No. 2, Vol. III (1965).
3. G. James, Proc. Symp. on Phys. and Chem. of Fission (Salzburg, 1965), Vol. 1, Vienna, IAEA (1965), p. 235.
4. C. Bowman et al., Phys. Rev. Letters, 18, 15 (1967).
5. E. V. Gaii et al., Yadernaya Fizika, 10, 542 (1969).
6. E. Migneco and G. Theobald, Nucl. Phys., A112, 603 (1968); A. Fubini et al., Phys. Rev. Letters, 20, 1373 (1968).
7. S. B. Ermagambetov and G. N. Smirenkin, Pis'ma Zh. Éksp. Teor. Fiz., 9, 510 (1969).
8. S. B. Ermagambetov and G. N. Smirenkin, Atomnaya Énergiya, 25, 527 (1968).
9. Neutron Cross Section, BNL-325, Suppl. No. 2, Vol. III (1965); W. Davey, Nucl. Sci. Engng., 26, 149 (1966).
10. D. Barton and P. Koontz, Phys. Rev., 162, 1070 (1967).
11. J. Lynn, Proc. Symp. on Phys. and Chem. of Fission, Vienna, IAEA (1969), p. 249.
12. M. Silbert, Report LA-4108-MS (1969).
13. S. B. Ermagambetov et al., Yadernaya Fizika, 8, 704 (1968).
14. A. S. Soldatov, Yu. M. Tsipenoyuk, and G. N. Smirenkin, Yadernaya Fizika, 11, 992 (1970).

DESIGN OF CASCADES FOR SEPARATING ISOTOPE MIXTURES

N. A. Kolokol'tsov, V. P. Minenko,
B. I. Nikolaev, G. A. Sulaberidze,
and S. A. Tret'yak

UDC 621.039.3

Interest is growing in the separation of isotope mixtures, and thus in the theory of the design of separation cascades, primarily because of the requirements of nuclear power. Not only the isotopes at the extreme ends of the mass scale must be separated, but also the intermediate isotopes or groups of intermediate isotopes. One problem in the design of such cascades is that the concentration of the intermediate-mass isotopes tends toward a maximum within the cascade [1, 2].

In this paper, we discuss continuous-profile cascades for separating intermediate isotopes and a method for modeling these cascades by real ones consisting of sections with constant fluxes. We will call these cascades "rectangular-stepped" cascades. To simplify the calculations, we will consider only symmetrical cascades, in which the fluxes having been separated in a step are sent to the following and preceding steps.

The system of transport equations for an m-component isotope mixture, for sampling part of the cascade with an arbitrary distribution of interstep fluxes L, can be written

$$\left.\begin{aligned} \frac{dN_i}{ds} &= N_i \sum_{j=1}^{m} \varepsilon_{ij} N_j - \frac{P}{L(s)} (N_i^P - N_i), \\ i &= 1, 2, \ldots, m-1; \\ \sum_{j=1}^{m} N_j &= 1, \end{aligned}\right\} \quad (1)$$

where N_i is the molar concentration of the i-th component in the s-th step; P is the flux in the cascade sample; N_i^P is the concentration in this sample; and ε_{ij} are the enrichment factors for the isotope pair i, j; these factors are additive,

$$\varepsilon_{ij} = \varepsilon_{ir} + \varepsilon_{rj}$$

and antisymmetric,

$$\varepsilon_{ij} = -\varepsilon_{ji}.$$

Below we assume that the isotopes are numbered in order of increasing mass.

Kucherov and Minenko [3] replaced the concentrations $N_i(s)$ by the functions $\varphi_i(s)$, and reduced system (1) with a continuous function L(s) to a single Volterra equation for one of these functions:

$$\varphi_i(s) + \sum_{j=1}^{m} \frac{PN_j^P}{L(s)} \int_0^s \varphi_i(t)\, e^{\varepsilon_{ji}(s-t)}\, dt = \sum_{j=1}^{m} \frac{N_i^f L^f}{L(s)} e^{\varepsilon_{ji} s} \quad (2)$$

and to the (m – 1)-th relation of the form

$$\varphi_j(s) = \varphi_i(s)\, e^{\varepsilon_{ij} s}, \quad (3)$$

Translated from Atomnaya Énergiya, Vol. 29, No. 6, pp. 425-429, December, 1970. Original article submitted July 6, 1970.

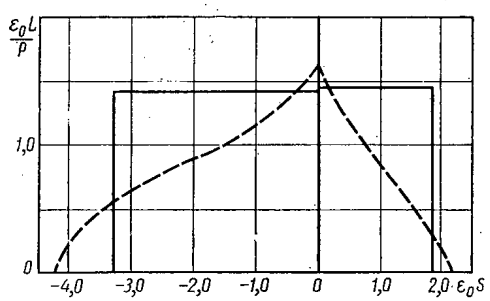

Fig. 1

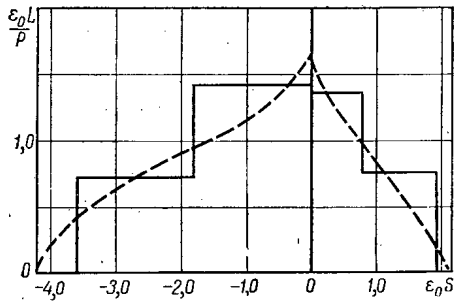

Fig. 2

Fig. 1. Two-section rectangular-stepped cascade with $\eta = 78.5\%$ for separating tungsten isotopes.

Fig. 2. Four-section rectangular-stepped cascade with $\eta = 91\%$ for separating tungsten isotopes.

where L^f and N^f_j are the flux and concentration at the supply point with $s = 1$; it is convenient to use the substitution $s = s^P - l$, where s^P is the number of steps in the sampling part. Then Eqs. (2) and (3) are rewritten

$$\varphi_i(l) - \sum_{j=1}^{m} \frac{PN_j^P}{L(l)} \int_0^l \varphi_i(t)\, e^{\varepsilon_{ji}(t-l)}\, dt = \sum_{j=1}^{m} \frac{N_j^P L(0)}{L(l)}\, e^{-\varepsilon_{ji} l}; \tag{4}$$

$$\varphi_j(l) = \varphi_i(l)\, e^{\varepsilon_{ji} l}, \tag{5}$$

where $L(0)$ is the flux at $l = 0$, i.e., at the end of the sampling.

The functions $\varphi_i(l)$ are related to the concentrations and flux in the cascade by

$$N_i(l)\, L(l) = \frac{N_i^P L(0) + N_i^P P \int_0^l \varphi_i(t)\, dt}{\varphi_i(l)}. \tag{6}$$

Introducing the notation $N_i L = \chi_i$, we find

$$\sum_{j=1}^{m} \chi_j(l) = L(l) \tag{7}$$

and thus

$$N_i(l) = \frac{\chi_i(l)}{\sum_{j=1}^{m} \chi_j(l)}. \tag{8}$$

For each given flux distribution $L(l)$ in the cascade, the functions $\varphi_i(l)$ and thus $N_i(l)$ are determined unambiguously.

We consider continuous-profile cascades which satisfy the condition

$$\varphi_i(l) = e^{Q_i l}, \tag{9}$$

where Q_i are some constants which, according to (5), should be related by

$$Q_i - Q_j = \varepsilon_{ij}. \tag{10}$$

Thus only one of the quantities Q_i can be chosen arbitrarily. For brevity, we will call those continuous-profile cascades which satisfy (9) "Q-cascades."

In minimizing the total flux of the cascade, it is natural to assume that the flux at the end is zero:

$$L(0) = 0. \tag{11}$$

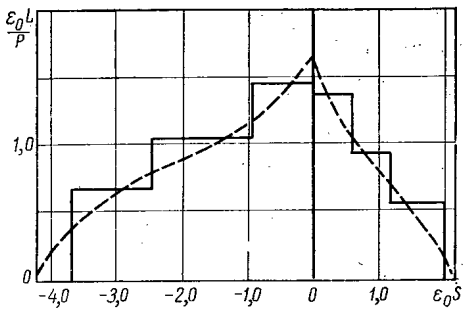

Fig. 3. Six-section rectangular-stepped cascade with $\eta = 94.6\%$ for separating tungsten isotopes.

TABLE 1. External Parameters of a Continuous-Profile Cascade for Separating Tungsten Isotopes [4]

i	M_i	N_i^F	N_i^P	N_i^W
1	180	0,0014	10^{-9}	0,0028
2	182	0,2646	0,0009	0,5363
3	183	0,1440	0,0238	0,2678
4	184	0,3060	0,4180	0,1906
5	186	0,2840	0,5573	0,0025

Substituting (9) into (6) and (7), and taking (11) into account, we find

$$\chi_i(l) = \frac{PN_i^P}{Q_i}(1 - e^{-Q_i l}); \tag{12}$$

$$L(l) = P\sum_{j=1}^{m}\frac{N_j^P}{Q_j}(1 - e^{-Q_j l}). \tag{13}$$

Equations (12) and (13) give the distribution of concentrations and flux in the sampling part of the Q-cascade.

Analogous equations can be written down for the dumping part:

$$\chi_i(l) = \frac{WN_i^W}{Q_i}(e^{Q_i l} - 1); \tag{14}$$

$$L(l) = W\sum_{j=1}^{m}\frac{N_j^W}{Q_j}(e^{Q_j l} - 1), \tag{15}$$

where W is the flux at the dumping part, N_i^W is the concentration of the i-th isotope there, and $l = s^W - s$.

We can use Eqs. (12)-(15) and (8) to express the concentrations N_i^P and N_i^W at the sampling and dumping points, respectively, in terms of the concentration N_i^f at the supply point:

$$N_i^P = \frac{Q_i N_i^f}{1 - e^{-Q_i s^P}} \Bigg/ \sum_{j=1}^{m}\frac{Q_j N_j^f}{1 - e^{-Q_j s^P}}; \tag{16}$$

$$N_i^W = \frac{Q_i N_i^f}{e^{Q_i s^W} - 1} \Bigg/ \sum_{j=1}^{m}\frac{Q_j N_j^f}{e^{Q_j s^W} - 1}. \tag{17}$$

It should be emphasized that the concentrations N_i^f at the supply point are in general not equal to the concentrations N^F in the supply flux. This equality can hold only if there is no mixing of concentrations in the supply.

Using the mass-balance equations

$$\left.\begin{aligned} PN_i^P + WN_i^W &= FN_i^F; \\ P + W &= F, \end{aligned}\right\} \tag{18}$$

we can eliminate N_i^f from Eqs. (16) and (17) and express N_i^P and N_i^W in terms of the concentrations N_i^F in the supply flux:

$$N_i^P = \frac{1 - e^{Q_i s^W}}{e^{-Q_i s^P} - e^{Q_i s^W}} N_i^F \Bigg/ \sum_{j=1}^{m}\frac{1 - e^{Q_j s^W}}{e^{-Q_j s^P} - e^{Q_j s^W}} N_j^F; \tag{19}$$

$$N_i^W = \frac{e^{-Q_i s^P} - 1}{e^{-Q_i s^P} - e^{Q_i s^W}} N_i^F \Bigg/ \sum_{j=1}^{m}\frac{e^{-Q_j s^P} - 1}{e^{-Q_j s^P} - e^{Q_j s^W}} N_j^F. \tag{20}$$

Equations (19) and (20) show that Q-cascades can concentrate isotopes of a certain part of the isotope spectrum with suitable choice of Q_i. This follows from the following arguments. We assume for definiteness that $Q_i > 0$ for the i-th isotope. In addition, it is natural to assume that we are dealing with long cascades,

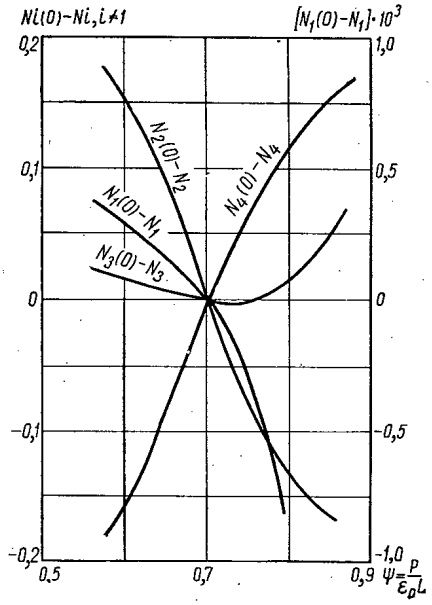

Fig. 4. Dependence of the boundary concentration N_i in the section of a rectangular-stepped cascade as a function of $P/\varepsilon_0 L$ [$N_i(0)$ is the concentration of the i-th component at a suitable point in the continuous-profile cascade].

for which s^P and s^W are large. In evaluating the separation effect, we make a sharp distinction between the isotopes for which Q_j is greater and less than zero.

For $Q_j > 0$, and assuming that the denominators in these equations are the same, we find from (19) without difficulty the following estimates:

$$\frac{N_i^P}{N_j^P} \approx \frac{N_i^F}{N_j^F}. \tag{21}$$

Analogously, if $Q_i < 0$, we find from (19) that

$$\frac{N_i^P}{N_j^P} \gg \frac{N_i^F}{N_j^F}. \tag{22}$$

For the depleted part of the cascade, analogous estimates are found for $Q_i < 0$.

If it is required that a certain intermediate isotope with a given number i is to be separated at the sampling point, we assume Q_i is given by

$$Q_i = k\varepsilon_{i,\,i+1} \approx k\varepsilon_0 (M_{i+1} - M_i), \tag{23}$$

where k is some quantity whose value is arbitrarily assumed, for the time being, to lie in the interval $0 < k < 1$; ε_0 is the enrichment factor for a pair of isotopes differing by unit mass; and M_i is the molecular weight of the i-th component. Then, according to (21) and (10), the concentrations of all isotopes for which $j < i$ will increase during the separation in the same ratio as the concentration of the i-th isotope. The concentrations of all isotopes with $j > i$ will decrease sharply.

It should be noted that the Q-cascades can separate all isotopes of a given element into two groups; in the first group the concentrations of all the isotopes increase simultaneously, while in the second group they all decrease sharply.

Design of cascades of this type has shown that k should be chosen equal to one-half for the least net flux ΣL.

It immediately follows that the concentration of an intermediate isotope at a sampling point cannot be increased without limit in a single Q-cascade, since the net concentration of the enriched isotopes must not exceed unity.

Two cascades can be used to solve the problem of producing an intermediate isotope of any practical purity. The first cascade would separate the group of isotopes in which the desired intermediate component is an extreme member, while the second cascade would eliminate the other members of this group.

It should be noted that the use of the so-called M*-cascades, found on the basis of slightly different arguments but leading to analogous results, was proposed in [4] to separate the intermediate isotopes. It should again be emphasized that Q-cascades are not ideal cascades, since the concentrations are mixed in them at the input; therefore, their efficiency should be compared with a certain "standard" cascade without such mixing. The introduction of a standard cascade was discussed in [5].

In this paper we consider another problem of practical importance: is it possible, having a continuous-profile cascade, in particular a Q-cascade, designed for given parameters, to replace it by a cascade consisting of rectangular sections, i.e., a rectangular-stepped cascade in such a manner that the output concentrations are the same? The possibility of this replacement is not obvious, since the effect of a disruption of the theoretical profile on the various components of the mixture is generally not the same. System (1) was solved analytically for the sections of a rectangular-stepped cascade with L = const in [3, 6]. For the computer design of a real cascade, however, it would be better to carry out a direct numerical integration of system (1).

Let us formulate the problem of designing a rectangular-stepped cascade in the following manner: we are to find the parameters of the cascade corresponding to a Q-cascade in output concentrations and having a specified efficiency.* The unknown parameters of the cascade are the number of sections, the flux L, and the number of steps in each section.

In contrast with the case of a two-component rectangular-stepped cascade, in which the specified concentration at the sampling point can always be arranged, when one changes the flux (i.e., one parameter) in a multicomponent cascade, one must find $m-1$ specified concentrations. However, analysis of the design of several rectangular-stepped cascades has shown that any part of a continuous-profile cascade can be replaced by a section of constant width with properly chosen flux, while all the component concentrations at the ends of the sections are held constant.

According to this result, the problem posed – the replacement of a continuous-profile cascade by a rectangular-stepped cascade with the same output parameters – can always be solved, and the specified efficiency can be achieved with a suitable choice of the number of sections.

The calculation is carried out in the following order.

1. A continuous-profile cascade is designed for the given parameters. This could be, in particular, a Q-cascade, but it could be any other type of continuous-profile cascade.

2. The number of sections is estimated on the basis of the required efficiency, and the continuous-profile cascade is broken up into parts. To fix the boundary of the section at this boundary, the concentration of one of the isotopes is set equal to the corresponding concentration in the continuous-profile cascade. That isotope whose concentration changes monotonically along the cascade is recommended for use to fix the boundary.

3. A certain initial flux is specified in each section in correspondence with the flux distribution in the continuous-profile cascade, and the concentrations of the other mixture components at the junctions are found. By varying the flux in each section, all the concentrations at the junction are made equal to the concentrations in the continuous-profile cascade, and the corresponding number of steps in each section is found.

4. Then the efficiency is determined:

$$\eta = \frac{\sum_{fl} L_{CPC}}{\sum_{fl} L_{RSC}}.$$

5. If the efficiency is not equal to the specified efficiency, the calculation is repeated with a corrected number of sections.

The use of this design procedure has been checked for several isotope mixtures. The calculations were carried out on an M-20 computer by a standard program for solving a system of differential equations by the Runge–Kutta method with automatic choice of step.

As an example, we show here the results of the design of a rectangular-stepped cascade modeling a continuous-profile cascade for separating tungsten isotopes (in the form of the gaseous compound WF_6); the external parameters of the continuous-profile cascade are shown in Table 1. The design of this cascade was described in [4]. Figures 1-3 show designs for modeling rectangular-stepped cascades with two, four, and six sections of constant width (the dashed lines in the figures show the flux distribution in the corresponding continuous-profile cascade). The output concentrations in all three cases are essentially equal to those at the output of the continuous-profile cascade.

Figure 4 illustrates the possibility of replacing a part of a continuous-profile cascade by sections of a rectangular-stepped cascade. The differences between the boundary concentrations of the isotopes in this part of the continuous-profile cascade are seen to simultaneously tend toward zero at the same L value (the quantity $P/\varepsilon_0 L$ is plotted in this figure).

It has thus been shown that by choosing the number sections properly, one can obtain practically any efficiency.

*By "efficiency" here we mean the ratio of the total flux of the Q-cascade (continuous-profile cascade) to the total flux of the corresponding rectangular-stepped cascade.

LITERATURE CITED

1. E. Schumacher and L. Clusius, Helv. Chim. Acta., 36, 949 (1953).
2. J. Meinrenken, Z. Naturforsch., A, 23, No. 2 (1963).
3. R. Ya. Kucherov and V. P. Minenko, Atomnaya Énergiya, 19, 360 (1965).
4. S. Levin, J. Chim. Phys. et Phys. Chim. Biol., 60, Nos. 1-2 (1963).
5. N. A. Kolokol'tsov et al., Atomnaya Énergiya, 29, 128 (1970).
6. A. Narten, Z. Naturforsch. A., 20a, No. 5 (1965).

STORAGE OF MULTIPLY-CHARGED IONS IN A RELATIVISTIC ELECTRON BUNCH

M. L. Iovnovich and M.M. Fiks

UDC 622.039.521:621.039.55

The method of collective ion acceleration proposed in [1] is being intensively developed at the present time. The possibility of obtaining stable electron–ion bunches is the basis for this method. Under certain conditions, the lifetime of the bunch is sufficient for effective acceleration of the bunch as a unit. During production of a bunch and during acceleration, the ions are confined within the bunch by the electron space charge. Since the translational velocity of the ions and electrons is identical, the ion energy is greater than the electron energy by a factor $MA/m\gamma$, where m and M are respectively the rest masses of the electron and nucleon; A is the ion mass number, and γ is the electron relativistic factor in the bunch at rest. The acceleration of ionized heavy atoms to high energies is therefore possible [2, 3].

The production of a two-component bunch takes place in the following manner. A thin ring of relativistic electrons is first formed in an external magnetic field. At this stage, there are practically no ions in the bunch; their storage occurs after the electron ring is essentially formed. Ion storage has been discussed previously [2, 3]. This paper considers the storage of multiply-charged ions of heavy atoms in a thin electron ring with major radius R and minor radius a.

Storage of Ions of a Monatomic Gas in a Relativistic Electron Bunch

Let neutral atoms with sufficiently small kinetic energy enter a bunch of relativistic electrons; as a result of collisions with the latter, the atoms become ionized.

At the same time, a change takes place in the potential energy of an ion which is within the field of the electronic space charge. This change in potential energy, which arises from the increased charge of the heavy particle, is much larger on the average than the kinetic energy transferred to the particle by collision. Therefore the majority of ions formed will be captured in the potential well of the electron ring.

During subsequent collisions with electrons, the charge of ions confined within the ring will increase. The probability of multiple ionization, where the charge of particles is increased by more than unity in a single interaction, is considerably less than that for single ionization. We shall therefore consider ionization to be a stepwise process, namely: particles with charge Z are formed from ions with charge Z – 1. In addition, it is reasonable to neglect recombination between relativistic electrons and ions of all charge states.

The variation of the concentration n_0 of neutral atoms averaged over the bunch per unit time is given by the expression [4]

$$\dot{n}_0 = -\lambda_i n_0 + \lambda_a (n_a - n_0);$$
$$\lambda_i = n_e c \sigma_0; \quad \lambda_a = \frac{S\bar{v}}{V}, \tag{1}$$

where n_a is the neutral atom concentration in the neighborhood of the bunch; n_e and c are respectively the concentration and velocity of the electrons in the ring; σ_0 is the cross section for ionization of a neutral atom by an electron; S is the area of the surface through which the atoms penetrate into the bunch; $\bar{v}$ is the average value of the neutral atom velocity component normal to the bunch surface, and V is the bunch volume.

Translated from Atomnaya Énergiya, Vol. 29, No. 6, pp. 429-433, December, 1970. Original article submitted January 4, 1970.

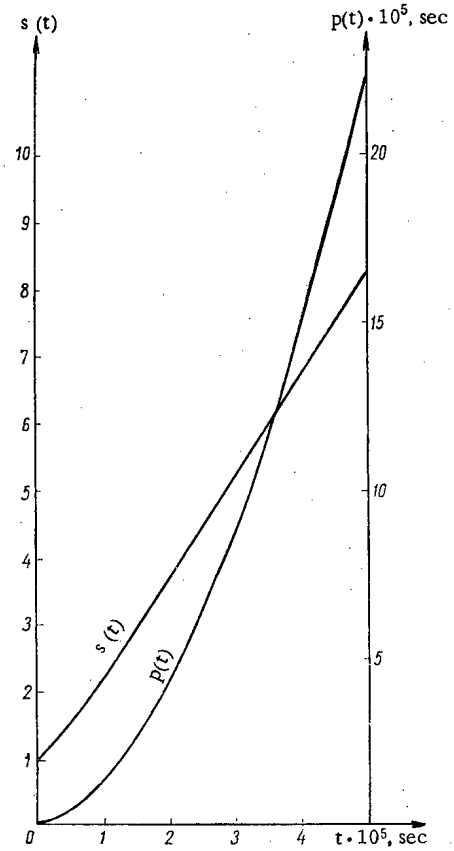

Fig. 1. Xenon storage in an electron bunch (atomic beam with $v_a = 4.76 \cdot 10^4$ cm/sec, $n_e = 10^{14}$ cm^{-3}, $a = 0.1$ cm, and $N_e = 10^{14}$).

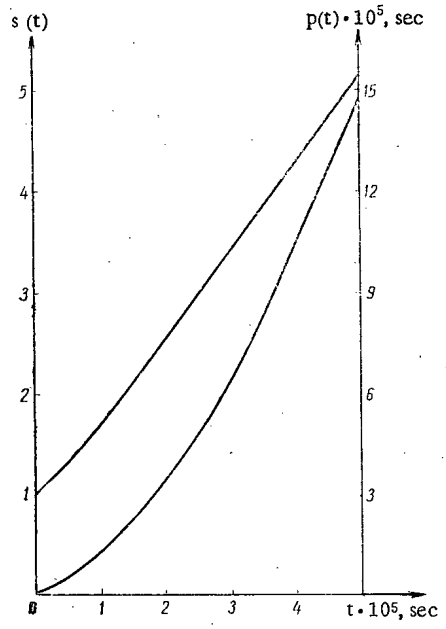

Fig. 2. Xe_{54}^{131} storage in an electron bunch (residual gas with I = 300°K, $v_T = 2.38 \cdot 10^4$ cm/sec, $n_e = 10^{14}$ cm^{-3}, $a = 0.1$ cm, and $N_e = 10^{14}$).

According to Eq. (1), the variation of neutral particle concentration in the bunch results from ionization by electrons and from the difference in the fluxes associated with difference in atom concentrations inside and outside the bunch. Depending on the method chosen for feeding atoms into the vacuum chamber in which the electron ring is formed, the concentration of neutral particles in the neighborhood of the bunch is given either by the density of the flux incident on the surface of the ring or by the partial pressure of the corresponding gas in the vacuum chamber. Let a thin ring of electrons intersect a flux of atoms at a velocity v_a directed along the axis of the ring. The average value of the velocity component normal to the surface of the bunch is then $\bar{v} = (2/\pi)v_a$, the area $S = 2\pi^2 Ra$, and hence $\lambda_a = (2/\pi)(v_a/a)$. If atoms of residual gas enter the ring and their thermal velocity is v_T, then [4] $\bar{v} = v_T/4$ and $\lambda_a = (v_T/a)/2$.

We write Eq. (1) in the following form:

$$\dot{n}_0 + \lambda_0 n_0 = \lambda_a n_a;$$
$$\lambda_0 = \lambda_i + \lambda_a. \tag{1a}$$

The time variation of the mean concentration n_1 of singly ionized atoms is described by the equation

$$\dot{n}_1 + \lambda_1 n_1 = \lambda_i n_0; \tag{2}$$

the equation for the concentration n_Z of ions with charge $Z > 1$ is

$$\dot{n}_Z + \lambda_Z n_Z = \lambda_{Z-1} n_{Z-1};$$
$$\lambda_Z = n_e c \sigma_Z, \tag{3}$$

where σ_Z is the ionization cross section for an ion with charge Z in a collision with an electron where $\lambda_{Z_0} = 0$ (Z_0 is the atomic number). Hence

$$\dot{n}_{Z_0} = \lambda_{Z_0-1} n_{Z_0-1}. \tag{4}$$

In the system of Eqs. (1a)-(4), no consideration is given to collisions between heavy particles which lead in particular, to ionization and charge exchange. The ion contribution in these processes is determined by the ratio of the characteristic collision times, which is $n_i \sigma_i v_i / n_e \sigma_e c$. The average velocity of an ion with

mass number A and charge Z undergoing oscillations in the potential well created by the electron space charge is $v_i = (Z/A)^{1/2}v_p$; the collison cross section [5] $\sigma_2 = Z^2\sigma_p$, where v_p and σ_p are respectively the average velocity and cross section for a proton. The proton velocity v_p in a bunch is $\approx 10^{-2}c$, and the cross section $\sigma_p \approx 10^3\sigma_e$. Consequently, if the ratio of the number of electrons and ions is

$$\frac{n_i}{n_e} \ll \frac{A^{1/2}}{10Z^{5/2}}, \tag{5}$$

the ion contribution can be neglected.

Assume that at t = 0, there are in the bunch only neutral atoms, $n_Z(0) = n_a\delta_{0Z}$. We shall write the solution of the equation system (1a)-(4) as the sum of a particular solution of the inhomogeneous system and the general solution of the homogeneous system:

$$\begin{gathered} n_0 = n_a\left(\frac{\lambda_a}{\lambda_0} + y_0\right); \\ n_Z = n_a\frac{\lambda_i}{\lambda_a}\left(\frac{\lambda_a}{\lambda_Z} + y_Z\right), \quad 1 \ll Z \ll Z_0 - 1; \\ n_{Z_0} = n_a\frac{\lambda_i}{\lambda_0}(\lambda_a t + y_{Z_0}), \end{gathered} \tag{6}$$

where the particular solution is represented by the first terms and the function y_Z is determined by the homogeneous system

$$\begin{gathered} \dot{y}_0 + \lambda_0 y_0 = 0; \\ \dot{y}_Z + \lambda_Z y_Z = \lambda_{Z-1}y_{Z-1}; \\ \dot{y}_{Z_0} = \lambda_{Z_0-1}y_{Z_0-1} \end{gathered} \tag{7}$$

with the initial conditions $y_0(0) = \lambda_i/\lambda_0$; $y_Z(0) = -(\lambda_a/\lambda_Z)$; $y_{Z_0}(0) = 0$.

An equation system similar to (7) describes decay in a family of radioactive elements [6]. Using the known solutions, we obtain expressions for the concentration of ions with a charge Z varying from one to $Z_0 - 1$:

$$n_Z = n_a\frac{\lambda_i}{\lambda_0}\left[\lambda_a\left(\frac{1}{\lambda_Z} - \sum_{k=1}^{Z}\frac{S_{Zk}}{\lambda_k}\right) + \frac{\lambda_i}{\lambda_0}S_{Z_0}\right] \tag{8}$$

and the concentration of completely ionized atoms

$$n_{Z_0} = n_a\frac{\lambda_i}{\lambda_0}\left[\lambda_a\left(t - \sum_{k=1}^{Z_0-1}\frac{S_{Z_0k}}{\lambda_k}\right) + \frac{\lambda_i}{\lambda_0}S_{Z_00}\right]. \tag{9}$$

Here, for $Z \ll Z_0 - 1$

$$S_{Zk} = \prod_{m=k}^{Z-1}\lambda_m \sum_{s=k}^{Z}\frac{e^{-\lambda_s t}}{\prod_{n=k}^{Z}\lambda_{ns}}; \quad S_{ZZ} = e^{-\lambda_Z t}, \tag{10a}$$

$$0 \ll k \ll Z - 1;$$

and for $Z = Z_0$

$$S_{Z_0k} = 1 - \prod_{m=k}^{Z_0-1}\lambda_m \sum_{s=k}^{Z_0-1}\frac{e^{-\lambda_s t}}{\prod_{n=k}^{Z_0-1}\lambda_{ns}}, \quad 0 \ll k \ll Z_0 - 1; \tag{10b}$$

$$\lambda_{ns} = \lambda_n - \lambda_s; \quad \lambda_{ss} = 1.$$

The concentrations of neutral and singly ionized atoms are respectively:

$$n_0 = n_a\left(\frac{\lambda_a}{\lambda_0} + \frac{\lambda_i}{\lambda_0}e^{-\lambda_0 t}\right); \tag{11a}$$

$$n_1 = n_a\frac{\lambda_i}{\lambda_0}\left[\frac{\lambda_a}{\lambda_1} - \frac{\lambda_i}{\lambda_{01}}e^{-\lambda_0 t} - \frac{\lambda_0(\lambda_a - \lambda_1)}{\lambda_1\lambda_{01}}e^{-\lambda_1 t}\right]. \tag{11b}$$

Summing the system (1a)-(4), we obtain an equation which the concentration of all heavy particles (atoms and ions), $n = \sum_{Z=0}^{Z_0} n_Z$, satisfies:

$$\dot{n} = \lambda_a (n_a - n_0). \tag{12}$$

In the case $n(0) = n_a$, its solution takes the form

$$s(t) \equiv \frac{n}{n_0} = 1 + \frac{\lambda_a \lambda_i}{\lambda_0} t - \frac{\lambda_a \lambda_i}{\lambda_0^2}(1 - e^{-\lambda_0 t}). \tag{13}$$

We also give the value of the quantity $p = 1/n_a \int_0^t n(t')dt'$:

$$p(t) = \left(1 - \frac{\lambda_a \lambda_i}{\lambda_0^2}\right) t + \frac{\lambda_a \lambda_i}{2\lambda_0} t^2 + \frac{\lambda_a \lambda_i}{\lambda_0^3}(1 - e^{-\lambda_0 t}). \tag{14}$$

If the ion storage time satisfies the condition $\lambda_0 t \gg 1$, $\lambda_1 t \gg 1$, . . . , $\lambda_Z t \gg 1$, the concentration of ions with the corresponding charge tends toward a limiting equilibrium value

$$n_Z = n_a \frac{\lambda_a}{\lambda_0} \cdot \frac{\sigma_0}{\sigma_Z}; \quad 0 \ll Z \ll Z_0 - 1, \tag{15}$$

which, like the time to reach this value, increases with an increase in ion charge. At the same time, the total concentration n of the heavy particles rises in proportion to the storage time.

The storage of xenon is shown in Figs. 1 and 2 (function s(t)). In one case (see Fig. 1), the neutral atoms reach the bunch from a directed flow with a velocity ~1.4 M, i.e., $v_a \approx 4.8 \cdot 10^4$ cm/sec; in the other case (see Fig. 2), xenon storage is accomplished from the residual gas in the vacuum chamber at a temperature T = 300°K, i.e., $v_T = 2.4 \cdot 10^4$ cm/sec. The final concentration of heavy particles can be increased by decreasing the time for filling the volume of the ring with neutral atoms. If $\lambda_a \gg \lambda_i$, the quantity λ_a/λ_0 should be replaced everywhere by its maximum value, which is unity.

Electron Loss during Ion Storage

The probability of electron scattering by atoms and ions increases as the concentration of heavy particles increases, leading to a limitation on the final value of the heavy particle concentration n. Since the amplitude of electron betatron oscillations is increased by scattering, one can assume that the electron will escape from the boundary of the circular beam if the square of this amplitude becomes larger than the square of the minor radius of the ring a^2. The average value over a betatron oscillation period of the square of the amplitude in the case of elastic scattering at a small angle ϑ is determined by the expression [7]

$$\overline{u^2} = u_0^2 + \frac{\vartheta^2 R^2}{2n_B}, \tag{16}$$

where u_0^2 is the square of the amplitude immediately before scattering and n_B is the magnetic field index.

An electron can be knocked out of the beam both by single collisions with heavy nuclei (large-angle scattering; bremsstrahlung emission in an atomic nucleus) and by small, frequently repeated changes in its trajectory.

Electron Loss through Single Collisions. Equation (16) indicates that an electron is removed from the beam as the result of a single scattering at an angle

$$\vartheta \geqslant \vartheta_0 = \sqrt{2n_B \frac{(a^2 - u_0^2)}{R^2}}. \tag{17}$$

Since scattering at an angle $\vartheta > \vartheta_0$ corresponds to impact parameters less than the atomic radius, it can be assumed that the scattering occurs in the atomic nucleus with a cross section which is given by the Rutherford scattering law. In this case, the electron scattering probability per unit time for an angle $\vartheta \geq \vartheta_0$ is

$$P(u_0^2, t) = cn(t) \int_{\vartheta_0}^{\pi} \sigma(\vartheta) d\vartheta = 2\pi \frac{Z_0^2}{\gamma^2} \cdot \frac{1}{n_B} r_e^2 cn(t) \frac{R^2}{a^2 - u_0^2}, \tag{18}$$

where $r_e = e^2/mc^2$ is the classical radius of the electron.

The relative electron loss because of single scattering is given by [7]

$$q_0 = 1 - \int_0^{a^2} du_0^2 F(u_0^2) \exp\left[- \int_0^t P(u_0^2, t')\, dt' \right], \tag{19}$$

where $F(u_0^2)$ is the electron distribution function at time t = 0 normalized to unity.

If $F = \delta(u_0^2)$, the relative loss can be expressed as

$$q_0 = 1 - \exp\left[-2\pi \frac{Z_0^2}{\gamma^2} \cdot \frac{1}{n_B} \cdot \frac{R^2}{a^2} r_e^2 c n_a p \right]. \tag{20}$$

Inelastic electron scattering can be taken into account if Z_0^2 in Eq. (20) is replaced by the number of electrons in the ionized atom, which is $Z_0 - Z$. It is obvious that the contribution from inelastic collisions of heavy atoms to the amount of loss will be insignificant.

A three-body interaction occurs during bremsstrahlung emission. Furthermore, electron losses from the ring occur even with the emission of soft γ-rays since the transfer of a large amount of momentum to the nucleus is possible. The amount of relative electron loss q_r can be estimated by means of the expression for the total cross section for bremsstrahlung emission, which is, for heavy atoms and for $1 \ll \gamma < 137 Z_0^{-1/3}$ [5],

$$\sigma_r = \frac{4Z_0^2}{137} r_e^2 (\ln 2\gamma - 1/3). \tag{21}$$

Hence

$$q_r = 1 - \exp[-\sigma_r c n_a p]. \tag{22}$$

Electron Loss through Multiple Scattering. From theoretical considerations of particle loss in accelerators [7], it follows that the relative electron loss produced by multiple scattering in atoms is determined by

$$\tau = \frac{c}{2} \int_0^t \frac{R^2}{n_B a^2} \cdot \frac{d\overline{\vartheta^2}}{dx}\, dt', \tag{23}$$

where the mean value of the square of the scattering angle per unit path length for an ultrarelativistic electron is [5]:

$$\frac{d\overline{\vartheta^2}}{dx} = \frac{8\pi}{\gamma^2} r_e^2 \sum_{Z=0}^{Z_0} Z^2 n_Z \ln \frac{\vartheta_{\max}}{\vartheta_{\min}}. \tag{24}$$

Equation (24) was obtained under the assumption the impact parameter in multiple scattering is considerably greater than atomic dimensions and the scattering occurs in ions with charge Z. We shall assume the maximum angle for multiple scattering is equal to the minimum angle for single scattering:

$$\vartheta_{\max} = \sqrt{2n_B} \frac{a}{R}. \tag{25}$$

The minimum scattering angle is determined by the maximum impact parameter which corresponds to the minor radius of the ring since the Debye screening radius is considerably greater than the minor radius of the ring in that case:

$$\vartheta_{\min} \simeq \frac{2Z}{\gamma} \cdot \frac{r_e}{a}. \tag{26}$$

As a result, we obtain

$$\tau = \frac{4\pi}{\gamma^2} \cdot \frac{1}{n_B} \cdot \frac{R^2}{a^2} r_e^2 c \sum_{Z=0}^{Z_0} Z^2 + \int_0^t n_Z(t')\, dt' \ln \sqrt{\frac{n_B}{2}} \cdot \frac{\gamma}{Z} \cdot \frac{a^2}{R r_e}. \tag{27}$$

To estimate the loss, one can make use of the fact that τ is always less than

$$4\pi \frac{Z_0^2}{\gamma^2} \cdot \frac{1}{n_B} \cdot \frac{R^2}{a^2} r_e^2 c n_a p L, \tag{28}$$

where L is the average value of the logarithm in Eq. (27).

By determining the value of τ and knowing the initial electron distribution with respect to betatron oscillation amplitudes, one can find the electron loss produced by multiple scattering [7]. A comparison of the loss equations shows that bremsstrahlung emission leads to considerably smaller losses than scattering. Obviously, the main source of loss is multiple elastic scattering of electrons at small angles. If an acceptable value for electron loss during the storage period is assumed to be 5-10%, the total concentration n of stored heavy particles (xenon) is bounded by the value $n/n_e \approx 10^{-3}$.

LITERATURE CITED

1. V. I. Veksler et al., Atomnaya Énergiya, 24, 317 (1968).
2. M. L. Iovnovich et al., JINR Preprint P9-4257, Dubna (1969).
3. Symposium on Electron Ring Accelerators, UCRL-18103, Berkeley (1968).
4. A. Simon, Phys. Fluids, 1, 495, (1958).
5. Experimental Nuclear Physics (E. Segre, editor) [Russian translation], Vol. 1, IL, Moscow (1955).
6. S. E. Bresler, Radioactive Elements [in Russian], Gostekhteorizdat, Moscow (1957).
7. A. A. Kolomenskii and A. N. Lebedev, Theory of Cyclic Accelerators [in Russian], Fizmatgiz, Moscow (1962).

ENERGY BALANCE IN THE PLASMA IN APPARATUSES OF THE "TOKAMAK" TYPE

Yu. N. Dnestrovskii and D. P. Kostomarov

UDC 621.039.626

In recent years a large number of theoretical papers has appeared on calculating the transport coefficients in toroidal systems on the basis of the classical mechanism of Coulomb collisions [1-4]. At the same time numerous experiments on "Tokamak" apparatuses indicate the absence of large-scale turbulent oscillations of the plasma under conditions for which hydrodynamic instabilities are suppressed [5, 6]. In this connection it is of great interest to calculate the energy balance of the plasma in such apparatuses on the assumption that the losses are of a classical character, and to compare the results of this calculation with experimental data. In the present paper results are given of a numerical solution of the thermal conductivity equations for ions and electrons, and the equations for the magnetic field of the current in a plasma pinch with allowance for the classical transport coefficients. These calculations allow the dependence of the ion and electron temperatures and the energy lifetime on the geometric dimensions of the plasma pinch, the plasma density, the longitudinal magnetic field intensity, and the magnitude of the discharge current to be investigated within the framework of the assumption made concerning the character of the losses. The results obtained are in good agreement with available experimental data [5-8]. This indicates the possibility of explaining the energy balance of the plasma in specified operating modes within the framework of classical concepts, and substantiates the conclusion of the theory to the effect that the confined particles play a special role in the transport processes.

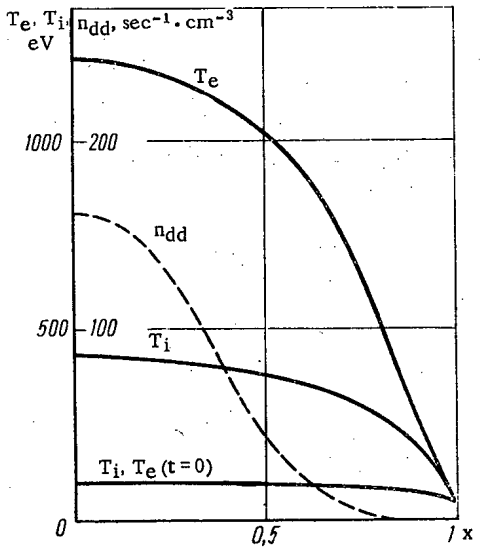

Fig. 1

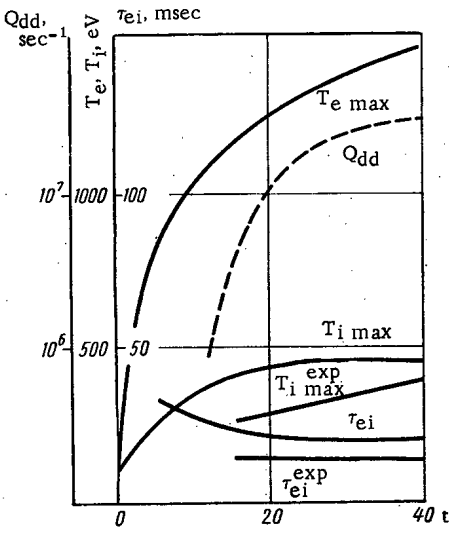

Fig. 2

Fig. 1. The dependence of T_e, T_i, and n_{dd} on the space coordinate $x = r/a$ for $t = 0$ and $t = 18$ msec ($R = 100$, $a = 12$, $H = 38$, $I = 110$, $N = 4$, $\xi_p = 0.3$, $\xi_d = 0.7$, $\gamma = 1$).

Fig. 2. The dependence of $T_{e\,max}$, $T_{i\,max}$, τ_{ei}, and Q_{dd} on the times ($R = 100$, $a = 12$, $H = 38$, $I = 110$, $N = 4$, $\xi_p = 0.3$, $\xi_d = 0.7$, $\gamma = 1$).

Translated from Atomnaya Énergiya, Vol. 29, No. 6, pp. 434-438, December, 1970. Original article submitted April 2, 1970.

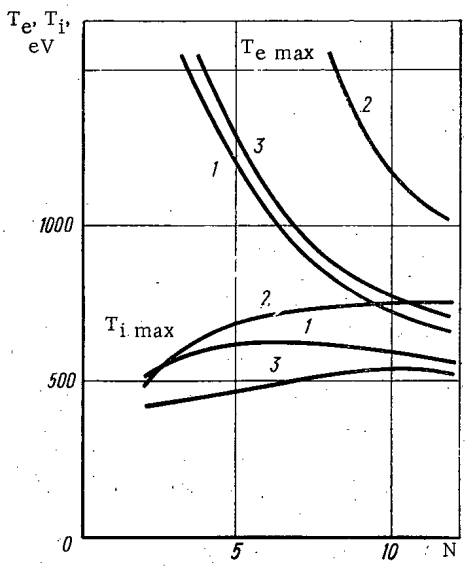

Fig. 3

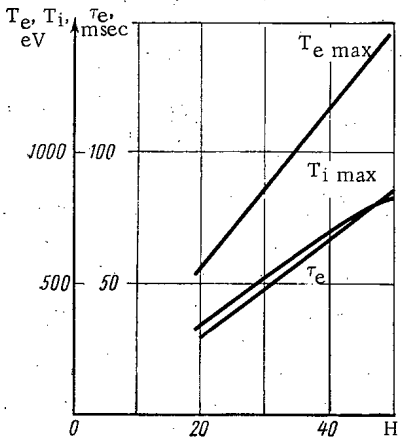

Fig. 4

Fig. 3. Dependence of the steady-state values of $T_{e\,max}$ and $T_{i\,max}$ on the density N for three versions (R = 100, a = 12, H = 38, I = 110). 1) $\xi_p = 1$, $\gamma = 1$; 2) $\xi_p = 1$, $\gamma = 3$; 3) $\xi_p = 0.3$, $\xi_d = 0.7$, $\gamma = 1$.

Fig. 4. Dependence of the steady-state values of $T_{e\,max}$, $T_{i\,max}$, and τ_e on the longitudinal magnetic field H[q(1, t) = 2.2 = const, R = 100, a = 12, N = 6, γ = 1, and I = 3.28H].

The Basic Equations

In formulating the equations which describe the energy balance of a toroidal plasma pinch in systems of the "Tokamak" type in the case of classical losses, we shall consider the fact that for such systems the diffusion lifetime is much longer than the energy lifetime [1-4]. This allows a) neglect of plasma diffusion in comparison with thermal conductivity, and b) the assumption that the plasma density is independent of time. As a result the system of equations describing the variation of the magnetic field of the current and the energy of the plasma [9] takes the form:

$$\frac{\partial \mu}{\partial t} = A\gamma \frac{1}{x} \cdot \frac{\partial}{\partial x}\left[\frac{1}{T_e^{3/2}} \cdot \frac{1}{x} \cdot \frac{\partial}{\partial x}(x^2\mu)\right]; \tag{1}$$

$$\frac{\partial T_e}{\partial t} = \frac{1}{nx} \cdot \frac{\partial}{\partial x}\left(xn\chi_e \frac{\partial T_e}{\partial x}\right) - C\frac{n}{T_e^{3/2}}(T_e - T_i) + B\gamma \frac{1}{nT_e^{3/2}}\left[\frac{1}{x} \cdot \frac{\partial}{\partial x}(x^2\mu)\right]^2 - Q_r; \tag{2}$$

$$\left.\begin{aligned} \frac{\partial T_i}{\partial t} &= \frac{1}{nx} \cdot \frac{\partial}{\partial x}\left(xn\chi_i \frac{\partial T_i}{\partial x}\right) \\ &\quad + C\frac{n}{T_e^{3/2}}(T_e - T_i). \end{aligned}\right\} \tag{3}$$

Here $\mu(x, t) = 1/q = RH_V/rH$ is a function which is proportional to the magnetic field H_V of the current; H is the longitudinal magnetic field $T_e(x, t)$ and $T_i(x, t)$ are the electron and ion temperatures; n(x) is the density of the plasma; $x = r/a$; r is the radial space coordinate; R and a are the large and small radii of the plasma torus;

$$A = \frac{6.1 \cdot 10^3}{a^2}; \quad B = \frac{2 \cdot 10^7 H^2}{R^2}; \quad C = \frac{470}{p}; \tag{4}$$

p is the ratio of the reduced mass of the ions in the mixture of hydrogen, deuterium, and tritium to the proton mass. The quantity Q_r in Eq. (2) denotes the possible additional energy losses by electrons. In the calculations the bremsstrahlung losses $Q_r = 7.2 \cdot 10^{-4}\, n\sqrt{T_e}$ were considered. In Eqs. (1)-(3) and in the subsequent equations the time is measured in milliseconds, the temperature in electron-volts, the density in 10^{13} cm^{-3}; R and a in centimeters, and H in kilooersteds.

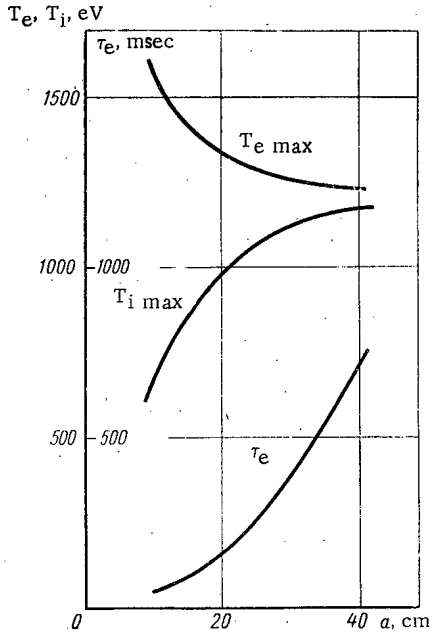

Fig. 5

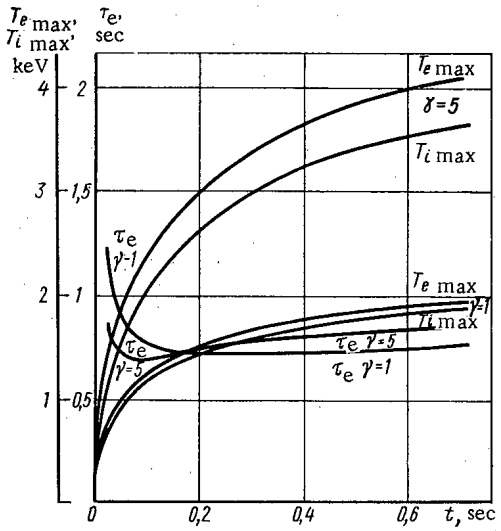

Fig. 6

Fig. 5. Dependence of the steady-state values of $T_{e\,max}$, $T_{i\,max}$, and τ_e on the radius a of the plasma [q(1, t) = 2.2 = const, H = 40, N = 6, R = 7a, I = 12.6a, and $\gamma = 1$].

Fig. 6. The dependence of $T_{e\,max}$, $T_{i\,max}$, and τ_e on time for a hypothetical apparatus for $\gamma = 1$ and $\gamma = 5$ (R = 150, a = 40, H = 50, I = 1000, N = 10, and $\xi_p = 1$).

The coefficients of thermal conductivity χ_e and χ_i of electrons and ions depend in a very complex way on the collison frequency ν and on the other parameters of the plasma in accordance with [2-4]. In the range of low collision frequencies the equations of [3, 4] are valid. If the explicit expressions for the collision frequencies are used and all of the quantities are written in the units given above, then the corresponding equations take the form

$$\chi_j = 300 \frac{F_j n q^2}{a^2 H^2 \sqrt{T_j}} \left(\frac{R}{ax}\right)^{3/2} J(\alpha_j) \quad (\alpha_j \leqslant \alpha_0), \tag{5}$$

where

$$J(\alpha) = 0.3 \int_0^\infty \frac{e^{-z} z^3\, dz}{\sqrt{z+\alpha}} \qquad (J(0) = 1); \tag{6}$$

$$\alpha_j = 420 f_j \frac{R^5 n^2 q^2}{T_j^4 (ax)^3};$$

$$\alpha_0 = 1.25 \left(\frac{q^2}{1+q^2}\right)^2 \left(\frac{R}{ax}\right)^3 \gg 1;$$

$$F_j = \begin{cases} \sqrt{p} & j = i, \\ \frac{5}{43} & j = e \end{cases} \qquad f_j = \begin{cases} 1 & j = i \\ 4 & j = e \end{cases} \tag{7}$$

For $\alpha_j \ll 1$ and $1 \ll \alpha_j < \alpha_0$ one can derive the following asymptotic equations from Eq. (5):

$$\chi_j = 300 \frac{F_j n q^2}{a^2 H^2 \sqrt{T_j}} \left(\frac{R}{ax}\right)^{3/2} \qquad (\alpha_j \ll 1); \tag{8}$$

$$\chi_j = 26 \frac{F_j T_j^{3/2} q}{\sqrt{f_j}\, a^2 H^2 R} \qquad (1 \ll \alpha_j \ll \alpha_0). \tag{9}$$

Finally, for $\alpha_j > \alpha_0$ the following equations in [2] are valid in the range of comparatively high frequencies:

$$\chi_j = 480 \frac{F_j n (1+q^2)}{a^2 H^2 \sqrt{T_j}} \qquad (\alpha_j \gg \alpha_0). \tag{10}$$

The limits of applicability of the equations given above are very sensitive to the parameters of the plasma. Usually, Eqs. (10) are valid for the thermal conductivity coefficients at the initial stage of the discharge while the temperature of the plasma is low. However, as the internal portion of the plasma pinch is heated up, the collision frequencies begin to decrease, and we go over to Eqs. (9); after that we may even reach the range of validity of Eqs. (8). The transition from one branch to the other does not occur simultaneously for the entire pinch. Therefore, in order to calculate the coefficients of thermal conductivity at different points it is necesary to use different equations. All this greatly complicates the problem, making its qualitative investigation difficult and allowing reliable quantitative results to be obtained only by means of numerical methods.

The factor γ is included in the terms of Eqs. (1) and (2), which are connected with the current. This factor allows a phenomenological description to be given of the resistance observed in the experiment. The case $\gamma = 1$ corresponds to the classical plasma resistance given by the Spitzer formula.

The initial and boundary conditions were chosen in the form

$$\mu(x, 0) = \mu_0(2 - x^2); \; T_j(x, 0) = T_{j0}(2 - x^2)\,(j = i, e); \tag{11}$$

$$\mu(1, t) = \mu_0 = 0.2\frac{RI}{a^2H}; \quad T_j(1, t) = T_{j0}\,(j = i, e), \tag{12}$$

where I is the total current in the plasma in kiloamperes. The radial density distribution of the plasma was assumed to be parabolic: $n(x) = N(1 - (1/2)x^2)$.

Equations (1)-(3) with the complementary conditions (11), (12) were integrated on an electronic computer. The time evolution of the electron and ion temperatures were investigated, as well as the dependence of the steady-state values of these temperatures on plasma density, longitudinal magnetic field, total current, and the dimensions of the plasma pinch. The results of the corresponding calculations are described below. In these calculations it was assumed that the total current I was independent of time and was distributed over the pinch cross section according to the parabolic law $f(x, 0) = 2I(1 - x^2)\pi$ at the initial time in accordance with the conditions (11). Thus, in the given series of calculations the problem of current penetration into the plasma during the initial stage of the process corresponding to an increase of the total current with time was not considered. Under these assumptions the function $\mu(x, t)$ and the current density $f(x, t)$ remain practically constant with time. A change in the electron and ion temperatures T_{0e} and T_{0i} on the boundary over fairly wide limits (10 to 100 eV) had a very slight effect on the solution of the problem. As far as the initial temperatures were concerned, they ceased to affect the solution after a time had elapsed which was 4-5 times as short as the energy lifetime.

The Results of the Calculations

As an example, Figs. 1 and 2 show the results of the numerical solution of the problem formulated above for parameter values corresponding to the parameters of the T-3 apparatus at the I. V. Kurchatov Atomic Energy Institute [5-7]. In the calculations it was assumed that

$$\begin{gathered} R = 100, \; a = 12, \; H = 38, \; I = 110, \\ T_{j0} = 50\,(j = i, e). \end{gathered} \tag{13}$$

Since the characteristic time of the process in this case is of the order of several tens of milliseconds, the integration of the system (1)-(3) was carried out till t = 40 msec. During this time T_e, T_i, and τ_e practically reach their steady-state values. The calculations were carried out for purely hydrogen plasma and for a mixture of hydrogen and deuterium having relative concentrations ξ_p and ξ_d ($\xi_p + \xi_d = 1$). In the latter case the yield of neutrons accompanying the d – d reaction was determined.

The energy lifetime τ_e was found according to the equation

$$\tau_e = E\left(Q - \frac{\partial E}{\partial t}\right)^{-1}, \tag{14}$$

where E is the thermal energy of the plasma; Q is the Joule heat released by the current. For purposes of comparison with experiment the energy lifetime $\tau_{ei} = E_i Q_i^{-1}$ of the ions was likewise calculated, where E_i is the energy in the ions, and Q_i is the heat flux from the ions to the wall. The density n_{dd} of the neutron yield and the total flux Q_{dd} of neutrons from the plasma were determined from the equations [10]:

$$\begin{gathered} n_{dd} = \xi_d^2 n^2 T_i^{-2/3} \exp(32 - 188 \cdot T_i^{-1/3}); \\ Q_{dd} = 4\pi^2 R a^2 \int_0^1 n_{dd} x\, dx. \end{gathered} \tag{15}$$

Figure 1 shows the dependences of the ion and electron temperatures of the space coordinate $x = r/a$. The dashed line shows the density n_{dd} of the neutron yield resulting from the d–d reaction. For the chosen value of plasma density the heat exchange between electrons and ions is relatively small, and therefore the "detachment" of the electron temperature from the ion temperature takes place during the heating process.

Figure 2 shows the dependence of $T_{e\,max}$, $T_{i\,max}$, and τ_{ei} on time for the same plasma parameters. The experimental curves for $T_{i\,max}$ and τ_{ei} were obtained on the T-3 apparatus. Good agreement between the results of the theory and experimental data indicates a possible explanation of the energy balance of the plasma in this case within the framework of classical concepts of heat exchange and losses, and substantiates the conclusion of the theory concerning the necessity of considering confined particles in the transport processes. Analogous calculations were carried out for the T-3 apparatus in other operating modes with modified values of the longitudinal magnetic field and total current. The results obtained under these conditions are in good agreement with experimental data.

The curves in Fig. 2 indicate a comparatively rapid establishment of the steady state in apparatuses of this type. In order to clarify the possibilities of ohmic heating of the plasma in such apparatuses the investigation of the dependence of the limiting steady-state values of the quantities $T_{e\,max}$, $T_{i\,max}$, and τ_e on the geometric dimensions of the plasma pinch and such parameters as the plasma density, the magnitude of the longitudinal fields, and the magnitude of the current is of great interest. Certain results of the investigation of these dependences have been presented in Figs. 3-5.

Figure 3 shows the dependence of the steady-state values $T_{e\,max}$ and $T_{i\,max}$ on density for hydrogen plasma and for a mixture of hydrogen and deuterium. The shape of the curves may be interpreted as follows. With increasing plasma density the heat exchange between electrons and ions improves, and due to the fixed total current the fraction of energy released per particle decreases. Both of these factors lead to an abrupt decrease in T_e with increasing N. The ion temperature first increases due to the improvement of heat exchange, and then begins to decrease. This is clearly evident for curves 1 and 3, while for curve 2 the corresponding value of density lies beyond the limits of the diagram. Note that as a whole the ion temperature is very "inert" to a change in the plasma parameters. Whereas the electron temperature in Fig. 3 differs by a factor of 2-3 in different operating modes, the change in ion temperature is 20 to 30%.

Figures 4 and 5 show the dependences of the steady-state values of $T_{e\,max}$, $T_{i\,max}$, and τ_e on the longitudinal magnetic field and the dimensions of the plasma pinch for hydrogen plasma at a constant value of density $N = 6$ and a value of the quantity $q(1, t) = 2.2$. In plotting Fig. 4 the values of the geometric parameters were chosen in accordance with Eq. (13), while the current varied with the magnetic field in accordance with the boundary conditions (12): $I = 3.28H$. Calculations show that in this case $T_{e\,max}$, $T_{i\,max}$, and τ_e increase with increasing H and I according to a practically linear law.

In calculating the curves in Fig. 5 the magnetic field was fixed ($H = 40$), while the current and the large radius R of the torus were varied along with the radius a of the plasma pinch: $I = 12.6a$, $R = 7a$. The shape of the curves in Fig. 5 may be qualitatively interpreted as follows. The linear dependence of I on a is connected with the decrease in current density with increasing a, which leads to a decrease of $T_{e\,max}$. However, since with increasing a the losses via thermal conductivity decrease, it follows that $T_{i\,max}$ (and especially τ_e) increases under these conditions.

Figure 6 is similar to Fig. 2. This figure shows the calculations for a hypothetical large apparatus. The time variations of the quantities $T_{e\,max}$, $T_{i\,max}$, and τ_e are shown for hydrogen plasma ($\xi_p = 1$) having a normal resistance ($\gamma = 1$) and an anomalous resistance ($\gamma = 5$). The characteristic time of the process is equal to 800 msec in this case. The high plasma density provides for good heat exchange between electrons and ions, and as a result the differences in their temperatures are insignificant. The temperature of the ions in the central portion of the plasma pinch reaches 1800 eV $\gamma = 1$, while for $\gamma = 5$ it reaches 3000 eV.

The authors express their deep thanks to Academician L. A. Artsimovich for stating the problem and discussing the results.

LITERATURE CITED

1. D. Pfirsch and A. Schüter, Max Planck Institute, Rep. MPI/Pa/7/62 (1962).
2. V. D. Shafranov, Atomnaya Énergiya, 19, 120 (1965).
3. A. A. Galeev and R. Z. Sagdeev, Zh. Éksperim. i Teor. Fiz., 53, 348 (1967).

4. L. M. Kovryzhnykh, Zh. Éksperim. i Teor. Fiz., 56, 877 (1969).
5. L. A. Artsimovich et al., Report CN-24/B-1 at the Third Conference on Research in the Field of Plasma Physics and Controlled Fusion Reactions [in Russian], Novosibirsk (1968).
6. L. A. Artsimovich et al., Report to the International Conference on Plasma Confinement in Closed Systems [in Russian], Dubna (1959).
7. H. Peacock et al., ibid. [Russian translation].
8. Yu. N. Dnestrovskii and D. P. Kostomarov, ibid. [in Russian].
9. B. B. Kadomtsev, in: Problems of Plasma Theory [in Russian], No. 5, Atomizdat, Moscow, p. 209.
10. L. A. Artsimovich, Controlled Fusion Reactions [in Russian], Fizmatgiz, Moscow (1961).

THERMODYNAMICS OF THE URANIUM – CARBON, URANIUM – NITROGEN, AND PLUTONIUM – CARBON SYSTEMS

V. V. Akhachinskii and S. N. Bashlykov

UDC 621.039.542.3:541.11

The Uranium – Carbon System

Heat Capacity at Low Temperature. Certain results of recent measurements of the low-temperature heat capacity of uranium carbides are presented in Table 1.

The data for U_2C_3 and UC_2 are in very good agreement, but for UC there is a certain difference, evidently caused by the different composition of the samples. In [1, 2], in a measurements of the heat capacity of UC, pieces of cast carbide were used, the carbon content in which only slightly exceeded the stoichiometric; moreover, in [1] the measurements were performed on a well characterized sample, and no correction was introduced for the small excess of bound carbon. In [2], however, a correction was made for the presence of UC_2, but the influence of oxygen, the amount of which in the carbide was rather high (1.9 mole %), was not taken into consideration.

The authors of [4] recommend that the average value from [1, 2] be used for the heat capacity of UC.

The results of a measurement of the heat capacity of UC, U_2C_3, and $UC_{1.94}$ in the interval 5-350°K [1, 4] are presented graphically in Fig. 1 [5].

Heat Capacity and Heat Content at High Temperature. Measurements of the true heat capacity of UC and UC_2, performed in [6] in an adiabatic calorimeter in the interval 373-473°K and in [7] on the determination of C_p of uranium monocarbide in the interval 300-900°K by the nonstationary system method with pulsed heating of the sample with a laser beam, should be considered insufficiently accurate.

The new technique, using pulsed heating (details unknown), was used in [8] to measure the heat capacity of a homogeneous sample of UC in the interval 600-2700°K. The systematic error of the method did not exceed 3-5%.

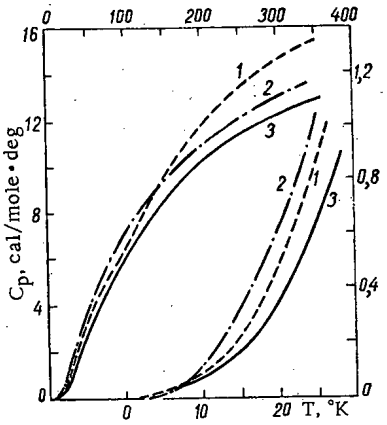

Fig. 1

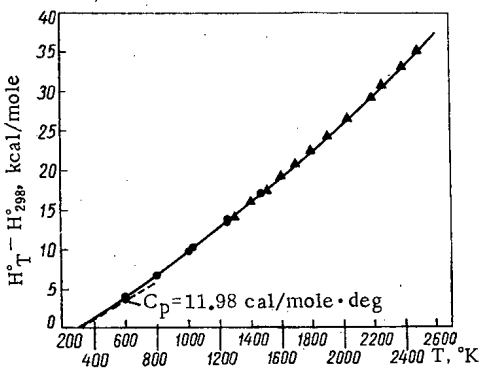

Fig. 2

Fig. 1. Heat capacity of U_2C_3 (1), $UC_{1.94}$ (2), and UC (3) at low temperature.

Fig. 2. Heat content of $UC_{1.0}$ at high temperature: ●) [9]; ▲) [10].

Translated from Atomnaya Énergiya, Vol. 29, No. 6, pp. 439-447, December, 1970. Original article submitted March 6, 1970.

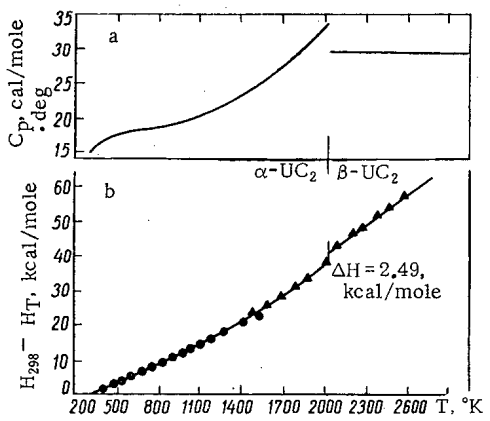

Fig. 3. Heat capacity (a) and heat content (b) of $UC_{1.9}$: ▲) [12]; ●) [13].

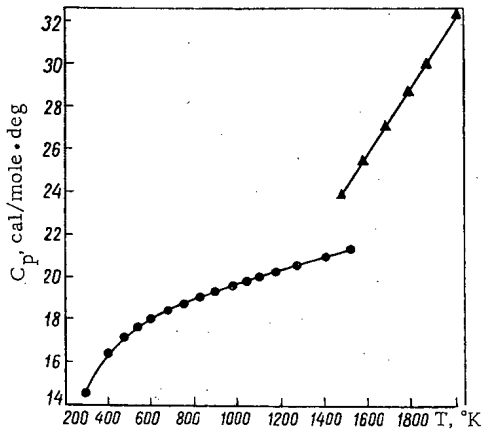

Fig. 4. Heat capacity of UC_2: ●) [13]; ▲) [12].

TABLE 1. Thermal Functions of UC, U_2C_3, and UC_2 at 298°K

Carbide	C_p°, cal/mole·deg	S°, cal/mole·deg	$H^\circ_{298.15} - H^\circ_0$, cal/mole	Presumed composition, mole%	Literature cited
UC	12,11	14,28	2193	$UC_{1,02 \pm 0,01}$	[1]
	11,84	14,03	2159	97,5 UC + 2,5 $UC_{1,9}$	[2]
U_2C_3	25,66	32,93	4829	U_2C_3	[3]
	25,55	32,91	4836	75,3 U_2C_3 + 10,6 UC + 4,1 $UC_{1,9}$ + 9,9 C	[2]
α—UC_2	14,46	16,30*	2513	72,05 $UC_{2,0}$ + 10,03 UC + 17,9 C	[1]
	14,52	16,33*	2521	$UC_{1,94}$	[3]
	14,50	16,31*	2522	95,3 $UC_{1,91}$ + 4,7 UC	[2]

* The entropy of mixing, characterizing the randomness in the arrangement of the C_1 and C_2 groups, is not included.

TABLE 2. Heat Capacity (in cal/mole·deg K) of UC at High Temperature

T, °K	Data of [8]	Data of [10]	T, °K	Data of [8]	Data of [10]
300	—	12,00	900	14,30	14,64
500	—	13,59	1100	14,85	15,08
700	13,80	14,19			

The heat capacity of the monocarbide can be calculated according to the results of measurements of the heat content in the intervals 300-1500°K [9] and 1287-2481°K [10], presented in Fig. 2, by the method of calorimetry of mixing. The data of these studies are in good agreement with the overlapping temperature interval and fit into the general curve expressed by equation [11] of the type

$$H_T - H_{298} = a + bT + cT^2 + dT^3 + \frac{e}{T}. \quad (1)$$

Table 2 presents for comparison the values of the heat capacity of UC, obtained in [8] and calculated in [11] according to the data of [10]. Table 3 presents the thermal functions of UC, calculated in [11].

Variation of the heat content of $UC_{1.93}$ in the interval 1484-2851°K and $UC_{1.90}$ in the interval 400-1500°K was determined in [12] and [13], respectively, by the method of calorimetry of mixing (Fig. 3). In the overlapping temperature interval, the values found for the change in the enthalpy coincide within the limits of the experimental errors, but the values of the heat capacity differ substantially. Thus, according to the data of [12], at 1490°K the heat capacity of $UC_{1.93}$ = 23.8 cal/mole·deg, while according to the data of [13] it is equal to 21.2 cal/mole·deg. Moreover, as can be seen from Fig. 4, the nature of the change in the heat capacity also differs. In [11] the data of the two investigations are compared and presented in the form of an equation of the type of (1). In Fig. 3 the sharp increase in the heat capacity of α-UC_2 close to the point of the $\alpha - \beta$ conversion is clearly visible.

The substantial increase in the heat capacity of UC_2 (and UC) in the region of high temperatures, which follows from the results of the measurements of [12], was the cause of the lack of confidence in these data. However, the author of [11] believes that there is no basis for doubt, since the heat content of other carbides was also measured, and in the case of TiC, ZrC, and TaC, an increase in the heat capacity was found, while in the case of HfC, NbC, and WC, it was not. Nonetheless, the results of measurements of the content of UC_2 above 1650°K should be treated with caution, since when UC_2 is cooled in the interval 2038-1650°K, there is frequently a precipitation of UC. Such precipitation probably occurred during the measurements in [12], which was noted by the authors of [20], who recalculated the data of [12] on the assumption that they pertain to a mixture of 0.055 UC + 0.945 $UC_{1.91}$ + 0.07 C. This theoretically correct correction somewhat lowers the value of the heat capacity of UC_2 but has little effect on the value of the free

TABLE 3. Thermal Functions of $UC_{1.0}$*

Temperature, °K	$H^\circ_T - H^\circ_{298}$, cal/mole	C°_p, cal/mole·deg	S°_T, cal/mole·deg	$-(F^\circ_T - H^\circ_{298})/T$, cal/mole·deg
298,15	0,0	11,98	14,15	14,15
500	2 618	13,59	20,82	15,58
700	5 402	14,19	25,50	17,78
900	8 285	14,64	29,12	19,91
1100	11 260	15,08	32,10	21,87
1300	14 320	15,58	34,66	23,64
1500	17 490	16,13	36,92	25,26
1700	20 780	16,77	38,98	26,76
1900	24 200	17,48	40,88	28,15
2100	27 780	18,27	42,67	29,45
2300	31 520	19,14	44,37	30,67
2500	35 440	20,10	46,01	31,83
2700	39 560	21,13	47,59	32,94
2823	42 200	21,81	48,55	33,60

* $H^\circ_T - H^\circ_{298.15} = -4.9624 \cdot 10^3 + 14.315\ T - 1.5130 \cdot 10^{-4}\ T^2 + 3.5038 \cdot 10^{-7}\ T^3 + 2.0828 \cdot 10^5/T$ cal/mole (298° – – 2.823°K) ± 0.4%.

TABLE 4. Thermal Functions of $UC_{1.90}$*

Temperature, °K	$H^\circ_T - H^\circ_{298}$, cal/mole	C°_p, cal/mole·deg	S°_T, cal/mole·deg	$-(F^\circ_T - H^\circ_{298})/T$, cal/mole·deg
α – 298,15	0,00	14,52	16,33	16,33
500	3 321,3	17,49	24,77	18,13
700	6 900,9	18,23	30,79	20,93
900	10 618	18,99	35,46	23,66
1100	14 527	20,187	39,37	26,17
1300	18 730	21,94	42,88	28,47
1500	23 344	24,30	46,18	30,62
1700	28 493	27,29	49,40	32,64
1900	34 304	30,92	52,62	34,57
2038	38 766	33,80	54,89	35,87
β – 2038	41 264	29,44	56,12	35,87
2100	43 089	29,44	57,00	36,48
2300	48 976	29,44	59,64	38,39
2500	54 864	29,44	62,14	40,19
2800	63 695	29,44	65,47	42,72
α – UC_2	$H^\circ_T - H^\circ_{298} = 8{,}377 \cdot 10^3 + 23{,}40\,T - 5{,}752 \times 10^{-3}\,T^2 + 2{,}727 \cdot 10^{-6}\,T^3 + 5{,}487 \cdot 10^5/T$			
β – UC_2	$H^\circ_T - H^\circ_{298} = -1{,}873 \cdot 10^4 + 29{,}44\,T$			

* The entropy of ordering is not included.

energy function $F^\circ_T - H^\circ_{298}/T$. Moreover, the correction cannot be accurate, since it cannot be established how much UC was precipitated during cooling in the calorimeter [12]. Taking the aforementioned into consideration, the author of [11] did not introduce any corrections into the data of [12] in the calculation of the thermal functions of UC (see Table 3) and UC_2 (Table 4). However, the thermal functions of UC_2 should evidently be corrected by adding the configurational entropy of ordering, calculated in [20] and equal to 0.60 cal/mole·deg, to the experimentally found entropy of UC_2.

There is no information on the high-temperature heat capacity of U_2C_3. Considering the unusual behavior of UC and UC_2, all attempts to estimate it will be extremely doubtful.

Enthalpy of Formation. The standard enthalpy of formation (ΔH°_{f298}) of uranium carbides was determined most accurately by the method of calorimetry of combustion. On the basis of mass spectrometric measurements [14], we detected a pronounced dependence of the enthalpy of formation of substoichiometric uranium monocarbide on the composition [21]. Therefore, samples with the composition $UC_{0.996}$ and $UC_{1.032}$ were taken for combustion, i.e., close to the stoichiometric. The enthalpies of formation were found equal to −23.3 ± 0.9 and −28.0 ± 1.0 kcal/mole, respectively [14]. Considering the results of our measurements [22] of the heats of formation of U_3O_8 and UO_2, these quantities should be approximately 0.8 kcal more negative, i.e., ΔH°_{f298} for $UC_{1.00} = -24.0 \pm 0.7$ kcal/mole. The value of the enthalpy of formation of UC_2 should also be corrected according to the same principle. Evidently, the most reliable value if ΔH_{f298} for $UC_{1.90} = -21.6 \pm 1.4$ kcal/mole. In [22] the enthalpy of formation of U_2C_3 was found equal to −44.0 ± 2 kcal/mole.

Free Energy of Formation. Figures 5-7 present the results of high-temperature measurements of the free energy of uranium carbides, obtained by different researchers, treated in [4]. The solid lines in Figs. 5 and 7 were constructed on the basis of the thermal function of $UC_{1.0}$ and $UC_{1.9}$ (see Tables 3 and 4) in such a way that they passed through the most reliable values obtained by the calorimetric method at the temperature 298°K.

The performance of measurements in different and frequently very limited temperature intervals and the substantial discrepancies between the results of different authors hinder a comparison of the data and do not give sufficiently reliable values of the free energy of uranium carbides within a broad temperature range. Noteworthy is the discrepancy in the values of the free energy, calculated from the purely calorimetric data and obtained by other methods. Analyzing the causes of this discrepancy, the authors of [4] hypothesized that the entropy of uranium (S°_{298}) may be equal not to 12, but to 14 cal/mole·deg. One of the causes of the discrepancy of the results of measurements of the vapor pressure may be an impurity of oxygen, especially when the investigated material is taken in the form of a powder or pulverized between individual experiments. Evidently a great role in the measurements is played by kinetic factors, since the processes of diffusion determine the concentration gradient.

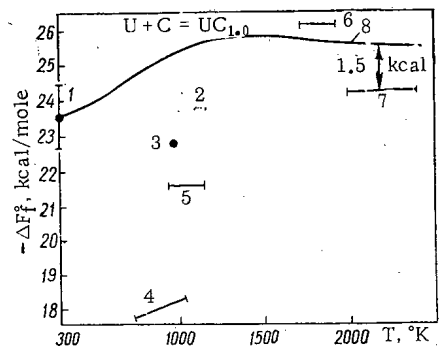

Fig. 5

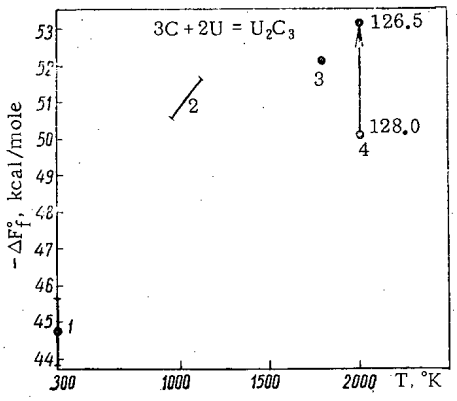

Fig. 6

Fig. 5. Free energy of formation of UC: 1) purely calorimetric method (ΔH_{298} = −23.3 kcal/mole) [14]; 2) equilibrium of UC + UC_2 and UC_2 + C with liquid bismuth [15]; 3) equilibrium of UC with liquid zinc [16]; 4) measurement of the emf [16]; 5) the same [17]; 6) equilibrium $UO_2 + 4C = UC_2 + 2CO$ [18]; 7) vapor pressure of uranium in the system U – C (ΔH_V = 128 kcal/mole) [19]; 8) see text.

Fig. 6. Free energy of formation of U_2C_3: 1) purely calorimetric data (ΔH_{298} = −43.3 kcal/mole) [19]; 2) measurement of emf [23]; 3 and 4) see text.

TABLE 5. Thermal Functions of UN

T, °K	C_p, cal /mole·deg	$H^\circ_T - H^\circ_{298}$, cal/mole	S°, cal /mole·deg	$(F^\circ_T - H^\circ_{298})/T$, cal/mole·deg
298	11,43	0	14,97	14,97
500	13,07	2 512	21,37	16,35
700	13,65	5 190	25,87	18,46
900	14,06	7 961	29,35	20,50
1100	14,45	10 811	32,21	22,38
1300	14,88	13 743	34,66	24,09
1500	15,36	16 767	36,82	25,64
1700	15,91	19 893	38,77	27,07
1900	16,52	23 125	40,57	28,41
2100	17,20	26 506	42,26	29,62
2300	17,95	30 021	43,86	30,81
2500	18,77	33 692	45,39	31,92
2700	19,66	37 534	46,87	32,97
2900	20,63	41 562	48,31	33,98
3125	21,79	46 333	49,94	35,12

To calculate the free energy, according to the data of evaporation, in addition to the activity of carbon it is necessary to know the heat of evaporation of uranium ($\Delta H_{V298°K}$). Its values, determined in different studies in the last ten years, vary from 117 to 126 kcal/mole. In the latter studies, even higher values were obtained – up to ~130 kcal/mole; a value of 128 kcal/mole was used in [4]. The free energy of uranium carbides calculated using this value does not coincide with the energy obtained according to purely calorimetric data, and the difference, as can be seen from the figures, comes to 1.5-2 kcal. This almost systematic discrepancy is elminated if we take the heat of evaporation of uranium equal to 126.5 kcal/mole.

For ΔF_f of U_2C_3, the following equation, correct within the interval 973-1173°K, was obtained in [23] (emf method):

$$\Delta F_f U_2C_3 = -43860 - 7T \text{ kcal/mole.}$$

The value of ΔF_f for U_2C_3 can be calculated, using data for UC and UC_2, from the equilibria

$$U_2C_3 = 0{,}758UC_{1{,}09} + 1{,}242UC_{1{,}75} \text{ (at 2000° K)}; \quad U_2C_3 + 0{,}78C = 2UC_{1{,}89} \text{ (at 1790° K).}$$

The corresponding values of ΔF_f for U_2C_3 are equal to −49.96 kcal/mole (at ΔH°_V = 128 kcal/mole) and −52.0 kcal/mole [4]. On account of the absence of certain necessary thermal data for U_2C_3, it is not known whether there is agreement between the values obtained. However, it is clear that when ΔH_V = 128 kcal/mole is used, the value of ΔF_f for U_2C_3 is too small, but it becomes more suitable if the calculation is performed at ΔH°_V = 126.5 kcal/mole.

The Uranium – Nitrogen System

In this article we shall discuss only the thermodynamic properties of uranium mononitride, UN, on the basis of the data of [26].

The heat capacity and heat content of UN were determined experimentally at low temperatures in [27, 28] and at high temperatures in [29, 30] (Fig. 8).

The results of both low-temperature measurements [27, 28] are in good agreement in most of the temperature region, but in the interval 250-350°K there is a slight discrepancy. The values of C_p obtained in

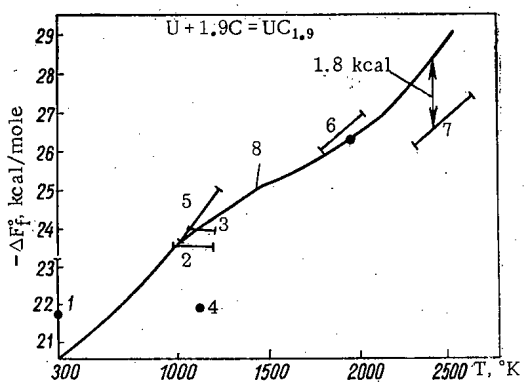

Fig. 7

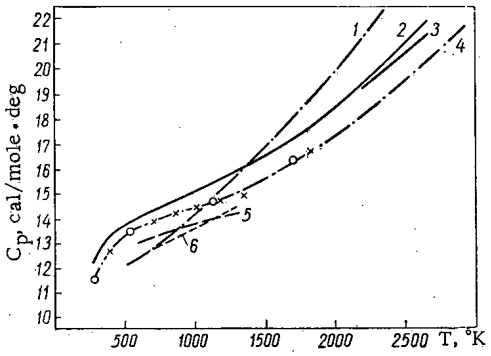

Fig. 8

Fig. 7. Free energy of formation of UC_2: 1) purely calorimetric data [24]; 2) measurement of emf [17]; 3) equilibrium of UC_2 + C with liquid bismuth [15]; 4) the same [25]; 5) measurement of emf [23]; 6) equilibrium $UO_2 + UC_2 = 4UC + 2CO$ [18]; 7) vapor pressure of uranium in the system U – C (ΔH_V = 128 kcal/mole) [19]; 8) see text (entropy of randomization taken into consideration).

Fig. 8. Heat capacity of UN: 1) data of [31]; 2) [11]; 3) [31], [29]; 4(○)) [26]; 4(×)) [29]; 5) [32]; 6) [30].

[28] are somewhat higher and in better agreement with the high-temperature measurements of [29], and for this reason are preferable.

Of the high-temperature measurements [29, 30], the data of [29] are better, since they were performed in a broader temperature interval. The calculated curves obtained [31, 32] were constructed as a result of a mathematical treatment of the experimental data [29, 30]. However, these curves do not coincide with the latter.

The author of [26], using the equation recommended [11] for the calculation of the temperature dependence of refractory compounds of the type of carbides, of the form

$$C_p = c_1 + c_2T + c_3T^2 + c_4T^{-2} \qquad (2)$$

and the experimental data of [29], also constructed the curves cited in Fig. 8. It is in good agreement with experimental data of [29] and almost parallel to the curve expressing the heat capacity of uranium monocarbide UC, cited in Fig. 8 for comparison.

Considering the similarity of the chemical bonds and the monotypic nature of the crystal lattices of UN and UC, such parallelism of the curves of C_p for UN and UC seems logical and is an additional confirmation of the curve constructed in [26].

The thermal functions of UN, calculated by the author of [26] using the formula that he obtained, as well as the values of the heat capacity C and the entropy S at 298°K, determined in [28], are cited in Table 5 and are recommended.

The heat of formation of UN was determined by two methods:

1) by measurement of the heat liberated in the reaction

$$U + \frac{1}{2}N_2 \rightarrow UN;$$

2) by the calorimetric method of combustion in fluorine or oxygen. The values of the heat of formation, measured by the second method, are more negative. The cause of this discrepancy is not known.

Evidently the data obtained by the first method are preferable [35, 36], since they were measured under conditions that better correspond to the practical conditions and are close to the heat of formation of UN, measured by the method of combustion in oxygen [37]. The average of the data of these three studies [35-37] is equal to −70.4 ± 0.7 kcal/mole and is recommended for the heat of formation of UN.

TABLE 6. Heat Capacity of $PuC_{0.87}$ at Low Temperature

T, °K	C_p°, cal/mole·deg	S_T°, cal/mole·deg	$H_T^\circ - H_0^\circ$, cal/mole
10	0,33	0,15	1,07
30	2,22	1,29	25,09
50	4,10	2,88	89,05
100	7,35	6,84	384,4
150	8,95	10,14	794,3
200	10,20	12,90	1274,1
250	11,21	15,29	1810,3
298,15	12,03	17,33	2370,4

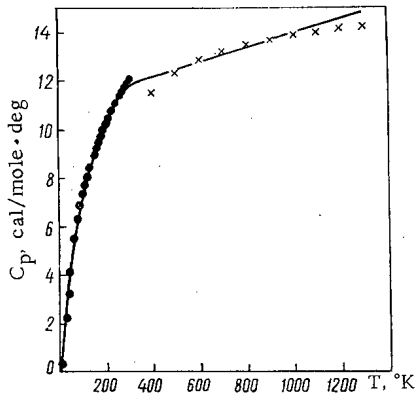

Fig. 9. Heat capacity of $PuC_{0.9}$: ×) data of [33]; •) [34].

TABLE 7. Thermal Functions of $PuC_{0.87}$*

T, °K	C_p, cal/mole·deg	S_T°, cal/mole·deg	$H_T^\circ - H_{298}^\circ$, cal/mole	$-(F_T^\circ - H_{298}^\circ)/T$, cal/mole·deg
298	11,794	17,300	0,0	17,300
500	12,413	23,543	2 443	18,657
700	13,040	27,819	4 988	20,693
900	13,671	31,172	7 659	22,662
1100	14,303	33,976	10 456	24,471
1300	14,935	36,417	13 380	26,125
1500	15,567	38,598	16 430	27,645
1700	16,200	40,585	19 607	29,052
1927	16,918	42,660	23 366	30,535

* The entropy of ordering is not included.

The Plutonium – Carbon System

Low-Temperature Heat Capacity. According to the communication [34], the heat capacity of plutonium monocarbide with the composition $PuC_{0.95}$ (49 atomic % carbon) was measured at Harwell. By metallographic analysis, 6.3 mole % Pu_2C_3 was detected in it, so that the "monocarbide" had a composition of $PuC_{0.86}$. The smoothed out results of the measurements are presented in Table 6. There are no other data on the low-temperature heat capacity of plutonium carbides.

High-Temperature Heat Capacity. There is information only on the heat capacity of $PuC_{0.87}$, measured by the method of calorimetry of mixing in the interval 425-1295°K [33]. The thermal functions of $PuC_{0.9}$ obtained are cited in Table 7.

It is scarcely possible to evaluate the heat capacity of Pu_2C_3 sufficiently reliably, since there are no data for compounds with such a structure.

Enthalpy of Formation. It should be considered that the values of ΔH_{f298}° for $PuC_{0.77}$ and Pu_2C_3, obtained by the method of calorimetry of combustion [38], were erroneous on account of the insufficiently accurate characterization of the combustible substances.

V. V. Akhachinskii has proposed a new method of evaluating the heats of formation of plutonium carbides [39]. He has noted that if in carbides formed by chemically similar metals (for example, TiC, ZrC, HfC) the values of the parameter $\Delta H_{subl.Me}/T_{m.Me} = K_1$ are close, then the values of $\Delta H_{f298MeC}/\Delta H_{subl.Me} = K_2$ and $\Delta H_{f298MeC}^\circ/T_{m.Me}$ are also close where $\Delta H_{subl.Me}$ and $T_{m.Me}$ are the heat of sublimation (at 298°K) and the melting point of the metal forming the carbide, while $\Delta H_{f298MeC}^\circ$ is the heat of formation of the carbide per g-atom of the metal. In the case of carbides of variable composition, ΔH_{f298} pertains to the carbide with maximum carbon content. As a result of the enthalpy of formation, the value of ΔH_{f298}° for $PuC_{0.87}$, Pu_2C_3, and PuC_2 was estimated at -14.5 ± 1.4, -29.0 ± 2.9, and 14.5 ± 1.4 kcal/mole.

Free Energy of Formation. Recently the pressure of plutonium above two-phase systems "PuC" + Pu_2C_3 and PuC_2 + C was measured by the vapor transfer method [40]. The Knudsen method has been used [41] to investigate two-phase regions "PuC" + Pu_2C_3 and Pu_2C_3 + C. The results of the measurements, performed by two groups of researchers in overlapping composition regions, differed by no more than 10%. The vapor pressure of plutonium above two-phase regions was expressed by the following equations:

$$\text{«PuC»} + Pu_2C_3 \quad \lg P_{atm} = 5.116 - \frac{18853}{T} \ (1325 - 1907^\circ K); \tag{3}$$

$$Pu_2C_3 + C \quad \lg P_{atm} = 4.39 - \frac{20330}{T} \ (1366 - 1835^\circ K); \tag{4}$$

$$PuC_{2-x} + C \quad \lg P_{atm} = 3.618 - \frac{18723}{T} \ (2017 - 2472^\circ K), \tag{5}$$

where the first equation is the result of a treatment of the experimental studies [40, 41] by the method of least squares. From these equations we can obtain expressions for the change in the free energy of the

TABLE 8. Thermodynamic Functions of $PuC_{0.87}$

T, °K	ΔH_f°, cal /mole	ΔS_f°, cal/mole · deg	ΔF_f, cal/mole
300	−10 400	2,89	−11 260
500	−11 110	1,19	−11 700
700	−11 220	1,01	−11 930
900	−11 540	0,56	−12 050
1100	−12 000	0,04	−12 040
1300	−11 700	0,29	−12 080
1500	−11 330	0,55	−12 160
1700	−10 870	0,84	−12 300
1927	−10 240	1,19	−12 530

following reactions, on the assumption that the carbon-rich boundary of the monocarbide phase corresponds to $PuC_{0.9}$, while Pu_2C_3 is a stoichiometric phase with a very low concentration interval:

$$2{,}5PuC_{0,9(sol)} \rightarrow 1.5PuC_{1,5(sol)} + Pu_{gas},$$
$$\Delta F = 86270 - 23.41T \text{ cal}; \quad (6)$$
$$PuC_{1,5(sol)} \rightarrow 1.5C_{(sol)} + Pu_{gas},$$
$$\Delta F = 93010 - 20.09T \text{ cal}; \quad (7)$$
$$PuC_{2-x(sol)} \rightarrow (2-x)C_{sol} + Pu_{gas},$$
$$\Delta F = 85710 - 16.55T \text{ cal}. \quad (8)$$

From Eqs. (6) and (7) it follows that

$$PuC_{0,9(sol)} \rightarrow 0.9C_{sol} + Pu_{gas},$$
$$\Delta F = 90320 + 21.42T \text{ cal} \; (1366 - 1835^\circ K). \quad (9)$$

Calculations using the second law of thermodynamics give a value of ΔH°_{f298} = 93.0 kcal for reaction (9), which is in good agreement with the value calculated according to the third law of thermodynamics and is equal to 93.4 kcal. Combining this value with the standard heat of sublimation of plutonium (83.0 ± 1.0 kcal), we can find that the standard enthalpy of formation of plutonium monocarbide ΔH°_{f298} for $PuC_{0.9}$(sol) = −10.4 kcal/mole.

In [42] the activity of plutonium in the two-phase regions PuC + Pu_2C_3 (971-1060°K) and Pu_2C_3 + C (974-1091°K) was measured by the emf method. Analyzing the results obtained, the author of [34] obtained for the reaction

$$Pu_{liq} + 0.9C_{sol} \rightarrow PuC_{0,9(sol)} \quad (10)$$

the equation

$$\Delta F^\circ_T = -15450 + 1.30T \text{ cal} \quad (970 - 1060^\circ K), \quad (11)$$

which differs somewhat from that cited in [42]. Evidently the slope of the line $\Delta F = f(T)$ according to the data of [42] is erroneous, since the value of ΔS of the reaction could not be determined accurately on account of the small temperature interval of the measurements. Calculations according to the third law, if ΔF_{1000}, calculated according Eq. (11), is taken as the basis, give a value of ΔH°_{f298} for $PuC_{0.9}$ = 12.5 kcal, which is close to the value obtained by V. V. Akhachinskii [39] as a result of an estimate.

For the reaction

$$2Pu_{liq} + 3C_{sol} = Pu_2C_{3(sol)} \quad (12)$$

the following function was found in [42]

$$\Delta F^\circ_T = -52500 + 14.7T \text{ cal} \quad (974 - 1091^\circ K). \quad (13)$$

At the present time, the results of measurements of the vapor pressure are preferable to the data obtained by the emf method on account of the good agreement of the results of various investigators and the good agreement with the theoretical data. Combining the latter with the calculated standard heat of formation of $PuC_{0.9}$ (−10.4 kcal/mole), we can obtain the thermodynamic functions cited in Table 8.

The free energy of formation can be represented by two equations:

$$Pu_{sol} + 0.9C_{sol} = PuC_{0,9(sol)},$$
$$\Delta F^\circ = -11060 - 1.16T \; (298 - 913^\circ K);$$
$$Pu_{liq} + 0.9C_{sol} = PuC_{sol},$$
$$\Delta F^\circ = -11510 - 0.48T \; (913 - 1927^\circ K).$$

The tables of thermodynamic functions for Pu_2C_3 and PuC_2 cannot be compared on account of the absence of thermal data. However, using the data of [43] on the evaporation of pure plutonium and the thermal data, cited in [44], we can find the values of ΔF° in the high-temperature region.

For the process

$$Pu_{liq} \rightarrow Pu_{gas} \quad (14)$$

$$\Delta F^\circ = 79570 - 22.39T \text{ cal} \quad (1366 - 1835^\circ K); \quad (15)$$

$$\Delta F^\circ = 81360 - 23.32T \text{ cal} \quad (2017 - 2472^\circ K). \quad (16)$$

From these equations and Eqs. (7) and (8), we find for

$$Pu_{liq} + 1.5C_{sol} = PuC_{(sol)} \quad (17)$$

$$\Delta F = -13440 - 2.3T \text{ cal} \quad (1366 - 1835^\circ K) \quad (18)$$

and for

$$Pu_{liq} + (2 - x)\,C_{sol} = PuC_{2-x\,(sol)} \quad (19)$$

$$\Delta F = -4350 - 6{,}77 \text{ cal} \quad (2017 - 2472^\circ K). \quad (20)$$

To eliminate certain contradictions, the author of [44] proposes that Eq. (20) be changed, and reduces it to the form

$$\Delta F = -7580 - 5.33T \text{ cal} \quad (1933 - 2495^\circ K). \quad (21)$$

There are no data on the thermodynamics of Pu_3C_2 (the ζ-phase).

Entropy. It may be assumed that the entropy of $PuC_{0.87}$ at 0°K is equal to R (0.13 ln 0.13 + 0.87 ln 0.87) = 0.77 cal/mole · deg. This value should be added to that found experimentally (see Table 7), and then S°_{298} for $PuC_{0.87}$ = 18.1 cal/mole · deg, which agrees with the value proposed in [39]. Evidently the thermal functions of $PuC_{0.9}$ cited in Table 7 should be recalculated, considering the new value of the entropy, increasing the absolute values of S°_T and $F^\circ_T - H^\circ_{298}/T$ by 0.77 cal/mole · deg. Correspondingly, the enthalpy of formation for $PuC_{0.9}$, calculated according to the evaporation data, using the third law of thermodynamics, proves equal to −9.0 kcal/mole.

In the report [39], the following values of the entropy are recommended for Pu_2C_3 and PuC_2: 41.6 ± 3 and 22.5 ± 2 cal/mole · deg, respectively.

LITERATURE CITED

1. E. Westrum, E. Suite, and H. Lonsdale, Advances in Thermophysical Properties at Extreme Temperatures and Pressures, S. Gratch (editor), ASME (1965), p. 156.
2. R. Andon et al., Trans. Farad. Soc., 60, 1030 (1964).
3. J. Farr, See [1], p. 162.
4. E. Storms, The Uranium–Carbon and Plutonium–Carbon Systems. Report at the Conference of Experts on the Thermodynamics of Uranium and Plutonium Carbides, IAEA, Vienna (September, 1968).
5. E. Westrum, Jr., Notes on the Thermodynamic Properties of Carbides of Actinides (Preliminary survey). See [4].
6. T. Mukaibo et al., Thermodynamics of Nuclear Materials, IAEA, Vienna (1962), p. 645.
7. J. Moser and O. Kruger, J. Appl. Phys., 38, 3215 (1967).
8. C. Affortit, Personal communication, made by R. Lalleman. See [4].
9. L. Harrington and G. Rowe, Carbides in Nuclear Energy, L. Russel (editor), Vol. 1 (1964), p. 342.
10. L. Levinson, ibid., p. 429.
11. E. Storms, The Refractory Carbides, Academic Press, New York–London (1967).
12. L. Levinson, J. Chem. Phys., 38, 2105 (1963).
13. A. Macleod and S. Hopkins, Proc. Brit. Ceramic. Soc., 8, 15 (1967).
14. E. Storms and E. Huber, J. Nucl. Mater., 23, 19 (1967).
15. I. Craig, Cited according to [4].
16. W. Robinson and P. Chiofti, Report JS-1061 (1966). Cited according to [4].
17. E. McIver, AERE-R 4983, Harwell (1966). Cited according to [4].
18. I. Piazza and M. Sinnot, J. Chem. Engng. Data, 1, 451 (1962).
19. E. Huber and C. Holley, Cited according to [4].
20. L. Leithaker and T. Godfrey, J. Nucl. Mat., 21, 175 (1967).
21. E. Storms, Thermodynamics, Vol. 1, IAEA, Vienna (1966), p. 309.
22. C. Holley, Letter to the Conference of Experts on the Thermodynamics of Uranium and Plutonium Carbides (August, 1968).

23. W. Behl and J. Egan, J. Electrochem. Soc., 113, 376 (1966).
24. E. Huber, E. Head, and C. Holley, J. Phys. Chem., 67, 1730 (1963).
25. P. Rice, R. Bajzhiser, and D. Ragone, Thermodynamics of Nuclear Materials, IAEA, Vienna (1966), p. 331.
26. H. Blank, The Ternary System U–C–N. Some Conclusions on the Behavior of Solid Solutions of UC–UN. See [4].
27. J. Counsell, R. Dell, and J. Martin, Trans. Farad. Soc., 62, 1736 (1966).
28. E. Westrum and C. Barber, J. Chem. Phys., 45, 635 (1966).
29. E. Speidel and D. Keller, BMJ 1633 (1963). Cited according to [26].
30. L. Harrington, CN-LM-4461 (1963). Cited according to [26].
31. T. Godfrey, J. Wolley, and J. Leitnaker, ORNL-TM-1596 (Rev. 1, 1966). Cited according to [26].
32. K. Spear and J. Leitnaker, ORNL-TM-2106 (1968).
33. O. Kruger and H. Savage, J. Chem. Phys., 40, 3924 (1964).
34. M. Rand, Thermodynamic Evaluation of the Plutonium–Carbon System. See [4].
35. P. Gross, C. Hayman, and H. Clayton, Thermodynamics of Nuclear Materials, IAEA, Vienna (1962), p. 653.
36. W. Hubard, T. J. D. ANL-15554 (1962). Cited according to [26].
37. F. Feder, See [35], p. 665.
38. E. Huber and C. Holley, Thermodynamics of Nuclear Materials, IAEA, Vienna (1962), p. 581.
39. V. V. Akhachinskii, The Heat and Entropy of Formation of Plutonium Carbides. See [4].
40. F. Harris et al., Cited according to [34].
41. W. Olson and R. Mulford, Thermodynamics of Nuclear Materials, IAEA, Vienna (1968), p. 467.
42. G. Campbell, L. Mullins, and J. Leary, ibid., p. 75.
43. Mulford, RNL, Thermodynamics, Vol. 1, IAEA, Vienna (1966), p. 231.
44. M. Rand. Atomic Energy Review, 4, Special Issue 1, IAEA, Vienna (1966), p. 7.

ABSTRACTS

SLOWING DOWN OF RESONANCE NEUTRONS IN MATTER

COMMUNICATION 4

D. A. Kozhevnikov and V. S. Khavkin

UDC 621.039.512.4

The time dependence of the neutron age $\tau_s(u, t)$ is examined. In the simplest (Wigner) spectral approximation, for isotropic scattering and constant mean free path

$$\tau_s(u, t)=\tau_s(u)+\frac{\lambda^2}{3}\left[x^2-1+\frac{2h}{\xi}(x+\ln x-1)\right]. \quad (1)$$

Here $\tau_s(u)$ is the total steady-state neutron age, h the total scattering probability, and $x = t/\langle t(u)\rangle$, where $\langle t(u)\rangle$ is the average slowing-down time.

The analytic features of the complete formal solution of the steady-state slowing-down problem are studied. The spatial, angular, and energy distributions of neutrons close to the source are obtained in explicit form. This result does not depend on the order of the B_N-approximation ($N \geq 1$) and has the same form for all spectral approximations:

$$\Psi(z, u, \mu)=\chi(z, u, \mu)\,\Psi_0(z, u); \quad (2)$$

$$\chi(z, u, \mu)=\frac{1}{2}\left\{1+\frac{[zZ(u, \mu)}{2\tau_0(u)}+\frac{z^2}{4\tau_0^2(u)}[\tau_s(u, \mu)-\tau_s(u)]+\ldots\right\}; \quad (3)$$

$$\Psi_0(z, u)=\frac{\Psi_0(u)\,e^{-z^2/4\tau_0(u)}}{\sqrt{4\pi\tau_0(u)}}\left\{1+\frac{z^2}{4\tau_0^2(u)}[\tau_s(u)-\tau_0(u)]+\ldots\right\} \quad (4)$$

The neutron spectrum $\Psi_0(u)$, the total age $\tau_s(u)$, the Fermi age $\tau_0(u)$, and the second spatial-angular moment $\tau_s(u, \mu)$ were calculated previously [1, 2] in four spectral approximations (Wigner, Weinberg–Wigner, and the generalized and standard Greuling–Goertzel approximations). The quantities $\tau_s(u, \mu)$ and $Z(u, \mu)$ (the first spatial-angular moment) depend on the angular distribution of the source neutrons. The condition for the applicability of (3) and (4) is formulated as the inequality

$$z \ll \frac{2\tau_0(u)}{\lambda_{\max}}, \quad (5)$$

where λ_{max} is the maximum slowing-down length in the interval. If condition (5) is satisfied the classical age approximation is valid for media with any hydrogen content but is not applicable to an absorbing moderator. The results (3)-(5) are valid for an arbitrary energy dependence of the reaction cross sections and, as is true of the more general formal solution, are easily generalized to take account of inelastic scattering and diffraction anisotropy.

At large distances from the source the spatial and energy neutron distributions are determined by the character of the energy dependence of the total interaction cross section. To explain the principal properties of the distribution function, determined by the resonance character of the $\Sigma(u)$ dependence, a single negative resonance (interference minimum) of the cross section is considered in the Wigner approximation for isotropic scattering.

In this case

$$\Psi_0(z, u)=B(u)\,F(z), \quad (6)$$

where the buildup factor B(u) describes the neutron spectrum, and F(z) is independent of energy and is

Translated from Atomnaya Énergiya, Vol. 29, No. 6, p. 448, December, 1970. Original article submitted May 20, 1970.

determined only by the width of the resonance Γ and the characteristics of the interaction h and ξ at the resonance energy:

$$F(z)=\frac{E_1(z/\lambda)}{\lambda\Gamma(\beta)}\left(\frac{2z}{\lambda}\right)^{\beta}\left\{1+0\left[\frac{1}{z}\ln\frac{z}{\lambda}\right]\right\}, \quad (7)$$

where $E_1(x)$ is the exponential integral, $\lambda = \Sigma_{min}^{-1}$, and $\beta = h\Gamma/2\xi$. This same result holds for two and more negative resonances having the same values of Σ_{min}. In the latter case $\beta \rightarrow \beta^* = \beta_1 + \beta_2 + \ldots$

LITERATURE CITED

1. D. A. Kozhevnikov and V. S. Khavkin, Atomnaya Énergiya, 27, 143 (1969).
2. D. A. Kozhevnikov and V. S. Khavkin, ibid., 29, 365 (1970).

INVESTIGATION OF THE CALIBRATION CHARACTERISTICS OF A RADIATION THERMODIVERTER IN HIGH-INTENSITY FIELDS OF IONIZING RADIATIONS

V. S. Karasev, S. S. Ogorodnik, and Yu. L. Tsoglin

UDC 621.039.564

An integrated heat flux calorimeter, known as a radiation thermodiverter (RTD), has been proposed for measuring heat generated by radiation; this device features high accuracy, high sensitivity, quick response, and arbitrary shape and size.

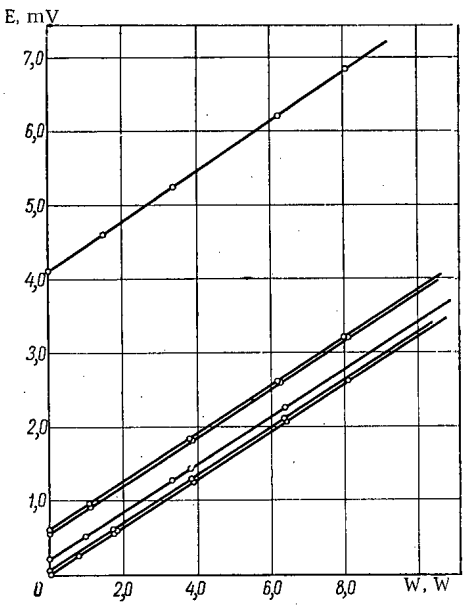

Fig. 1. Calibration curves of RTD (radiation thermodiverter) exposed to pile radiations of different intensity.

The behavior of the calibration curves of the RTD in response to irradiation were studied experimentally in this article, and the results of long-term radiation stability tests directly in the core of the nuclear reactor are reported.

The experimental procedure is designed to take separate account of the effects of intensity, integrated fast flux, and γ-radiation. The transport channel in a reflector at the interface with the reactor core, and an experimental channel in a spent-fuel storage pool, were selected as the exposure zones in the experiment. An RTD with a cylindrical cavity 20 mm in diameter, 20 mm in height, 0.30 mV/W sensitivity, was tested in the reactor channel, and another RTD with an inner cavity 9 mm in diameter and 12 mm in height, with a sensitivity of 66.6 mV/W, was tested in the pool channel.

Results of the RTD calibrations at different positions in the height of the reactor channel, at different stages in the exposure, are plotted in Fig. 1.

The integrated fast (sulfur) flux amounted to $1.2 \cdot 10^{19}$ neutrons/cm^2 by the time the experiment was over.

For long-term testing for radiation stability, a thermodiverter unit made up of copper–constantan thermopiles with mica interlayers sandwiched between them as electrical insulation, was placed in a hermetically sealed capsule which was

Translated from Atomnaya Énergiya, Vol. 29, No. 6, p. 449, December, 1970. Original article submitted March 26, 1970.

inserted into a reactor core cell, replacing one fuel element. The capsule was exposed to irradiation rated at 10 MW for over three months, and received over that time span an integrated fast flux (sulfur) of $4.3 \cdot 10^{20}$ neutrons/cm^2, and an integrated thermal flux (gold) of $6.7 \cdot 10^{20}$ neutrons/cm^2, with an integrated γ-radiation dose (lead) of $2.7 \cdot 10^6$ Mrad. A monotonic decline in the dose rate in lead, referred to 1 MW, was observed, ending up at 4.65% by the end of the exposure, and this was accounted for by a decrease in the intensity of the soft component of the γ-radiation stemming from fuel burnup in neighboring fuel elements in the core.

These experiments demonstrated that the calibration curves of the thermodiverter retain their linearity and stability in high-intensity fields of ionizing radiations. The practical feasibility of long-term service of the thermodiverter for in-pile measurements was thereby demonstrated.

CALCULATION OF PHOTONEUTRON DISTRIBUTION BY MONTE CARLO METHOD

A. A. Morozov and A. I. Khisamutdinov

UDC 539.125.5.348:546:45

The conditions of the problem are as follows. A pulsed source of γ-rays placed at a height h above the surface of the earth emits 1.667-2.2 MeV photons in a cone of a given angle. The photons fall on beryllium-bearing rock and initiate photonuclear reactions in beryllium, producing neutrons which pass through the air. The beryllium is assumed to be uniformly spread through the rock.

The quantities investigated are the integrated neutron fluxes in given time and energy intervals at various distances from the source. The neutron flux depends on the parameters of the beryllium-containing rock as well as on height, time, energy, and distance from the source.

Plane symmetry in the neutron part of the problem and the uniformity of time were used in finding the required integrated fluxes by a specially developed modification of the Monte Carlo method. Local flux calculations were thus avoided. In the process of solving the problem the neutron trajectory was displaced to the proper point in phase space and then the corresponding "importance of production" was calculated at the point of actual production.

Time histograms were obtained and interpreted for beryllium-bearing granite with porosities of 0, 3, and 6%, energy intervals of 0-0.4 and 0.4-400 eV, heights h of 20, 45, and 100 m, and distances from the source r of 0 and 10 m. The time axis of the histograms contains the time intervals 10^{-5}-10^{-3}; 10^{-3}-$5 \cdot 10^{-3}$; $5 \cdot 10^{-3}$-10^{-2}; 10^{-2}-$5 \cdot 10^{-2}$; and $5 \cdot 10^{-2}$-10^{-1} sec.

The results of the calculations confirm the possibility of air prospecting for beryllium from a height of 45-60 m with a γ-source $\sim 5 \cdot 10^{12}$ photons/sec for a beryllium density of $\sim 10^{-5}$ g/cm^3, and can contribute to the choice of optimum instrument characteristics.

Translated from Atomnaya Énergiya, Vol. 29, No. 6, pp. 449-450, December, 1970. Original article submitted November 11, 1969; revision submitted February 26, 1970; abstract submitted June 23, 1970.

PRECISION SYSTEM FOR THE DETERMINATION OF OXYGEN BY FAST NEUTRON ACTIVATION

I. P. Lisovskii and L. A. Smakhtin*

UDC 621.039.564

A method for determining oxygen from the reaction $O^{16}(n, p)N^{16}$ is suggested. The samples are irradiated in stainless steel ampoules in an NG-160 neutron generator which is provided with a device for interrupting the deuteron beam (diameter of the ampoules 15 mm, length 20 mm, and internal volume 1.6 cm^3). The maximum flux at the point of irradiation amounts to $5 \cdot 10^8$ neutrons/$cm^2 \cdot$ sec. The integral neutron flux through the internal volume of an ampoule (sample) is directly proportional to the flux through the ampoule walls. This makes it possible to use the induced activity of the ampoule (reaction $Fe^{56}(n, p) \cdot Mn^{56}$) as the flux monitor. The sample position during the irradiation need not be exactly determined.

The γ-emission of the samples and of standards was measured with a detector (NaI(Tl) crystal with a size of 150 mm × 100 mm and with a hole of 20 mm diameter and 50 mm depth) and an LP4050 512-channel analyzer.

The N^{16} activity was measured in the range 4.8 to 8 MeV. Lucite ($C_5H_8O_2$) was used as an oxygen standard. The ampoules were transported in an automated pneumatic shuttle. The irradiation time was 30 sec, the delay time 0.9 sec, and the exposure time 30 sec. The background generated by the ampoule was taken into account. The accuracy of the determinations amounted to 1-2.5 relative percent, depending upon the oxygen concentration. The sensitivity was 10^{-4} g O_2.

VVR REACTOR SEMIAUTOMATIC ACTIVATION ANALYSIS SYSTEM

I. P. Lisovskii, L. A. Smakhtin, N. V. Filippova, and V. I. Volgin†

UDC 621.039.56

A semiautomatic pneumatic shuttle system for a nuclear reactor is described. The specimens were irradiated in hermetically sealed polyethylene capsules which were placed in the shuttle rabbit. After ten rabbits with specimens have been placed in the loader, all further operations (irradiation exposure, extraction of capsule with specimen from the rabbit and delivery of specimen to the laboratory for measurements) are handled automatically. The total time elapsed from the end of the irradiation exposure to the beginning of measurements is 10 to 20 sec (depending on the size of the capsules).

Work done in activation analysis with the aid of this semiautomatic shuttle and irradiation system is reviewed. Operating experience with this pneumatic shuttle, over a four-year period, has demonstrated the versatility, reliability, and ease of operation of the system.

*Translated from Atomnaya Énergiya, Vol. 29, No. 6, p. 450, December, 1970. Original article submitted March 20, 1970.

†Translated from Atomnaya Énergiya, Vol. 29, No. 6, p. 450, December, 1970. Original article submitted March 20, 1970.

METHOD OF ATTENUATING RADIAL BETATRON OSCILLATIONS IN CYCLIC ACCELERATORS

L. A. Roginskii and G. F. Senatorov

UDC 621.384.6.07

Systems for the attenuation of betatron oscillations are of great importance for the development and use of cyclic accelerators designed for high intensities and energies. The conventional attenuation systems [1-4] comprise pickup electrodes, which measure the deviation of the beam from the chamber axis (sensors), and electrostatic deflectors (correctors), which adjust the transverse momentum of the particles. The present article is a theoretical consideration of an attenuation method slightly different from the conventional method. The principle of the present method, which was suggested by the author of the article and by Yu. S. Ivanov in the Radiotechnical Institute of the Academy of Sciences USSR, is based on the fact that the voltage of several accelerating sections is modulated by a signal proportional to the signal of a sensor measuring the beam shift. The momentum change which is induced in the particle's momentum by the modulation of the longitudinal accelerating field causes a shifting of the particles in radial direction. The system parameters can be selected so that the radial force attenuates the betatron oscillations.

Compared with the conventional methods, the present method is characterized by the advantage that the existing accelerating sections can be used as correctors (without affecting their actual purpose); thus, special deflectors, which would occupy additional space, are unnecessary. The relatively low efficiency is the principal disadvantage of the method. The low efficiency results from the fact that the indirect effect upon the radial motion (by modifications of the longitudinal momentum) is small. Nevertheless, one can accomplish in such a system a constant attenuation which is equal to several ten revolutions, and this suffices for suppressing certain transverse beam instabilities (e.g., drag instabilities).

The article describes in detail one of the versions of the proposed attenuation system consisting of a sensor and two accelerating sections used as correctors. The voltage of the first section (first section, as far as the motion of the particles is concerned) is modulated with a signal which is proportional to the sensor signal. Therefore, after passage through the resonator, the particles which arrive in the equilibrium phase acquire a momentum different from the equilibrium momentum. A radial force proportional to the relative momentum deviation caused by the modulation of the accelerating voltage acts upon the particles. The phase of the voltage applied to the second resonator is opposite to the modulation of the first resonator, and therefore, the momentum deviation of the particles vanishes after the passage of the particles through the resonator, and the particle motion is not affected by a radial force.

The system was described with a matrix method. The attenuation decrement and the stability regions were determined. It could be shown that the distance between the sensor and the first section must be equal to an integer of the wavelength of the betatron oscillations in order to obtain the highest efficiency; the distance between the sections must be equal to a half integer of the betatron oscillation wavelength.

LITERATURE CITED

1. C. Pruett, Fifth International Conference on High Energy Accelerators, Frascati (1965), p. 363.
2. J. Martin, Fifth International Conference on High Energy Accelerators, Frascati (1965), p. 347.
3. H. Barton, A Summary of the Cosmotron Experiments on the Coherent Vertical Instability, MOB-7 (November 27, 1963).
4. P. R. Zenkevich, Thesis, Moscow (1965).

Translated from Atomnaya Énergiya, Vol. 29, No. 6, pp. 450-451, December, 1970. Original article submitted November 20, 1969; abstract submitted June 17, 1970; revision submitted June 17, 1970.

PERMANENT ELECTROMAGNET WITH BUILT-IN RADIOISOTOPE THERMOELECTRIC DIRECT CONVERTER

A. Kh. Cherkasskii and V. S. Makarov

UDC 621.362

An independently functioning electromagnet with a built-in thermoelectric direct converter for direct conversion of the heat energy of radioactive decay into electrical energy, and combining the positive features of a permanent magnet (continuous and independent operation without the aid of external power supplies) with the advantages of an electromagnet (high field strength, high flux density, linearity of B–H characteristics, stability to effects exerted by strong externally applied magnetic fields, capability of service at temperatures well above the Curie point of ferromagnetic materials), is proposed by the authors and examined.

This "quasipermanent" magnet (see Fig. 1) consists of the thermopiles 1 and 2 placed on the surface of the fuel slug 3 and the electrically closed winding 4, which envelops the ferromagnetic core 5. A part of the core is cut off to form a working gap. The fuel slug consists of several capsules with radioactive isotope 6 placed within a current-conducting casing 7. The heat energy of radioactive decay is converted by the thermoelectric cells into electrical energy, so that a short-circuit current appears in the magnet winding, and a magnetic field is established in the working gap.

The current in question depends on the parameter $Y \equiv \alpha\sigma/\varkappa$ of the thermoelectric material, which is expressed in A/W units:

$$I = \frac{q_0 b l_{Fe}}{(1+m+zT)} Y \text{ A}, \tag{1}$$

where $\alpha, \sigma, \varkappa$ are the thermal emf, electrical conductivity, and thermal conductivity of the thermoelectric cell; q_0 is the density of the heat flux flowing through the thermoelectric cell; bl_{Fe} is the heat contact surface; m is the ratio of the winding resistance to the resistance of the pn pair; zT is the Ioffe criterion. When the number of turns $\omega_{opt} = [(1 + zT)/m]^{1/2}$ has been optimized, the field intensity in the working gap will be

$$H_\delta = \frac{q_0 l l_{Fe}}{2km_0\sqrt{1+zT}\, l_\delta} Y \text{ A/m}; \tag{2}$$

and the magnetic flux density in the working gap will be:

$$B_\delta = \frac{\mu_0 q_0 b l_{Fe}}{2km_0\sqrt{1+zT}\, l_\delta} Y \text{ ml}, \tag{3}$$

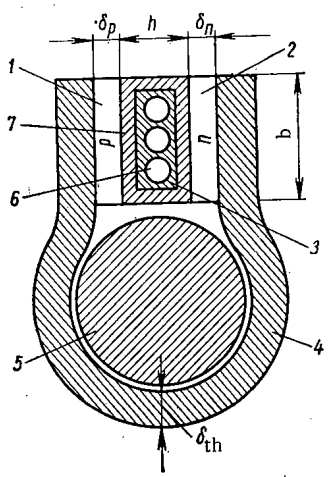

Fig. 1. Layout of permanent electromagnet.

while the volume density of electromagnetic energy in the working gap will be:

$$W_\delta = \frac{H_\delta B_\delta}{2} = \frac{\mu_0}{4}\left[\frac{q_0 b l_{Fe}}{km_0\sqrt{1+zT}\, l_\delta} Y\right]^2 \text{ J/m}^3, \tag{4}$$

and the specific electromagnetic energy referred to the weight of the core will be:

$$W_{Fe} = \frac{H_\delta B_\delta S_{Fe} l_\delta}{\gamma_{Fe} S_{Fe} l_{Fe}} = \frac{\mu_0}{4}\left[\frac{q_0 b Y}{km_0\sqrt{1+zT}}\right]^2 \frac{l_{Fe}}{l_\delta}\cdot\frac{1}{\gamma_{Fe}} \text{ J/kg}, \tag{5}$$

where $m_0 = m/\omega^2$; l_δ, S_δ are the length and area of the working gap; l_{Fe}, S_{Fe}, γ_{Fe} are the length, cross-sectional area, and specific weight of the core; μ_0 is the magnetic permeability constant; k is a multiplicative factor characterizing the contribution made by the core resistance to the total circuit resistance.

Calculations for basic parameters of this autonomous electromagnet made from thermopiles of silicon–germanium alloy for various types of

Translated from Atomnaya Énergiya, Vol. 29, No. 6, pp. 451-452, December, 1970. Original article submitted March 3, 1970.

radioactive fuel, including: Sr^{90}, Pu^{238}, Cm^{244}, U^{232}, Ce^{144}, Po^{210}, and Th^{228}, are cited. It is shown that other types of built-in director converters can be used along with the thermoelectric converter, e.g., thermionic converters or thermophotoelectric converters.

EXPERIMENTAL STUDY OF THE CHARACTERISTICS OF THE IR-100 RESEARCH REACTOR

L. V. Konstantinov, I. N. Martem'yanov,
V. A. Nikolaev, A. A. Sarkisov,
V. F. Sachkov, A. V. Sobolev,
S. V. Chernyaev, and I. S. Chesnokov

UDC 621.039.521:621.039.55

The water-cooled, water-moderated IR-100 teaching and research reactor was commissioned in 1967; it was designed for a thermal power of 100 kW and used uranium dioxide (10% enriched) as nuclear fuel. Sheathless fuel cassettes were used for the first time in the IR-100, in conjunction with small graphite displacers and a demountable graphite reflector; these enabled a variety of critical-composition configurations to be created.

The release of heat from the active zone of the reactor is effected by the natural directional circulation of water. The water is cooled in a heat exchanger built into the vessel of the reactor. In order to improve the natural circulation of the water, the reactor vessel contains a concentric cylindrical barrier situated below the active zone. The barrier separates the active zone and the space above it filled with hot water from the water cooled in the heat exchanger.

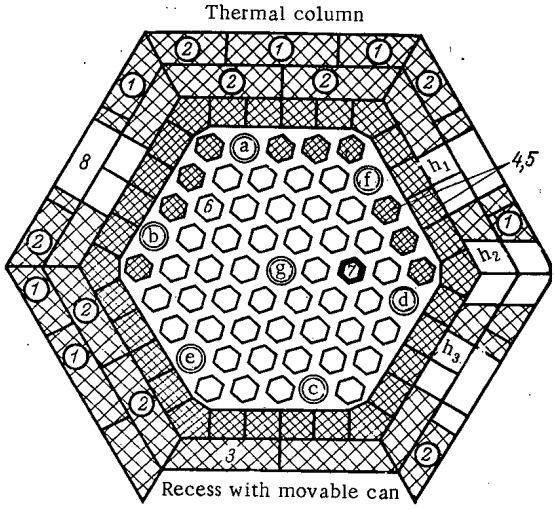

Fig. 1. Schematic chart indicating the loading of the active zone and the arrangement of the experimental sections in the IR-100 reactor: 1) ionization-chamber channels; 2) vertical experimental channels (VEC); 3) graphite reflector; 4, 5) graphite displacers; 6) fuel cassette; 7) photoneutron source; 8) shuttle channel; a) automatic-control rods; b, c, d) scram rods; e, f) manual-control rods; g) CEC; h_1-h_3 HEC.

A description of the construction of the IR-100 and its rated physical and technological parameters was given earlier [1, 2].

In this paper we shall present the results of some measurements carried out during the introductory period and the subsequent running of the reactor, characterizing its experimental potentialities.

A schematic chart representing the loading of the active zone and the arrangement of the experimental sections of the reactor are presented in Fig. 1. The working load (charge) of the active zone comprises 43 fuel cassettes (2.4 kg U^{235}), 40 graphite displacers, and one beryllium photoneutron source.

The reactivity reserve of the reactor with the experimental sections empty is 0.58%. The total compensating capacity of the control rods is 4.7%.

The reactivity introduced by the mobile can [1] is 0.06% on filling it with graphite and 0.05% on filling it with water. Filling the central experimental channel (CEC) with water increases the reactivity of the reactor by 0.48%. Filling the other experimental regions with water has no effect on the reactivity of the system.

Table 1 presents the thermal-neutron fluxes and the dose rate of γ-radiation in the vertical experimental

Translated from Atomnaya Énergiya, Vol. 29, No. 6, pp. 453-454, December, 1970. Original article submitted January 23, 1970.

TABLE 1. Thermal-Neutron Fluxes and Dose Rate of γ-Radiation in the Experimental Systems

Experimental system	Thermal-neutron flux, $\cdot 10^{12}$ neutrons/cm^2 · sec	Dose rate of γ-radiation, $\cdot 10^6$ R/h	Experimental system	Thermal-neutron flux, $\cdot 10^{12}$ neutrons/cm^2 · sec	Dose rate of γ-radiation, $\cdot 10^6$ R/h
CEC	2,75	22	VEC-5	0,99	1,9
VEC-1	1,12	2,1	VEC-6	0,97	1,9
VEC-2	1,11	2,2	VEC-7	0,3	0,71
VEC-3	0,34	0,72	VEC-8	0,22	0,70
VEC-4	0,24	0,68	Can	0,1	0,36

TABLE 2. Characteristics of the Horizontal Experimental Channels

Experimental system	Dose rate of γ-radiation, R/h	Thermal-neutron flux, neutrons/cm^2 · sec	Fast-neutron flux, neutrons/cm^2 · sec
HEC-1 (h_1)	$6{,}8 \cdot 10^5$	$1{,}43 \cdot 10^8$	$2{,}86 \cdot 10^7$
HEC-2 (h_2)	$5{,}5 \cdot 10^5$	$2{,}53 \cdot 10^7$	$1{,}65 \cdot 10^7$
HEC-3 (h_3)	$7{,}7 \cdot 10^5$	$1{,}54 \cdot 10^8$	$3{,}52 \cdot 10^7$

channels (VEC) and on the front wall of the unloaded "drawbridge" can at the level of the center of the active zone, referred to the nominal reactor power of 100 kW.

The thermal-neutron fluxes were determined by reference to the absolute activity of a set of gold indicators, using the method of (β, γ)-coincidences (maximum error 7%). The dose rate of γ-radiation was measured with small-scale γ-chambers (maximum error 20%).

Table 2 gives the thermal and fast-neutron fluxes and the dose rate of γ-radiation at the exit from the horizontal experimental channels (HEC) for the case of open gates (valves), measured with a universal radiometer of the RUS-7 type and referred to the nominal reactor power of 100 kW.

Practical experience showed that the cooling system employed in the IR-100 reactor had a considerable reserve factor, enabling the reactor power to be raised to between 200 and 300 kW without seriously changing the loading of the active zone.

LITERATURE CITED

1. Yu. M. Bulkin et al., Atomnaya Énergiya, 21, 363 (1966).
2. Yu. M. Bulkin et al., Byull. Izobret., No. 30, 184 (1968).

EFFECT OF THE FLOW VELOCITY OF A VAPOR – LIQUID MIXTURE OF COOLANT, AND OF VAPOR CONTENT, ON SURFACE HEAT-TRANSFER COEFFICIENT IN BOILING OF WATER INSIDE TUBES

F. F. Bogdanov

UDC 621.039.534.44

The literature contains surprisingly little data on the effect of steam content and the flow velocity of a coolant vapor–liquid mixture on surface heat-transfer coefficients in the case of boiling in channels and tubes. This appears to stem from the fact that many investigators have failed to detect any such effects in their experiments at all. One of the reasons for this would be insufficient attention on the part of investigators to keeping the heating surface sufficiently clean. Experience has shown that the presence of a 0.02-0.03 mm thick oxide film on the heating surface will result in an appreciably steep rise in thermal resistance over the path of the heat flux in boiling, offsetting any comparable drop in steam content or in the flow-speed of the vapor–liquid mixture. Hence, only those investigators who stage their experiments on sufficiently clean heating surfaces will have any success in detecting the influence exerted by the above factors on surface heat transfer when water is boiled in channels.

Generalizations about boiling heat transfer within tubes consequently either fail to take account of the effect of vapor content and of the flowspeed of the vapor–liquid coolant mixture at all, or else take account of the effect of vapor content alone, and that in at best a highly approximate manner.

These circumstances render it more convenient to seek out some new form for making generalizations on experimental data, one which would take into account the effect on surface heat-transfer coefficients of changes in the relative steam content by weight, and in the flowspeed of the vapor–liquid coolant mixture.

At the basis of these generalizations, we placed our improved formula from reference [1], with thermodynamic similitude criteria brought into the picture, and proposed for the purpose of determining the surface heat-transfer coefficients in boiling of water on clean heating surfaces when steam content is either positive or negative, as well as the recommendations in reference [2] on treating the effect exerted on heat-transfer coefficients in boiling of a liquid phase in tubes where the flowspeed of the liquid phase is linear, and laminar flow goes over into turbulent flow.

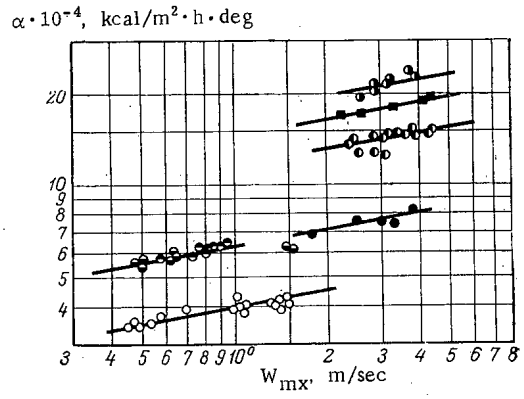

Fig. 1. Dependence of surface heat-transfer coefficients for boiling in tubes on flowspeed of vapor–liquid mixture: ○) author's data for boiling in slightly oxidized tubes (pressure p = 55 atm, heat flux q = $2.6 \cdot 10^5$ kcal/m²·h, liquid-phase flowspeed w_0 = 0.4 m/sec); ◒) same, at p = 125 atm, q = $4 \cdot 10^5$ kcal/m²·h, w_0 = 0.35 m/sec; ◓) same, for p = 140 atm, q = $3.7 \cdot 10^5$ kcal/m²·h, w_0 = 0.4 m/sec; ●) data borrowed from reference [1], for boiling of water in tubes (p = 170 atm, q = $2 \cdot 10^5$ kcal/m²·h, w_γ = 1245 kg/m²·sec); ◑) same for q = $4.5 \cdot 10^5$ kcal/m²·h; ■) same, for q = $6 \cdot 10^5$ kcal/m²·h; ◐) same, at q = $8 \cdot 10^5$ kcal/m²·h.

Translated from Atomnaya Énergiya, Vol. 29, No. 6, pp. 454-456, December, 1970. Original article submitted June 3, 1969; revision submitted November 13, 1969.

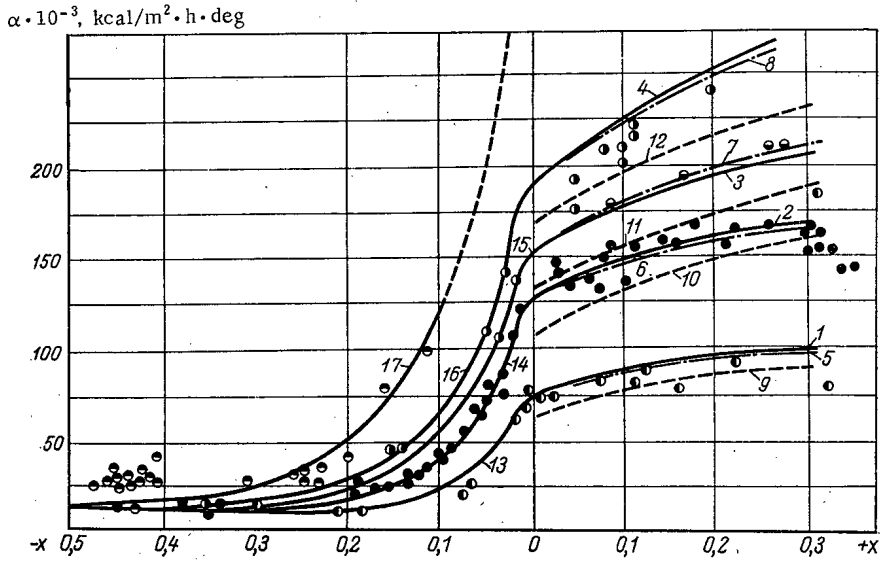

Fig. 2. Dependence of the surface heat-transfer coefficients on the total effect exerted by vapor void content and vapor–liquid mixture flowspeed: ◓) data borrowed from reference [1] for a vapor–liquid mixture at p = 170 atm and q = $2 \cdot 10^5$ kcal/m$^2 \cdot$h; ●) same, at q = $4.5 \cdot 10^5$ kcal/m$^2 \cdot$h; ◒) same, at q = $6 \cdot 10^5$ kcal/m$^2 \cdot$h; ◑) same, at q = $8 \cdot 10^5$ kcal/m$^2 \cdot$h. Curves 1, 2, 3, 4 are theoretical curves plotted on the basis of formula (3) for q values of $2 \cdot 10^5$, $4.5 \cdot 10^5$, $6 \cdot 10^5$, and $8 \cdot 10^5$ kcal/m$^2 \cdot$h, respectively; curves 5, 6, 7, 8 are curves plotted on the basis of the formula recommended by the authors of reference [1] for the same heat fluxes, respectively; curves 9, 10, 11, 12 are curves plotted on the basis of formula (3), for p = 100 atm and the same respective heat fluxes; curves 13-16 are plotted on the basis of formula (4), for p = 170 atm and the same respective heat fluxes; curve 17 is plotted on the same basis, but for concentric slit orifices, at q = $1.2 \cdot 10^6$ kcal/m$^2 \cdot$h.

Experimental data borrowed from references [1, 3], and taken from our own experiments, were used in processing the experimental results: 1) on surface heat transfer when subcooled water is boiled on the practically clean heating surfaces of narrow annular channels, and obtained at very high heat flux levels [q = 10^6 to $3 \cdot 10^6$ kcal/m$^2 \cdot$h] and at pressure p = 175 atm; 2) on surface heat transfer in the case of boiling in oxide-coated tubes, and obtained at pressures of 50, 120, and 140 atm.

The experiments were carried out by a procedure described in the literature [2], but the arrangement was modified slightly.

A tube of 1Kh18N9T steel with an outer diameter of 23.5 mm and wall thickness of 1.25 mm, total length l = 3290 comprising two sections to be heated: l_1 = 345 mm, and l_2 = 1020 mm, and with a stabilized section left unheated, of length l_0 = 805 mm, was used as the working section in the experiments.

Four Chromel–Alumel thermocouples 0.2 mm in diameter were used on each of two cross sections on the l_2 interval of tubing, and four thermocouples were used in one cross section on the l_1 interval. The thermocouples measured the temperature of the external surface of the experimental tube; the temperature of the tube inner surface was determined by calculations based on K. D. Voskresenskii's formula.*

The experiments were carried out under rigorously stationary conditions. Only the heat load on the economizer lengths of tubing was varied before each series of experiments. As a rule, the maximum heat load was established in the first experiments in each series, and was found to decrease from one experiment to the next. When the heat load on the economizer tube lengths remained unaltered, five to six experiments each lasting 30 min were carried out.

*This formula was derived by K. D. Voskresenskii upon the present author's request back in 1949, but has unfortunately remained unpublished. The formula is as follows:

$$\Delta t_w = \frac{q_l}{2\pi\lambda l}\left[\left(\frac{\ln d_2/d_1}{1-d_2^2/d_1^2}-0{,}5\right)-\ln\frac{d_2}{d_1}\,q_h\right]^0 C,$$

where q_h accounts for heat losses to the surroundings.

The steam content by weight of the coolant varied only insignificantly (by a few percent), making it possible to discern the effect exerted by the flowspeed of the vapor–liquid mixture on the surface heat-transfer coefficients, independently of the vapor content, since the direct effect exerted by the vapor phase on the heat-transfer process remains practically unaffected. At the same time, the vapor content by volume varied appreciably from one experiment to the next, and the flowspeed of the vapor–liquid mixture also underwent appreciable changes.

Data from these experiments are plotted in Fig. 1 in the form of the dependence $\alpha = f(w_{mx})$. The experimental data points plot out with a modest spread (relative to the skewed straight lines giving the slope n = 0.16 at all the heat fluxes and pressures measured). This means that the change in heat flux and pressure over the range investigated will have no effect on the way heat transfer accompanying boiling of water in tubes is affected by the flowspeed of the vapor–liquid mixture. But the diagram also shows experimental data from reference [1] on heat transfer when water boils in tubes. A correction intended to eliminate any direct effect of the vapor content by weight was introduced into the values of the surface heat-transfer coefficients in this case. The experimental data from [1] corrected in this manner fit with very little spread about the skewed straight lines representing the slopes n = 0.16. Accordingly, the effect of the flowspeed of the vapor–liquid coolant mixture on the surface heat-transfer coefficients in boiling in tubes and channels can be taken into account by means of the power-law multiplier $w^{0.16}$ at those parameters, or by the simplex $(w_{mx}/w_{cr})^{0.16}$ in generalized formulas, at any pressures of the vapor–liquid coolant mixture. This dimensionless criterion links the rate of surface heat transfer, in boiling in channels, with the hydrodynamics of two-phase flow. When we also take into account the recommendations put forth in reference [1] on handling the effect exerted on heat transfer by the steam content by weight in boiling, the total effect of the flowspeed of the vapor–liquid coolant mixture and of the vapor content by weight in this mixture on heat transfer when the coolant boils in the channels in forced flow, can be treated properly by using the dimensionless complex:

$$x^{0.4}\left(\frac{w_{mx}}{w_{cr}}\right)^{0.16}. \tag{1}$$

The magnitude of the component of the surface heat-transfer coefficient ascribed to boiling can be determined with sufficient accuracy by using the formula

$$\alpha_b = C\left(\frac{p_{cr}}{p_1}\right)^{0.12}\left(\frac{T_s}{T_{cr}-T_s}\right)^{2/3} q^{0.7}\ \frac{\text{kcal}}{\text{m}^2\cdot\text{h}\cdot\text{deg}}. \tag{2}$$

Hence, the convective component will be determined from Eq. (2) multiplied by the complex (1). The total heat-transfer coefficient in boiling in tubes is given by the formula

$$\alpha = C\left(\frac{p_{cr}}{p_1}\right)^{0.12}\left(\frac{T_s}{T_{cr}-T_s}\right)^{2/3} q^{0.7}\left[1+x\left(\frac{w_{mx}}{w_{cr}}\right)^{0.4}\right]^{0.4}\frac{\text{kcal}}{\text{m}^2\cdot\text{h}\cdot\text{deg}}. \tag{3}$$

Figure 2 shows experimental data from reference [1] on heat transfer in boiling of water in tubes and when the vapor content is positive, as approximated by formula (3). The free proportionality factor in this formula was adopted in accordance with our recommendations for a weakly oxidized surface, with the assigned value 0.8. The broken curves on this graph are averaging curves [1] plotted for the corresponding heat flux levels.

The theoretical curves based on formula (3) describe the experimental data in [1] quite closely, and almost coincide with the averaging curves based on those data. Figure 3 also shows the theoretical curves based on formula (3) for the pressure p = 100 atm. It is clear from the diagram that these curves are equidistant from the theoretical curves plotted for p = 170 atm.

Here we also have the experimental data from [1] relating the same heat flux levels at negative vapor content (subcooled liquid), at the pressure 170 atm. The experimental data are approximated by the theoretical curves plotted on the basis of a formula in which the multiplicative factor taking the convective component into account is raised to the negative power recommended by the authors of reference [1]. In that case, the computational formula becomes

$$\alpha = C\left(\frac{p_{cr}}{p_1}\right)^{0.12}\left(\frac{T_s}{T_{cr}-T_s}\right)^{2/3} q^{0.7}\left[1+x\left(\frac{w_{mx}}{w_{cr}}\right)^{0.16}\right]^{-2.8}\frac{\text{kcal}}{\text{m}^2\cdot\text{h}\cdot\text{deg}}. \tag{4}$$

The coefficient C is assigned the value 0.8 in this case.

It is clear from the diagram that the experimental data in reference [1] referring to the case of negative vapor void content are described quite closely by formula (4). Our experimental data on surface heat transfer in boiling of subcooled water at the pressure p = 170 atm on a practically clean heating surface of annular channels, with forced flow (indicated by circles blackened in top half), also plotted in that diagram, are again approximated closely by formula (4). The free proportionality factor is assigned the values of 1 and 2 in that case, depending on how clean the heating surface is. These experimentally derived data points fit the approximating curve with a very small spread.

LITERATURE CITED

1. N. V. Tarasova, A. A. Armand, and A. S. Kon'kov, in: Heat Transfer at High Heat Flux Levels, and Other Special Conditions [in Russian], A. A. Armand (editor), Gosénergoizdat, Moscow (1959), p. 6.
2. F. F. Bogdanov, Izv. Akad. Nauk SSSR, Otd. Tekh. Nauk, No. 4, 136 (1955).
3. W. Elrod et al., Trans. ASME, 89, No. 3 (1967).

NEUTRON YIELD FROM THICK TARGETS BOMBARDED WITH 11.5 AND 23.5 MeV PROTONS

V. K. Daruga and E. S. Matusevich

UDC 621.384.633

The measurements were performed at the FÉI cyclotron. The energy of the proton beam was determined by the range in aluminum foils and by a semiconductor detector. At the time of the measurements the energy was 11.5 ± 0.5 MeV (molecular hydrogen) and 23.5 ± 0.7 MeV (atomic hydrogen).

The targets of Li, Be, C, Mg, Al, Ti, Fe, Co, Ni, Cu, Zn, Nb, Cd, Ta, W, Pb, Bi, and U had their natural isotopic compositions, and thicknesses equal to the range of the bombarding protons.

The experimental procedure and technique were described earlier [1].

Absolute measurements were made with a BF_3 long counter. The angular distributions of neutrons from the targets were measured with a ZnS(Ag) scintillator in Plexiglas and a B^{10} + ZnS(Ag) scintillator with a polyethylene neutron moderator 5 cm thick. Backgrounds were determined with a shadow cone. The total yields were obtained by integrating the areas under the angular distribution curves, taking account of the neutron spectra and the detector characteristics. The shape of the angular distribution in the $\theta > 140°$ region was obtained by extrapolation. The angular distributions for all targets except carbon fall smoothly from $\theta_{lab} = 0$ to $\theta_{lab} = 180°$. The neutron yield from carbon increases in both the forward and backward directions.

Table 1 shows the absolute neutron yields in 4π and in the $\theta_{lab} = 0°$ direction. Table 2 gives the characteristics of the neutron spectra in the range E_n = 1-6 MeV for E_p = 23.5 MeV, listing values of the parameters T_W and T_L for describing the spectra in the form $\sim E_n \exp(-E_n/T_W)$ and $\sim E_n^{5/11} \exp(-E_n/T_L)$ respectively. The spectra of neutrons emitted in the $\theta_{lab} = 0°$ direction from light targets (Li, Be, C) are very different from spectra of evaporated neutrons. All spectra have different values of T in the ranges $E_n < 3$ MeV and $3 < E_n < 6$ MeV. The data on neutron spectra for E_p = 11.5 MeV are given in [2].

TABLE 1. Absolute Neutron Yields from Thick Targets

Target	E_p = 11.5 MeV		E_p = 23.5 MeV	
	Y (0°), neutrons/sr·μCi	$Y_{4\pi}$, neutrons/μCi	Y (0°), neutrons/sr·μCi	$Y_{4\pi}$, neutrons/μCi
Li	—	—	$9{,}5 \cdot 10^9 \pm 13\%$	$5{,}5 \cdot 10^{10} \pm 16\%$
Be	$6{,}3 \cdot 10^9 \pm 10\%$	$3{,}9 \cdot 10^{10} \pm 15\%$	$2{,}2 \cdot 10^{10} \pm 10\%$	$1{,}1 \cdot 10^{11} \pm 14\%$
C	$1{,}75 \cdot 10^7 \pm 6\%$	$1{,}1 \cdot 10^8 \pm 27\%$	$1{,}3 \cdot 10^8 \pm 9\%$	$8{,}0 \cdot 10^8 \pm 25\%$
Mg	—	$6{,}1 \cdot 10^8 \pm 17\%$	$1{,}0 \cdot 10^9 \pm 8\%$	$7{,}5 \cdot 10^9 \pm 15\%$
Al	$1{,}7 \cdot 10^8 \pm 10\%$	$1{,}35 \cdot 10^9 \pm 18{,}5\%$	$1{,}5 \cdot 10^9 \pm 8\%$	$1{,}15 \cdot 10^{10} \pm 13\%$
Ti	—	$4{,}8 \cdot 10^9 \pm 23\%$	$3{,}95 \cdot 10^9 \pm 10\%$	$3{,}6 \cdot 10^{10} \pm 14\%$
Fe	—	—	$2{,}8 \cdot 10^9 \pm 10\%$	$2{,}5 \cdot 10^{10} \pm 16\%$
Co	—	$5{,}0 \cdot 10^9 \pm 16\%$	$4{,}35 \cdot 10^9 \pm 10\%$	$3{,}7 \cdot 10^{10} \pm 14\%$
Ni	—	$4{,}6 \cdot 10^8 \pm 18\%$	$1{,}35 \cdot 10^9 \pm 8\%$	$1{,}0 \cdot 10^{10} \pm 16\%$
Cu	—	—	$4{,}1 \cdot 10^9 \pm 8\%$	$3{,}9 \cdot 10^{10} \pm 15\%$
Zn	—	$2{,}6 \cdot 10^9 \pm 23\%$	$3{,}3 \cdot 10^9 \pm 11\%$	$3{,}0 \cdot 10^{10} \pm 17\%$
Nb	$4{,}1 \cdot 10^8 \pm 7\%$	$4{,}6 \cdot 10^9 \pm 15\%$	$5{,}0 \cdot 10^9 \pm 8\%$	$5{,}0 \cdot 10^{10} \pm 12\%$
Cd	—	$3{,}7 \cdot 10^9 \pm 19\%$	$5{,}0 \cdot 10^9 \pm 8\%$	$5{,}2 \cdot 10^{10} \pm 14\%$
Ta	—	$1{,}2 \cdot 10^9 \pm 16\%$	$3{,}95 \cdot 10^9 \pm 10\%$	$5{,}0 \cdot 10^{10} \pm 14\%$
W	$9{,}5 \cdot 10^7 \pm 10\%$	$1{,}05 \cdot 10^9 \pm 19\%$	—	—
Pb	$5{,}0 \cdot 10^7 \pm 10\%$	—	$2{,}95 \cdot 10^9 \pm 11\%$	$3{,}5 \cdot 10^{10} \pm 18\%$
Bi	—	$5{,}6 \cdot 10^8 \pm 18\%$	—	—
U	$7{,}4 \cdot 10^7 \pm 7\%$	$9{,}0 \cdot 10^8 \pm 17\%$	$5{,}7 \cdot 10^9 \pm 11\%$	$7{,}0 \cdot 10^{10} \pm 14\%$

Translated from Atomnaya Énergiya, Vol. 29, No. 6, pp. 456-458, December, 1970. Original article submitted June 30, 1970.

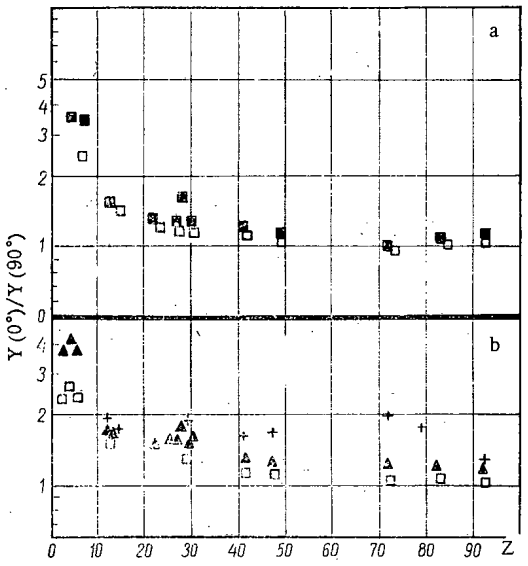

Fig. 1. Ratio of neutron yields Y(0°)/Y(90°) from thick targets bombarded with protons. a) E_p = 11.5 MeV, mean square error $\pm\delta$ = 5-10%; b) E_p = 23.5 MeV, $\pm\delta$ = 10-15%; □) $E_n > 0$; ■) $E_n > 1.6$ MeV; ▲) $E_n > 1.8$ MeV; +) $E_n \geq 8$ MeV from [3].

TABLE 2. Parameters for the Analytic Description of Spectra

Target	θ = 0°		θ = 90°	
	T_W, MeV	T_L, MeV	T_W, MeV	T_L, MeV
Li	0,7—1,2	0,8—1,4	0,7—1,0	0,8—1,1
Be	0,9—2,3	1,1—2,9	0,80—2,1	0,95—2,6
Al	1,0—2,7	1,2—3,9	0,9—2,2	1,1—2,6
Cu	0,95—1,55	1,2—1,8	0 8—1,2	0,95—1,4
Cd	0,85—1,15	1,0—1,3	0,75—1,1	0,95—1,25
Pb	0,85—1,1	1,1—1,25	0,8—0,9	1,0—1,1
U	1,0—1,27	1,25—1,45	0,95—1,25	1,25—1,4

Figure 1 shows the ratio of the yields Y(0°)/Y(90°) as a function of the Z of the target nuclei.

The authors thank V. A. Dulin and N. N. Pal'chikov for help with the measurements, and A. A. Ognev for measuring the proton energy.

LITERATURE CITED

1. V. K. Daruga et al., Preprint FÉI [in Russian] (1970).
2. V. K. Daruga et al., Bulletin of the Nuclear Data Information Center [in Russian], No. 6, Atomizdat, Moscow (1970).
3. B. Cohen, Phys. Rev., 98, 49 (1955).

A METHOD OF DETERMINING THE IRON CONTENT OF CORROSION PRODUCT DEPOSITS

B. A. Alekseev, N. N. Kozhenkov, and G. A. Kotel'nikov

UDC 621.039.553.36

The current method of analyzing the amount of accumulated corrosion product deposits in nuclear reactor circuits, using specimens of zirconium alloys, is based on boiling the deposits in 6N HCl. However, solution is very slow and systematic errors may be incurred owing to incomplete solution of these products (chiefly iron oxides). These difficulties can be eliminated by determining the content of the corrosion product deposits from their γ-radiation.

Study of the deposits was performed on specimens from outside the active zone – in the heat-transfer agent of the forced-circulation loop of the MR reactor of the I. V. Kurchatov Institute of Atomic Energy. The specimens were prepared from zirconium alloys. The spectrum of the γ-quanta, measured by means of a Ge(Li) detector, clearly displayed Co^{60} and Cr^{51} isotopes. The iron content was determined by means of o-phenanthroline. The error of the iron determination was assessed by the accuracy of the spectrophotometric method. Thus, during the experiment we determined how the activity of Co^{60} in the sweeping-out liquor depends on its iron content.

Analysis of the experimental data revealed that in the corrosion product deposits, the activity of Co^{60} is proportional to the iron content to within ~10% (see Table 1). This fact may be used for rapid and remote-controlled determinations of accumulated iron concentration of specimens, and also in pipelines (for studying the kinetics of sweeping away of deposits), and other similar problems.

We thank V. F. Kozlova for helping with the assembly of the spectrometer, V. A. Ermakov for his useful advice, and V. F. Leonov for operating the apparatus.

TABLE 1. Activity of Co^{60} versus Concentration of Accumulated Iron

Fe, mg/liter ($\cdot 10^3$)	11	12	18	19	22	27	29	32	34	42	44	54	57	58	69
Co^{60}, counts /sec	4,0	6,5	8,5	8,0	10,0	12,0	13,0	10,5	14,5	19,0	16,5	21,0	17,0	23,0	27,0

Translated from Atomnaya Énergiya, Vol. 29, No. 6, p. 458, December, 1970. Original article submitted July 17, 1969; revision submitted June 1, 1970.

GROUP SEPARATION OF FISSION PRODUCTS BY THE CHROMATOGRAPHIC METHOD

L. N. Moskvin and N. N. Kalinin

UDC 543.544.6

Analysis of radioactive elements in the water of the reactor primary loop is protracted and complicated, no matter whether the methods of analysis used are sedimentation techniques, extractive techniques, or chromatographic techniques [1-3]. The appearance of Ge(Li)-detectors in γ-ray spectroscopy has made the job of identifying radioactive elements a much simpler one. It has become possible to estimate the content of individual isotopes directly from the γ-ray spectrum of the primary loop water in the reactor system [4]. But because of the different yields in fission, different activation cross sections for impurities, and peculiar spectral features, some of the radioactive isotopes may escape detection directly against the γ-ray spectrum background of the total sum of active products present in the coolant stream.

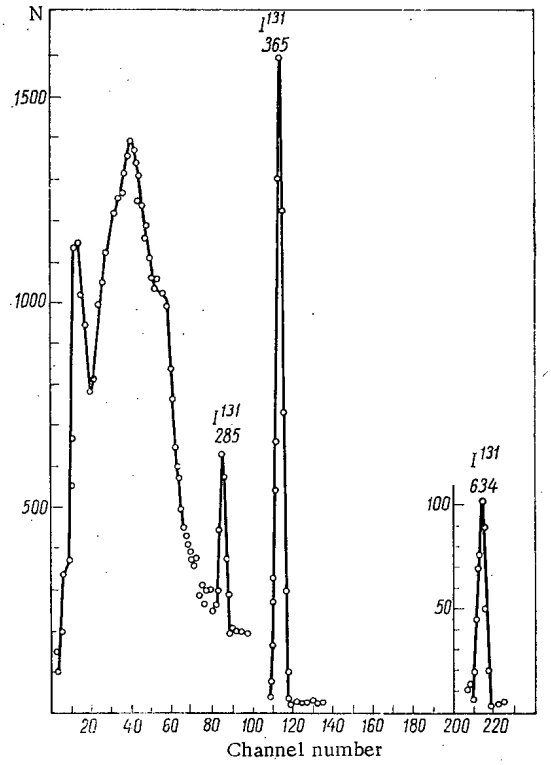

Fig. 1. γ-Ray spectrum of fraction separated out on column packed with AB-17 anion-exchange resin.

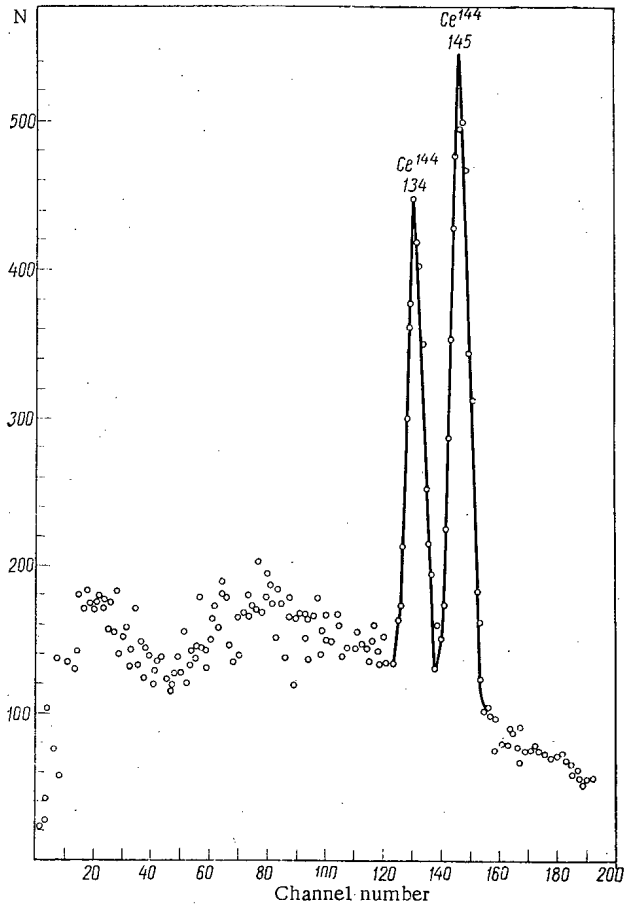

Fig. 2. γ-Ray spectrum of fraction separated out on column with di-2-ethylhexylphosphoric acid.

Translated from Atomnaya Énergiya, Vol. 29, No. 6, pp. 458-461, December, 1970. Original article submitted January 4, 1970; revision submitted April 2, 1970.

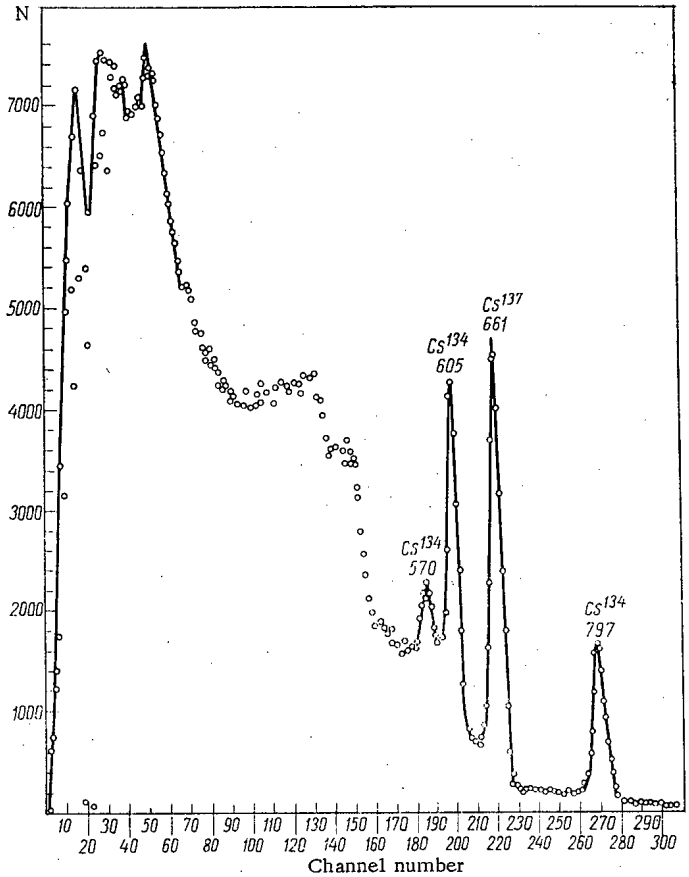

Fig. 3. γ-Ray spectrum of fraction separated out on third column in first two free volumes of eluate.

The authors of the present article made some attempts to combine group express chromatographic separation of fission products with subsequent identification on a Ge(Li)-spectrometer, an approach which makes provisions for singling out the most highly active impurities in the reactor loop water (viz., iodine and alkali metals) and considering them in separate groups.

Radioactive elements have to be stabilized in a single chemical form in order to isolate them in quantitative work. The introduction of formic acid is important in setting up conditions favorable to chromatographic separation of fission fragments. As a strong reducing agent, formic acid contributes to the conversion of different forms of iodine and bromine to a single reduced form, I^- or Br^-, which then makes it possible to isolate these elements quantitatively on a column with a strongly basic anion-exchange resin (AB-17 in our case) in the formate form. The acidity of the solution needed in order to separate out the rare earths from the alkali and alkali earth metal on a chromatographic partition column of Teflon coated with di-2-ethylhexylorthophosphoric acid as the stationary organic phase is achieved at the same time, and with ease.

A system of columns made of glass, all of the same dimensions (100 mm in height, 12.5 mm in diameter) and connected in series, was utilized in the chromatographic separation. The first column was filled with AB-17 anion-exchange resin with grain sizes from 100 to 250 μ, in the formate form (HCO_2^-). The second column consisted of Teflon in pellet form, coated with di-2-ethylhexylorthophosphoric acid. The preparation of this type of column has been described in detail in the literature [5]. The third column was filled with Dowex-50X8 cation-exchange resin, grain sizes 100 to 250 μ, in the H^+-form. Cation-exchange resin KU-2 lends itself equally well to this application.

The aqueous solution to be analyzed (100 to 250 ml in volume), containing traces of iodine, cesium, barium, lanthanum, and cerium, was acidified to pH = 2 with formic acid, and was passed under pressure, at a flowspeed of 8 to 10 ml/min, through the array of columns. The eluate was collected in a receptacle and checked for activity. All the activity contained in the solution under analysis was retained in the system of columns after the solution had made one traversal of the system.

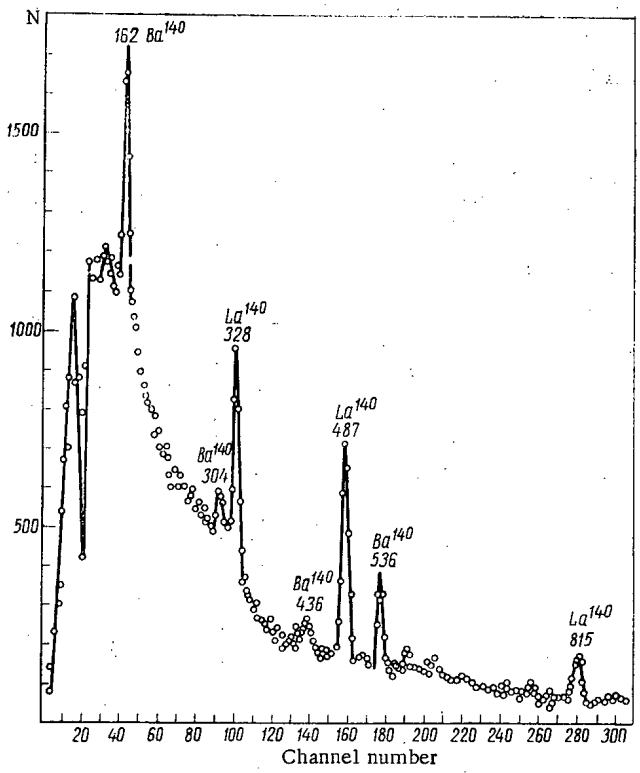

Fig. 4. γ-Ray spectrum of fraction separated out on third column.

The columns, together with the vessel for the original working solution, were washed with 10 to 20 ml 0.01 M solution of formic acid. No activity was detected in the wash effluent. The coating and washing operations take 15 to 20 min. After washing, the system was analyzed. The third column was washed with 10 ml 6 N hydrochloric acid (1.5 to 2 free volumes). Each column and the test tube with the eluate from the third column were covered with stoppers and measured on a γ-ray spectrometer with a 512-channel analyzer.

As was to be expected, quantitative absorption of iodine takes place in the first column: the γ-ray spectrum (Fig. 1) indicates the presence of the isotope I^{131}. No other elements were detected in the first column. The γ-ray spectrum of the second column (Fig. 2) is indicative of the presence of isotopes Ce^{141} and Ce^{144}, i.e., absorption of rare earths is observed in the second column. No isotopes of other elements were detected. The isotope La^{140} is lacking, since the measurements were taken 19 days after the chemical separation had been effected. Isotopes Cs^{137} and Cs^{134} (see Fig. 3) were detected in the eluate from the third column. Ba^{140} and its daughter La^{140} remained in the column (Fig. 4). The extent to which the separation of each group of elements in the respective fraction went to completion is confirmed by the absence of activity in the filtrate taken from the system of columns, and by the absence of mutual contamination of the distinct fractions.

The scheme of express chromatographic groupwise separation of fission products contained in the reactor loop waters, with subsequent identification of the isotope composition on a semiconductor γ-ray spectrometer as described, is thus proposed as a regular technique.

The authors take this opportunity to express their deep thanks to Yu. E. Loginov for having made it possible to use the Ge(Li)-γ-ray spectrometer for the measurements, and for the assistance which he kindly rendered in the work.

LITERATURE CITED

1. Radiochemical Studies of Fission Products, Vol. I-III, New York (1951).
2. Radiochemical Analysis of Fission Products [in Russian], Yu. M. Tolmachev (editor), Izd-vo AN SSSR, Leningrad (1960).

3. Yu. P. Saikov, Atomnaya Énergiya, 20, 123 (1966).
4. O. A. Miller et al., Atomnaya Énergiya, 25, 524 (1968).
5. B. K. Preobrazhenskii et al., Radiokhimiya, 10, 377 (1968).

EXPERIMENTAL VERIFICATION OF THE RADIATION-CHEMICAL METHOD FOR PRODUCING TETRACHLOROALKANES

A. A. Beér, P. A. Zagorets,
V. F. Inozemtsev, L. A. Maiorov,
V. I. Slavyanov, G. A. Artyushov,
I. F. Sorygaev, and V. A. Novozhilov

UDC 541.15

A pilot plant designed to produce new products, tetrachloroalkanes, by radiation-chemical methods was put on stream in late 1967 at the Grozny chemical combine. At the present time, the experimental operations have been pretty much completed, and current plans envisage expanding the facility to full industrial scale.

The tetrachloroalkanes are of great interest to the chemical processing industry, as semifinished products useful in the synthesis of polymeric materials, additives, lubricants, pesticides, stabilizers, plasticizers, etc., [1]. Tetrachloropropane and tetrachloropentane are acquiring special importance.

The tetrachloroalkanes are obtained by a reaction of telomerization from ethylene and carbon tetrachloride:

$$x \cdot C_2H_4 + CCl_4 = Cl(CH_2CH_2)_xCCl_3.$$

This reaction is usually initiated by free radicals obtained via thermal decomposition of peroxides or azo-compounds. It has been shown [2-4] that this reaction is initiated by γ-emission from Co^{60}, and the radiation method of initiation has certain advantages here. Subsequently, the radiation-chemical process has been described in the literature by other investigators as well [5, 6].

On the basis of their research findings, the present authors designed and built a pilot plant with two divisions, one for telomerization, the other for rectification, of the tetrachloroalkanes. The basic layout of the telomerization division is shown in Fig. 1.

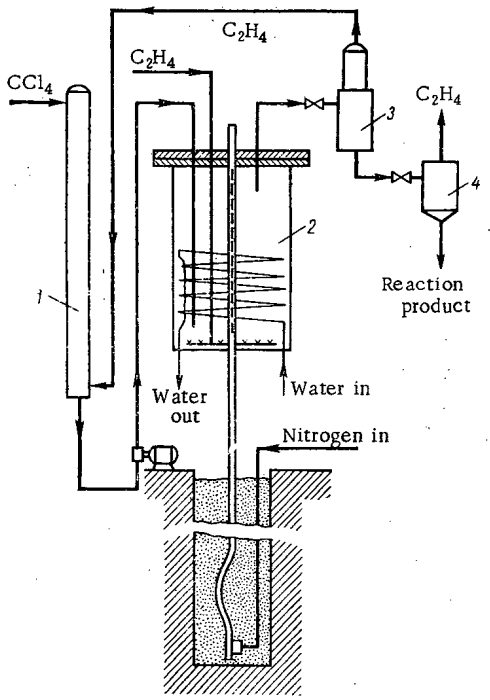

Fig. 1. Basic layout and flowsheet of facility designed for radiation telomerization between CCl_4 and C_2H_4 (reaction unit).

Carbon tetrachloride is supplied by the pump to the absorber tower 1 for absorption of unreacted ethylene. The solution enters the reactor 2, into which compressed ethylene is bubbled. The sources (total activity ~18 kg-equivalents radium) are raised up from their storage pool into the central irradiator tube of the reactor under pressure from compressed nitrogen [7]. The irradiated mixture from the reactor is then throttled to 3-5 atm in the separator 3. The unreacted ethylene from the separator is directed to the absorber tower 1, where it is dissolved in carbon tetrachloride and recycled to the process. Liquid reaction products leaving the separator 3 are throttled to atmospheric pressure in the separator 4, and pass

Translated from Atomnaya Énergiya, Vol. 29, No. 6, pp. 461-463, December, 1970. Original article submitted June 10, 1970.

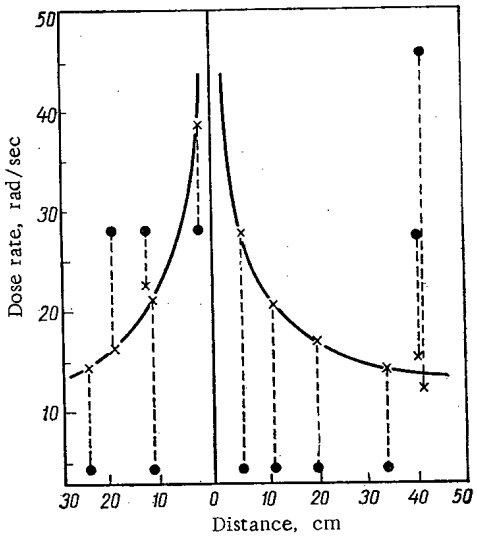

Fig. 2. Dose field of reactor (according to data provided by ferrosulfate dosimeters): •) location of dosimetric capsule; ×) dose rate.

from there to the rectification step so that the unreacted carbon tetrachloride can be driven off (and recycled to the process), and the pure tetrachloroalkanes can be isolated.

All of the process equipment was made of Kh18N10T steel. The absorber tower was packed with porcelain rings. The reactor, 550 liters in volume and 800 mm in diameter, was equipped with a coil for heating or cooling, and a bubbler for feeding the ethylene stream.

The process is carried out at 15-20 atm and 100°C, for 6 h, and the resulting reaction mixture contains ~80% unreacted carbon tetrachloride and approximately equal quantities of tetrachloropropane and tetrachloropentane. The impurity content remains the same, to within a fraction of a percent.

The assigned process parameters correspond to the molar composition of the irradiated mixture $R = [CCl_4]/[C_2H_4] = 5 \sim 10$. Any change in this composition will mean a change in the content of the distinct tetrachloroalkanes in the mixture, as described by the equations

$$F_1 = \frac{C_1 R}{(C_1 R + 1)}; \quad F_2 = \frac{C_2 R}{(C_1 R + 1)(C_2 R + 1)};$$

$$F_3 = \frac{C_3 R}{(C_1 R + 1)(C_2 R + 1)(C_3 R + 1)} \text{ etc.}$$

where F_i is the molar fraction of the telomer in the mixture; R is the molar ratio $[CCl_4]/[C_2H_4]$; C_i is the transfer constant.

The transfer constants, according to the data collected by the present authors, have the following values:

Temperature, °C	C_1	C_2	C_3
0	0.045	3	10
20	0.059	2.9	9
50	0.89	2.8	7
100	0.155	2.7	5
140	0.218	2.6	4.7

A drop in the reaction temperature will depress the content of tetrachloroalkanes in the reaction mixture slightly, since the energy of activation of the reaction is 5.5 kcal/mole.

Dosimetric monitoring of the reactor (with the aid of a methylene blue solution) showed the average absorbed dose rate to be 10 rad/sec. The dose field in the interior of the reaction, taken from readings of ferrosulfate dosimeters, is given by the curve plotted in Fig. 2.

The radiation-chemical yield (converted to the dose rate 1 rad/sec) is 22,000 to 27,000 molecules of tetrachloroalkanes per 100 eV of radiation absorbed. According to laboratory data, the yield is inversely proportional to the dose rate, with the exponent 0.73, and is equal to 30,000 molecules per 100 eV at a dose rate of 1 rad/sec.

The radiation efficiency is 0.23, which is below the rating (0.38).

The formula

$$P = 3.7 \cdot 10^{-9} M_{av} g' (\eta A)^{0.27} (V\rho)^{0.73},$$

where P is the reactor throughput, in kg/h; g' is the radiation-chemical yield at a dose rate of 1 rad/sec, M_{av} is the average molecular weight of the tetrachloroalkanes, η is the radiation efficiency; A is the source

activity [gram-equivalents radium]; V is the reactor effective volume [liters]; ρ is the specific weight of the irradiated mixtures [g/cm^3], was proposed for large-scale simulation of the process, and was checked for experimental verification.

The experimental verification revealed that the process takes place in a stable manner, responds amenably to control measures, and ceases immediately after the sources are removed from the reactor core. A slight induction period was discovered. The process parameters and the composition of the resulting mixture were found to be in close agreement with laboratory data.

The discharge coefficient of the carbon tetrachloride at the telomerization step is 0.8 to 0.9 (the theoretically predicted discharge coefficient is 0.78). Ethylene losses are negligible.

The tetrachloroalkanes obtained after rectification exhibit the required degree of purity.

This flowsheet is a reliable one, but could be improved. The process equipment should be made of titanium, since stainless steel is still subject to corrosive attack.

Optimization calculations were performed, on the basis of prevailing prices, with due attention to the basic features of the process, on reactor dimensions and activity of radiation sources for different levels of productivity. It was found economically feasible to utilize a reactor of fairly large volume with low-level irradiators. For example, the optimum reactor volume for a throughput of 200 kg/h was found to be ~5 m^3, with the activity of the sources set at 55 to 60 kg-equivalents radium.

Engineering cost calculations showed that the net cost of tetrachloroalkanes in full-scale industrial production is 600 to 700 rubles/ton. Compared to the process achieved with azo-bis-isobutyronitrile, the radiation-chemical method requires much less initiator (the amount required is cut by 10 to 20 times).

LITERATURE CITED

1. R. Kh. Freidlina and Sh. A. Karapetyan, Telomerization and New Synthetic Materials [in Russian], Izd-vo AN SSSR, Moscow (1961).
2. M. A. Besprozvannyi, A. A. Beér, and G. B. Ovakimyan, Inventors' Certificate No. 106988, Byull. Izobret., No. 14 (1957).
3. A. A. Beér et al., in: Radioactive Isotopes and Nuclear Radiations in the National Economy of the USSR [in Russian], Gostoptekhizdat, Moscow (1961), p. 211.
4. A. A. Beér et al., Neftekhimiya, 2, 617 (1962).
5. C. David and P. Gosselian, Tetrahedron, 18, 369 (1962).
6. M. Takehisa, M. Yasumoto, and J. Hosaka, Kogyo Kagaku Zasshi, 65, 531 (1962); ibid., 66, 259 (1963).
7. V. A. Dobrovol'skii, B. I. Ryabov, and Yu. V. Kastrup, Inventors' Certificate No. 166975, Byull. Izobret., No. 24 (1961).

USE OF XENON PROPORTIONAL COUNTER ESCAPE PEAKS FOR X-RAY RADIOMETRIC ANALYSIS OF TUNGSTEN IN ORES

N. G. Bolotova, V. V. Kotel'nikov, and E. P. Leman

UDC 550.835

The use of proportional counters significantly expands the technical capabilities of x-ray radiometric ore analysis and increases the number of elements which can be determined by this method. For example, the high accuracy and sensitivity of x-ray radiometric analysis in the determination of elements with atomic numbers $Z \leq 30$ by means of the characteristic radiation of the K series can only be achieved with the help of proportional counters [1]. An increase in dimensions and an increase in filling-gas pressure to atmospheric makes it possible to increase the efficiency of xenon proportional counters to the extent that elements with a Z of 40-55 are determined from the K series with satisfactory accuracy and sensitivity [2, 3]. For elements with $Z > 60$, the analysis can be made on the basis of the characteristic radiations of the L series [4] since the detection efficiency for 60-100 keV photons is very small in proportional counters. Use of the K series of these elements for proportional counter analysis is only possible in practice by recording the escape peaks [5].

The escape peaks of xenon counters are of particular interest in the determination of heavy elements (with $Z \geq 70$) in ores, and particularly tungsten. Tungsten determination by means of the L series is complicated by the fact that it is close in energy (8.5 keV) to the K lines of iron (6.5 keV), copper (8.0 keV), and zinc (8.6 keV), which are often present in ores along with the tungsten, and the counter resolution in

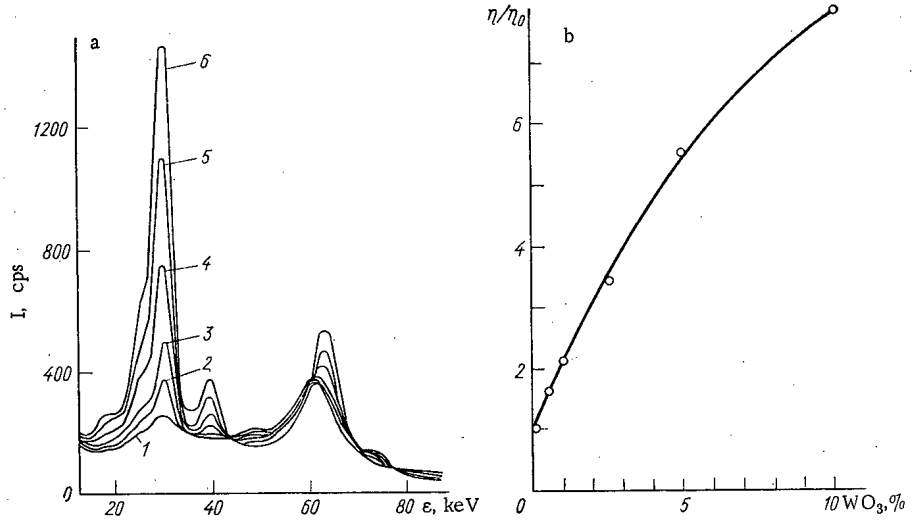

Fig. 1. Example of the use of escape peaks in an SRPO-12 xenon proportional counter for determination of tungsten content in ores by means of the K-series characteristic x-ray radiation (Co^{57} source): a) secondary γ-spectra obtained from simulated samples with varying content of tungsten trioxide; 1) 0; 2) 0.5%; 3) 1%; 4) 2.5%; 5) 5%; 6) 10%; b) dependence of spectral ratios on tungsten trioxide content in simulated samples.

Translated from Atomnaya Énergiya, Vol. 29, No. 6, pp. 463-465, December, 1970. Original article submitted May 14, 1970.

this energy region, which is 18-20%, is insufficient for complete separation. The tungsten K lines (57-59 keV) efficiently excite the characteristic radiation of the xenon filling in a proportional counter. The xenon is practically transparent to its own characteristic x radiation, and the radiation consequently leaves the counter or is absorbed in the counter walls producing clearly defined escape peaks. The intensity of an escape peak is determined by the photon flux in the characteristic K radiation from tungsten and the position of the peak in the secondary spectrum – the energy difference between the K radiations of xenon and tungsten (see Fig. 1a).

An SRPO-12 xenon proportional counter was used as the detector. The characteristic tungsten x radiation was excited with a Co^{57} source (123 keV). Measurements were made with an AI-8 spectrometer on simulated samples of tungsten ores (a mixture of quartz sand and gypsum was used as filler) over a large solid angle without collimation of the radiation. A maximum was observed in the 60 keV region of the secondary instrumental spectra which resulted from the superposition of the tungsten K lines (57-59 keV) and the xenon K-series escape peak for singly scattered radiation (~90 keV) from the Co^{57} source. This situation, along with the low detection efficiency for photons with energies above 50 keV, prevents the use of xenon counters for the determination of tungsten in ores by means of the characteristic K radiation.

A different picture was observed in the spectral region 20-40 keV where one finds the xenon escape peaks associated with the tungsten K series. Three peaks were very clearly distinguished: the first (in the 25 keV region) corresponds to the energy difference between the tungsten K_α lines and the xenon K_β lines; the second (in the 29 keV region) is equal to the difference between the energies of the xenon and tungsten K_α lines; the third (with energies of 37-38 keV) results from the difference between the energies of the K_β line of tungsten and the K_α line of xenon. The intensity of the escape peaks increases with an increase in tungsten concentration. The most intense peak is the second one, which can be used as an analytic line for spectral ratio techniques.

Figure 1b gives the curve for the dependence of spectral ratios on tungsten trioxide content in simulated samples. Scattered radiation at 46 keV was chosen as the internal standard for background. The spectral ratios η were normalized to the value η_0 in the ore-free sample. The η/η_0 curve is close to linear in the tungsten trioxide concentration range 0-5%. The sensitivity of the analysis can be increased by using collimation of the radiation and by reducing the scattered radiation background in the region of the escape peaks. Thus x-ray radiometric analysis of some heavy elements, and of tungsten in particular, by means of characteristic K-series x radiation can be performed with the help of the escape peaks from xenon proportional counters when direct recording of the K radiations of these elements proves to be impossible or inefficient. Such a method can be used for the determination of tungsten in tungsten and molybdenum–tungsten ores. In the analysis of antimony–tungsten or tin–tungsten ores, the use of this technique is complicated by the fact that the xenon escape peaks resulting from the presence of tungsten coincide in energy with the analytic K lines of antimony and tin.

LITERATURE CITED

1. R. I. Plotnikov et al., Instruments and Methods in X-Ray Analysis [in Russian], No. 2, Izd. SKBRA, Leningrad (1967), p. 126.
2. E. P. Leman et al., Development of Geology and Mine-Survey Services in Nonferrous Metallurgical Enterprises (Mining Industry Series) [in Russian], Izd. TsNIItsvetmetinformatsiya, Moscow (1970), p. 31.
3. A. L. Yakubovich, E. I. Zaitsev, and S. M. Przhiyalgovskii, Nuclear Physics Methods for the Analysis of Minerals [in Russian], Atomizdat, Moscow (1969).
4. I. V. Tomskii, V. N. Mitov, et al., Instruments and Methods in X-Ray Analysis [in Russian], No. 5, Izd. SKBRA, Leningrad (1969), p. 111.
5. R. I. Plotnikov et al., Instruments and Methods in X-Ray Analysis [in Russian], No. 2, Izd. SKBRA, Leingrad (1967), p. 121.

DIAGNOSTICS OF AN ELECTRON – ION BUNCH USING BREMSSTRAHLUNG

M. L. Iovnovich, V. P. Sarantsev, and M. M. Fiks

UDC 533.95:621.039.61

A new method has been proposed [1] for the collective acceleration of ions. The method is based on the possibility of creating electron–ion bunches which are accelerated as a unit in external electromagnetic fields. The creaction of a bunch begins with the formation in an external magnetic field of a thin ring of relativistic electrons (major radius of the ring is R, minor radius is a) where storage of ionized atoms occurs. The storage process has been discussed [2-4]. During storage, bremsstrahlung from the electrons arises through electron collisions with atoms and ions, and this bremsstrahlung can be used for bunch diagnostics.

The bremsstrahlung from a relativistic electron in an atomic nucleus is essentially anisotropic. For $\gamma \gg 1$ (γ is the electron relativistic factor in the bunch at rest), almost all the radiation is concentrated in a small solid angle $\Omega = 4\pi \sin^2(\theta/2)$, where $\theta/2 = 1/\gamma$ is the angle between the photon direction of propagation and the tangent to the trajectory at the point of radiation [5].

The average number N of photons with energies $\varepsilon = h\nu/mc^2 \geq \varepsilon_0$ emitted by the ring per unit time into an angle Δ, within which the "illuminated" portion of the radiation detector is seen, is determined by the expression

$$\frac{dN}{dt} = \sum_{Z_0} \int_{\varepsilon_0}^{\varepsilon} d\varepsilon' \Phi(Z_0, \varepsilon')\, dQ \sum_{Z=0}^{Z_0} n_{Z_0 Z} j_e R \frac{4\pi}{\Omega_0} \int d\varphi \sin^2 \frac{\Delta}{4}, \quad (1)$$

where $\Phi(Z_0, \varepsilon)$ is the cross section for emission of photons with energies in the range ε, $\varepsilon + d\varepsilon$ from a nucleus of charge Z_0, $n_{Z_0 Z}$ is the concentration of heavy particles (Z_0 is the nuclear charge and Z is the ionic charge), and j_e is the electron current density in the ring.

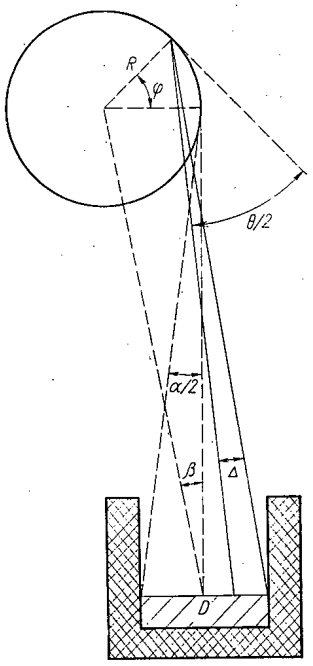

Fig. 1. Diagram of the arrangement of the bremsstrahlung detector D.

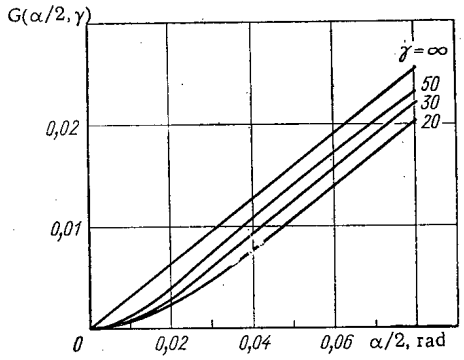

Fig. 2. Ratio of bremsstrahlung intensity incident on the detector to the total intensity from the entire ring.

Translated from Atomnaya Énergiya, Vol. 29, No. 6, pp. 465-467, December, 1970. Original article submitted January 4, 1970.

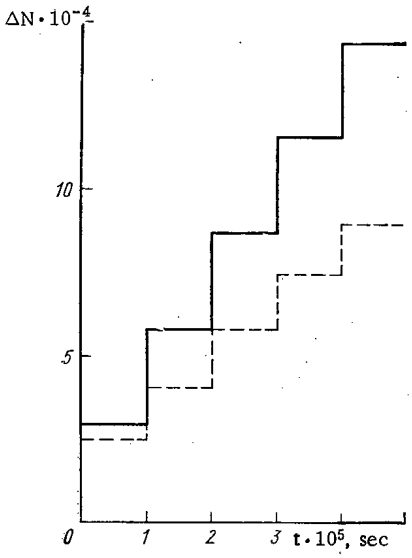

Fig. 3. Number of photons with energies $0.1 \leq h\nu \leq 1.0$ MeV incident on the detector in an interval $\Delta t = 10^{-5}$ sec: ——) storage from atomic beam; – – – –) storage from residual gas; $n_e = 10^{14}$ cm^{-3}, $a = 0.1$ cm, $N_e = 10^{14}$, $\alpha/2 = 0.02$.

Integration is carried out over the ring cross section $Q = \pi a^2$. Equation (1) was obtained under the assumption the electron current was transparent to photons.

If the detector dimension $d \gg a$ and the electron and heavy particle concentrations are constant over the cross section Q of the ring, then

$$\frac{dN}{dt} = N_e c \sum_{Z_0} \int_{\varepsilon_0}^{\varepsilon} d\varepsilon' \Phi(Z_0, \varepsilon') \sum_{Z=0}^{Z_0} n_{Z_0 Z} \frac{2}{\pi} \gamma^2 \int d\varphi \sin^2 \frac{\Delta}{4}, \tag{1a}$$

where N_e is the total number of electrons in the ring.

The function $\Delta(\varphi)$ and the equations which determine the limits of integration over φ are found from simple geometric considerations (see Fig. 1). In the case where not only $1/\gamma \ll 1$ but also $\alpha/2 \ll 1$, $\beta < 1$, one can obtain an approximate evaluation of the geometric factor $G(\alpha/2, \beta, \gamma) = (2/\pi)\gamma_2 \int d\varphi \sin^2(\Delta/4)$ in analytic form:

$$G\left(\frac{\alpha}{2}, \gamma\right) \approx \begin{cases} \frac{1}{3\pi}\left(3\frac{\alpha}{2} - \frac{1}{\gamma}\right) & \frac{\alpha}{2} \geqslant \frac{1}{\gamma}; \\ \frac{1}{3\pi}\gamma^2\left(\frac{\alpha}{2}\right)^2\left(3\frac{1}{\gamma} - \frac{\alpha}{2}\right) & \frac{\alpha}{2} \leqslant \frac{1}{\gamma}. \end{cases} \tag{2}$$

The family of curves $G(\alpha/2, \beta, \gamma)|_{\substack{\gamma=\text{const} \\ \tan\beta = 2.5\tan(\alpha/2)}}$ is shown in Fig. 2.

During storage of a single type of ion of a monatomic gas, the radiation intensity and the number of photons incident on the detector in a time t are given by

$$\frac{dN}{dt} = \left(\frac{dN}{dt}\right)_0 G\left(\frac{\alpha}{2}, \beta, \gamma\right) s(t); \tag{3}$$

$$N(t) = \left(\frac{dN}{dt}\right)_0 G\left(\frac{\alpha}{2}, \beta, \gamma\right) p(t), \tag{4}$$

where

$$\left(\frac{dN}{dt}\right)_0 = N_e c n_a \int_{\varepsilon_0}^{\varepsilon} d\varepsilon' \Phi(Z_0, \varepsilon') \tag{5}$$

is the radiation intensity of the entire bunch at the initial time $t = 0$; n_a is the neutral atom concentration near the bunch, and the functions $s(t) = \sum_{Z=0}^{Z_0} n_{Z_0 Z}/n_a$ and $p(t) = \int_0^t s(t')dt'$ are defined in [4].

Small values of ε make the main contribution to the integral in Eq. (5). For reason of computational convenience, we therefore use an expression for $\Phi(Z_0, \varepsilon)$ which is valid for the case of small energies (complete screening) [5]:

$$\Phi(Z_0, \varepsilon) = \frac{4Z_0^2}{137} r_e^2 \frac{1}{\varepsilon}\left\{\left[1 + \left(1 - \frac{\varepsilon}{\gamma}\right)^2 - \frac{2}{3}\left(1 - \frac{\varepsilon}{\gamma}\right)\right] \ln(183 Z_0^{-1/3}) + \frac{1}{9}\left(1 - \frac{\varepsilon}{\gamma}\right)\right\}, \tag{6}$$

where $r_e = e^2/mc^2$ is the classical radius of the electron. Equation (6) is applicable for photon energies up to the value $\varepsilon_{max} \approx \gamma^2/137 + \gamma$. Following integration, we obtain

$$\left(\frac{dN}{dt}\right)_0 = \frac{4Z_0^2}{137} N_e c n_a r_e^2 \left\{\left[\frac{4}{3}\ln 183 Z_0^{-1/3} + 1/9\right]\left[\ln\frac{\varepsilon}{\varepsilon_0} + \frac{\varepsilon - \varepsilon_0}{\gamma}\right] + \frac{\varepsilon^2 - \varepsilon_0^2}{2\gamma^2}\ln 183 Z_0^{-1/3}\right\}. \tag{7}$$

The limits of integration, ε_0 and ε are determined by the spectral sensitivity of the detector. The number of photons detected during the time of storage depends on the spectral sensitivity of the detector and the detection efficiency. For bunch diagnostics, one can use a germanium–lithium detector, for which the maximum spectral sensitivity is in the photon energy range 0.1-1.0 MeV, and the detection efficiency is a few tens of percent with an energy resolution of ~2%. The frequency of electron synchrotron radiation, which forms the background in these measurements, is many orders of magnitude less than that of the radiation detected. By measuring the radiation intensity, one can determine the total concentration of heavy particles in the ring with an accuracy of a few percent.

Figure 3 shows the number of photons in the energy range mentioned reaching the detector during storage of xenon ($Z_0 = 54$) (broken down into intervals $\Delta t = 10^{-5}$ sec). This data indicates that one can study the process of xenon storage in bunches having electron numbers $N_e \gtrsim 3 \cdot 10^{12}$.

The study of ions formed from diatomic gases, particularly protons, requires special consideration. Nevertheless, one can assume that in a bunch with $N_e = 10^{14}$, the observation of proton storage is feasible if the concentration of hydrogen molecules in the region of the bunch is roughly two orders of magnitude greater than the concentration of residual gas molecules.

We note in conclusion that the proposed diagnostic technique also allows one to determine the total number of electrons in a ring since the initial concentration of heavy particles is known.

The authors thank A. B. Kuznetsov, Yu. Ts. Oganesyan, and N. V. Rubin for discussions of the problems involved.

LITERATURE CITED

1. V. I. Veksler et al., Atomnaya Énergiya, 24, 317 (1968).
2. M. L. Iovnovich, N. B. Rubin, and V. P. Sarantsev, JINR Preprint, P9-4257, Dubna (1969).
3. Symposium on Electron Ring Accelerators, UCRL-18103, Berkeley (1968).
4. M. L. Iovnovich and M. M. Fiks, this issue p. 1199.
5. Experimental Nuclear Physics [Russian translation], E. Segre (editor), Vol. 1, Izd-vo IL, Moscow (1955).

EXCITATION OF RADIAL BETATRON OSCILLATIONS BY A LONGITUDINAL ACCELERATING FIELD

Yu. S. Ivanov, A. A. Kuz'min, and G. F. Senatorov

UDC 621.384.6

In the adjustment and use of proton synchrotrons it is essential to be in possession of adequate information regarding the frequency of the betatron oscillations during the whole cycle of acceleration.

Usually at the beginning of the cycle one encounters intrinsic coherent oscillations of the center of gravity of the beam of accelerated protons, due to the nonzero initial conditions prevailing on injection; however, the period of their "coherence," which is mainly determined by the distribution function of the particles in the beam with respect to the betatron-oscillation frequencies, is not very long. For example, in the case of the 70 GeV accelerator of the Institute of High-Energy Physics, under normal operating conditions the period of coherence is no longer than 3 to 5 μsec.

In order to measure the frequencies of the betatron oscillations throughout the whole acceleration cycle, the oscillations must first be excited [1].

In this paper we shall consider one of the methods of exciting coherent radial betatron oscillations. The method is of the resonance type; however, in contrast to the method described earlier [2], the periodic stimulating force varies the longitudinal rather than the transverse momentum of the center of gravity of the beam.

It is well known [3] that the radial betatron oscillations of a particle with a momentum differing from the equilibrium value are described by the equation

$$\frac{d^2x}{dt^2}+Q^2\omega^2x=\omega^2r_0\frac{\delta p}{p}, \qquad (1)$$

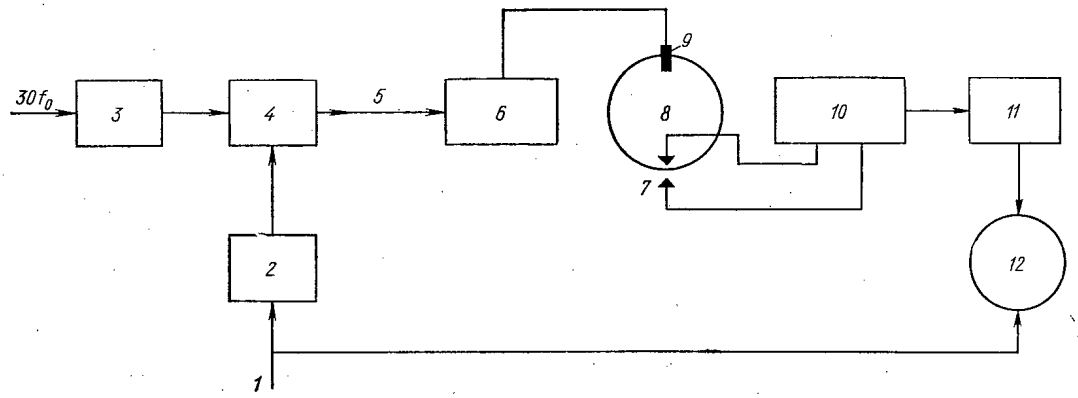

Fig. 1. Arrangement for the excitation and observation of betatron oscillations: 1) pulse initiating the excitation; 2) control system; 3) frequency divider; 4) key; 5) modulating voltage; 6) accelerating stage; 7) signal electrodes; 8) ring; 9) resonator; 10) differential amplifier; 11) low-frequency filter; 12) oscilloscope.

Translated from Atomnaya Énergiya, Vol. 29, No. 6, pp. 467-469, December, 1970. Original article submitted December 17, 1969.

where x is the radial deviation of the particle from the equilibrium value; ω is the frequency of revolution; t is the time; Q is the frequency of the betatron oscillations; δ_p is the deviation of the longitudinal momentum from equilibrium; p is the total momentum of the particle; and r_0 is the average radius of the accelerator.

If the voltage on one of the accelerating stages is modulated in accordance with a law of the f(t) type, then

$$\frac{d^2x}{dt^2}+Q^2\omega^2x=r_0\omega^2\sum_{n=0}^{N-1}\frac{\Delta p_0}{p}f(t)\,H(t-n\tau_0), \tag{2}$$

where Δp_0 is the maximum possible difference of the momentum from equilibrium; H is a unitary function; τ_0 is the period of rotation of the particle; and N is the number of turns.

Let us consider simply the forced solution of (2):

$$x=\omega r_0\Delta p/pQ\int_0^t\sum_{n=0}^{N-1}f(t)\,H(t-n\tau_0)\sin Q\omega(t-\tau)\,d\tau. \tag{3}$$

If f(t) = sin qωt (where q is an arbitrary number), then expression (3) takes the form

$$x=\omega r_0\Delta p_0/pQ\sum_{n=0}^{N-1}\sin q\,\omega n\tau_0\int_{n\tau}^{t}\sin Q\omega(t-\tau)\,d\tau, \tag{4}$$

or finally

$$x=r_0\Delta p_0/2pQ^2\left\{2\sum_{n=0}^{N}\sin 2\pi nq+\cos Q\vartheta\sum_{n=0}^{N}[\sin 2\pi n(q+Q)+\sin 2\pi n(q-Q)]+\sin Q\vartheta\sum_{n=0}^{N}[\cos 2\pi n(q-Q)-\cos 2\pi n(q+Q)]\right\}, \tag{5}$$

where $\vartheta = \omega t$.

When

$$Q\pm q=m$$

(where m = 0, ±1, ±2, . . .), solution (5) assumes the resonance form.

The most interesting case is that in which m is the closest whole number to the frequency of the betatron oscillations Q. This corresponds to the lowest modulation frequency, and it constitutes an important factor, since the accelerating stages are quite narrow-banded (the band width of the accelerating stages in the Institute's synchrotron is of the order of 80 to 100 kc/sec).

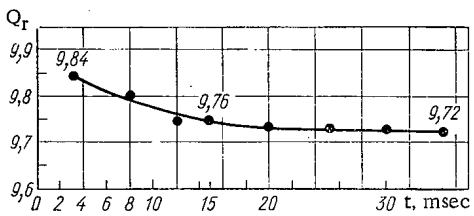

Fig. 2. Time dependence of the betatron-oscillation frequency.

The frequencies of the phase oscillations differ considerably from the frequencies qω, and the mutual influence of the radial and phase oscillations may be neglected [2]. In order to confirm the theoretical results we carried out some experiments on the excitation of radial oscillations in the Institute's proton synchrotron.

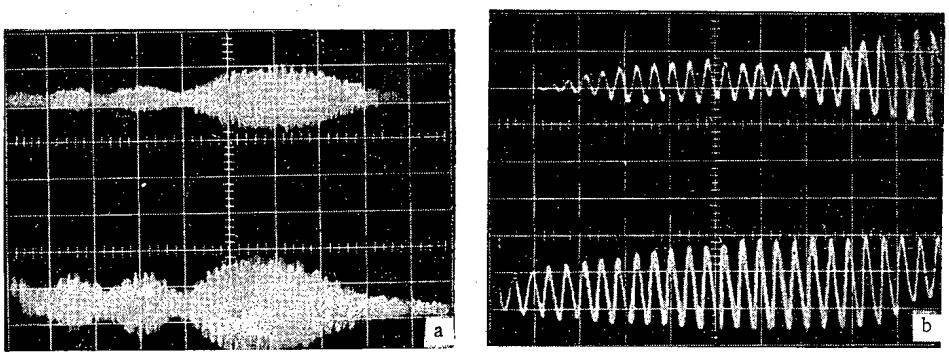

Fig. 3. Oscillograms of the build-up of radial and vertical betatron oscillations: a) sweep 200 μsec/cm; b) sweep 70 μsec/cm.

A block diagram of the arrangements for exciting and observing the betatron oscillations is presented in Fig. 1. The voltage from a master generator with a frequency of $30f_0$ (f_0 being the frequency of rotation of the particles) is fed to a frequency divider, which divides this frequency by a whole number n (n may vary in unit steps from 67 to 300). The signal at a frequency of $30f_0/n$ is amplified, passes through a timer-controlled key, and is applied to the grid of the output tube of the accelerating stage, as a result of which the amplitude of the accelerating voltage is modulated.

The measuring system is also controlled by a timer and contains low-frequency filters considerably increasing its sensitivity.

An oscillograph incorporating a memory enables information relating to the betatron oscillations to be analyzed directly from the screen; alternatively, the processes may be photographed and analyzed later.

Our experiments enabled us to measure the frequency of the radial betatron oscillations and also to establish the relationship between the radial and vertical oscillations at individual points of the cycle up to energies of the order of 2 GeV. For energies greater than 2 GeV the betatron oscillations of the beam could not be increased to amplitudes sufficient to allow accurate measurement (~0.5 mm) using only one accelerating stage.

Figure 2 shows the experimental time dependence of the betatron-oscillation frequency in the accelerating cycle. This relationship may be varied by adjusting the accelerator.

Figures 3a and b present photographs of two oscillograms obtained when studying the development of betatron oscillations. The upper oscillograph beam represents the excitation of the radial oscillations and the lower beam represents that of the vertical oscillations arising from the coupling between the radial and vertical oscillations of the beam. The processes give the appearance of passing through resonance, and in Fig. 3b (corresponding to a faster sweep) we see how the energy is transferred from one form of oscillation to the other.

These results demonstrate the efficiency of the proposed method of exciting radial betatron oscillations at low energies. The use of this method requires no special excitation apparatus and hence demands no space for locating such apparatus in the accelerator ring.

In conclusion, the authors wish to thank V. E. Pisarevskii, A. M. Gudkov, and V. P. Ustinov for help in the experiments.

LITERATURE CITED

1. V. A. Uvarov and G. F. Senatorov, Pribory i Tekh. Éksperim., No. 6, 20 (1968).
2. A. A. Kolomenskii and A. N. Lebedev, Theory of Cyclical Accelerators [in Russian], Fizmatgiz, Moscow (1962).
3. A. Shoch, Theory of Linear and Nonlinear Perturbations of Betatron Oscillations in Alternating-Gradient Synchrotrons, CERN, Geneva (1958).

NEWS

LIEGE MAY 1970 INTERNATIONAL SYMPOSIUM ON MODERN ELECTRIC POWER GENERATING STATIONS

P. A. Andreev

An international symposium on modern electric power generating stations was held in Liege (Belgium) in May 1970, and attracted over 500 specialists from 22 countries. A total of 52 papers was presented at this symposium, dealing the design, fabrication, investigation, adjustment, and operation of heat process equipment and electromechanical equipment for modern electric power stations. Topics covered in the papers ranged over: nuclear-fueled electric power stations, gas turbine plants and gas turbines, hydroelectric power stations, and electric power generating stations burning fossil fuels.

Attention was centered on nuclear power at this symposium; topics focused upon were equipment and operating experience, in relation to nuclear power stations based on different types of reactors, with a large number of papers taking up these questions and provoking a lively discussion. Equally close attention was given to the urgent problems of reliability and efficient use of the basic power equipment in modern nuclear power stations with water-cooled reactors and above all water-moderated water-cooled reactors (reactors, steam generators, steam turbines, and circulating pumps). The outlook for nuclear power development and forecasts projecting into the future of nuclear power were discussed to a lesser extent.

Awareness of the damage suffered by the thermal shielding in reactors similar in design to the American Westinghouse Corp. reactors (e.g., the damage to the SENA Franco–Belgian power station reactor) lent added interest to a report on experience in the adjustment and startup of the Obrigheim (West Germany) power station.

The first full-scale tests of an unloaded reactor to probe into temperature and fluid dynamic conditions brought on severe vibrations in the thermal shielding because of the impact of the stream of water. These vibrations resulted in severe damage to the surfaces of the reactor pressure vessel, on which the thermal shielding, 28 tons in weight, rested freely. After trying out several variants in fastening the shielding structures which failed to pay off, even after over 1500 h of testing, a reliable design was worked out which was checked out again after fuel had been loaded in. A special feature of this successful design variant is seen in the six support brackets with welded-on retaining vertical backup plates to which the thermal shielding is pinned. This mode of fastening allows free radial and axial temperature expansion of the shielding while holding it rigidly fast against any rotational displacements.

Another source of malfunction and misalignment in the performance of the power station was the excessively high moisture content of the steam feed to the turbine, as a result of the unsuccessful design of the first and second stages of the steam separator. Attempts to cope with this led to working out a new design of the separator first stage on full-scale models, with a horizontal cyclone, and using thin moisture traps manufactured by the Peerless firm as the second separator stage. The separation system thereafter brought about a moisture content of not more than 0.25% in the steam under the entire range of operating conditions of the nuclear power station.

Because of the excessive amount of wear on the seals, malfunctions of the main circulation pumps were also reported; the rapid wear on ring seals made of tungsten carbide is accounted for by the high boron content in the primary coolant. A satisfactory solution was found through the use of ring seals coated with chromium oxide.

It is interesting to note that computer process monitoring of the operation of the Obrigheim nuclear power station, using the Siemens-305 computer, shows much promise, with 450 analog variables monitored and ~2200 binary signals processed.

Translated from Atomnaya Énergiya, Vol. 29, No. 6, pp. 470-471, December, 1970.

The symposium discussed cleanup of primary loop water at nuclear power stations. Since the commonly encountered water treatment systems using ion exchange, degassing, and evaporation equipment fail to provide efficient filtration of active corrosion products, it was proposed that the problem be solved through recourse to special mechanical filters.

A report presented by the Belgian concern Cocril–Ugrais–Providence made a convincing demonstration of the advantages of upright steam generators; data on the advantages of inconel as a material in the fabrication of steam generators, instead of the stainless steel AJSJ-316, were also presented.

Some of the reports dealt with improved design of water-cooled water-moderated reactors, and their operation. Most of the authors of reports analyzing reasons for breakdown of heat processing and transfer machinery at nuclear power stations, reach the unanimous conclusion that the overwhelming majority of failures are due to insufficient knowledge of hydrodynamical phenomena, which are responsible for damaging vibrations, generated under certain sets of operating conditions. Work is now underway everywhere on developing means and techniques for keeping a check on vibrations executed by the internal components of reactors and steam generators.

Lowering capital costs and improving the reliability of power station equipment are of vital significance in efforts to achieve economically competitive nuclear power. This explains the very serious attention being given to the building of more powerful high-efficiency and highly reliable steam turbines for nuclear power stations. Many of the papers presented by leading turbomachinery manufacturing concerns in france, West Germany, Czechoslovakia, the USA, and Switzerland dealt with the design and fabrication of low-speed turbines with extremely high specific power ratings, development and improvements in the design and fabrication of blading for the last stages of turbomachinery (TsND blading) of critically extended blade length, general principles in the design of steam turbines for nuclear power stations, designs of last stages, operating experience, and unitization and typization principles in the standardization of turbomachinery.

Most of the firms view the use of low-speed turbines (in the 1800 rpm or 1500 rpm speed range) as correct for nuclear power stations, but justify this solely in terms of cost considerations, without bringing into question the reliability of modern high-speed turbines. Maximum interest was evoked by a report submitted by the Czechoslovak Skoda works, containing extremely valuable information on the characteristics of the exhaust stages of turbines with blades extending to 1000 mm in length, and with turbine runner speeds up to 3000 rpm, depending on the choice of structural material and on the selection of blade fastening arrangement. Results of an investigation of anticorrosion coatings for long blades designed for service in wet steam, and designs of stator guide blading with suction drainage slits, are presented. Methods for eliminating dangerous vibrations of turbine blades are described.

Valuable experience in coping with and overcoming defects in turbomachinery is communicated in a report devoted to a description of startup operations at the Gundremingen nuclear power station (in West Germany) centered around a 237 MW boiling-water reactor. Repeated failures and fractures of turbine blades in the first stages of a cylinder of an AEG turbine at 1500 rpm resulted in repeated breakdown of power station operations, with downtime lasting over nine months. The reason for the damage lay in pulsations of the stream of steam deriving from uneven moisture distribution in the piping leading to the TsND (the existence of zones with moisture content as high as 12% when the average moisture content only reached 1%). The introduction of changes in the design of the feed pipe connection brought about more uniform distribution of steam moisture; the design of the blade shanks in the first stages and runner disks of TsND.

A report on heavy-water power reactors which presented Canadian experience in this area in a systematic manner evoked considerable interest as did a report on high-temperature gas-cooled reactors.

The French EdF concern, in a report shedding light on five years of operating history of basic heat exchangers, drew the inference that the use of heat-transfer surfaces of complex configuration is not justified, because of difficulties in inspection and removal of flaws, and that efforts should rather be directed to the design of simpler heat exchangers (specifically, smooth-tube exchangers are recommended).

The design of a Japanese experimental fast reactor with a power output rating of 50 MW(e) was also of some interest.

JUNE 1970 PRINCETON SYMPOSIUM ON PLASMA STABILIZATION BY FEEDBACK AND DYNAMICAL TECHNIQUES

D. A. Panov

The extensive development undergone by research on methods for suppressing plasma instabilities by feedback systems or by dynamic stabilization provided the basis for convening a symposium, organized under the sponsorship of the Plasma Physics Laboratory of Princeton University, at Princeton (USA) in June, 1970. The symposium drew participation from scientists of Britain, Italy, Norway, the Soviet Union, France, and West Germany. Forty-eight papers were presented at the sessions of the symposium.

The work done by V. V. Arsenin and V. A. Chuyanov, and published in 1968 [1], has provided a stimulus for developing research on feedback stabilization of plasma, and has furnished a basis for successful experiments on suppressing flute instabilities in the plasma in the magnetic trap of the OGRA-2 thermonuclear fusion machine [2]. The use of a feedback system to stabilize plasma instabilities was first proposed by A. I. Morozov and L. S. Solov'ev in 1964 [3].

Work on plasma stabilization by feedback systems, as presented and discussed at the symposium, touched on many questions ranging from classification of the stabilization mechanisms to the use of feedback in the study of specific modes of instability.

J. Taylor and C. Lashmore-Davis (Britain) showed that relevant feedback systems can be subdivided into two types, active and reactive, depending on the modes of instability to be suppressed. Instabilities of the interchange type, characterized by negative or positive energy of oscillation, belong to the first category. The signal has to be phase-shifted $\pm 90°$ in order to suppress such instabilities in a feedback system. The choice of sign depends on the sign of the energy of oscillation. Instabilities of the interchange type characterized by zero energy of oscillation being in the second category. The conclusion is that the allowable phase shift for the stabilization of such stabilities is either 0° or 180°.

Most of the experimental papers presented at the symposium on the subject of feedback dealt with active plasma stabilization techniques. In those cases, it is possible to write out the dispersion equation with the effect of the feedback loop taken into account, and to derive a theoretical dependence of the shift in the real part of the frequency, of the size of the increment, and of the displacement of the instability threshold, on the gain and on the phase shift in the feedback loop. An excellent concordance between measured dependences and theoretically predicted dependences was demonstrated. The most typical results of that sort are to be found in the papers submitted by T. Symonen (USA) and D. Jessby et al. (USA); these experiments were conducted with alkali plasma generated in Q-machines. Similar results were communicated in a report by B. Anker-Johnson et al. (USA).

A paper submitted by V. A. Zhil'tsov et al. (USSR) demonstrated that when a surface of finite conductivity is placed parallel to the boundary of a plasma, energy absorption in that surface due to the flowing of induced currents in the surface will be greater, under optimized conditions, than the rate of increase in the energy associated with unstable ion-cyclotron oscillations. At the same time, attenuation greater than the instability growth rate is introduced into the plasma. The feedback loop will behave, at a certain phase shift, like a surface of finite conductivity. Results of experiments on the suppression of an ion-cyclotron instability in the plasma in the magnetic trap of the OGRA-2 thermonuclear machine were reported.

In most of the earlier experiments on suppression of instabilities by feedback, the control components used were electrodes placed outside the plasma, or Langmuir probes immersed in the plasma. For understandable reasons, neither of these approaches is applicable to the case of a dense high-temperature plasma.

Translated from Atomnaya Énergiya, Vol. 29, No. 6, pp. 471-473, December, 1970.

On that account, close attention was given in the reports presented at the symposium to techniques involving electrodeless and contactless manipulation of the plasma. Reports by A. Huang et al. (USA) put forth results of successful suppression of a trapping instability in an alkali plasma by microwave radiation at the upper hybrid frequency (~10 GHz) modulated by the feedback loop signal. A report by F. Cheng (USA) drew attention to the fact that direct utilization of microwave radiators to set up a contactless feedback loop is fraught with difficulties in the case of a thermonuclear plasma. To cope with the problem, he suggested recourse to a system of a pair of CO_2 gas lasers situated in a such a way that the nonlinear interaction between the two infrared laser rays would produce a difference frequency equal to the upper hybrid frequency of the plasma. According to the estimates cited in the paper, the laser power output required to seriously affect plasma oscillations is well within reasonable limits.

In the papers referred to above, as well as others submitted at the symposium, it was demonstrated that the mechanism underlying active suppression of plasma instabilities characterized by either positive or negative energy has been given sufficient study, as evidenced by the excellent agreement between theoretical calculations and experimental findings.

The experiments and theory of reactive feedback stabilization of plasma were presented in far less generous volume. Only the reports by V. A. Chuyanov (USSR) and E. Murphy (Britain) gave information on experiments dealing with stabilization of instabilities of that type, specifically flute instability of a plasma in a magnetic field of a simple mirror configuration. A single-electrode feedback loop has been used successfully in stabilizing the first mode of the plasma flute instability. But the suppression of flute instabilities of the first mode is accompanied by a buildup of oscillations at other frequencies determined by the characteristics of the feedback loop. Plasma losses accompanying the activation of the feedback loop are smaller. In a theoretical paper, C. Lashmore-Davis (Britain) posed the question of the optimum frequency response of a feedback loop for stabilizing a flute instability. But no satisfactory solution of this problem meeting practical needs has been found.

Practically all of the work described in the experimental papers was done with the aid of a single feedback loop. A model of homogeneous boundary conditions was used, however, in the theoretical analysis of the problem. The validity of the use of such a model was the subject of a paper by J. Crowley (USA). The example of a six-pole feedback loop designed to suppress plasma flute instabilities was brought up to show that all modes of flute instability below the sixth mode can be suppressed provided the loop gain is above a certain critical value. But flute oscillations with a mode number of seven or higher continue to build up, even if the plasma density has not reached the level at which these oscillations become unstable when the feedback loop is switched off.

Some of the reports presented results of a theoretical analysis of the feasibility of suppressing Kruskal–Shafranov instabilities in Tokamak type systems. A paper by J. Clarke and R. Dorey (USA) solved the problem of stabilizing a corkscrew instability in a pinch, and showed that currents stabilized by a feedback loop in a surface enveloping a plasma are capable of stabilizing unstable modes of oscillation which have no radial modes. Practical realization of a system of that type would require first that some complicated engineering problems be solved. G. Furth (USA) presented a brief review of problems pertaining to the use of feedback loops to stabilize plasma instabilities in Tokamak machines. Among the other problems considered was the possibility of controlling currents in loops replacing the copper liner of Tokamak facilities by a feedback system. The removal of the copper liner would open the way for using magnetic compression in order to heat up the plasma more effectively.

Several theoretical papers dealt with the possible use of feedback where the feedback system is activated only for very brief time intervals, to match signals from transducers recording displacements of the plasma surface. Analysis of systems of the type described revealed that the difficulties attendant upon stabilization of interchange instabilities by a linear feedback loop have been overcome to an appreciable extent. This problem was discussed in greatest detail in application to stabilization of plasma in Tokamak type facilities, in a paper submitted by A. Milner (USA).

The use of high-frequency fields to stabilize plasma instabilities has been the object of research for a fairly protracted period. This problem appears to have been tackled for the first time by S. M. Osovets (USSR) back in 1957 [4]. Further development of this work can be traced in contributions of a theoretical nature by Ya. B. Fainberg, V. D. Shapiro, V. P. Silin, L. I. Rudakov, and A. A. Ivanov (USSR), J. Teichman (Czechoslovakia), and other authors as well.

The problems touched upon in most of the theoretical reports presented at the symposium involve improvements and refinements on work done earlier, or finding stabilization conditions applicable to specific experiments. Of greatest interest in this context was a theoretical report by A. A. Ivanov and V. F. Murav'ev (USSR) which demonstrated that the ordinary wave and the helicon mode are capable of suppressing electrostatic instabilities such that $k_z \ll k$, whenever the frequency of the mode excited is much higher than the frequency of the instability. The example of a cone instability was brought up to show that recourse to a helicon type mode is preferable, since the amplitude of the magnetic field on the wave in this case will have to be lower.

There was great interest shown in a paper by M. Alcock and B. Keen (Britain) citing results on suppression of a drift-dissipative instability in the plasma of the positive column of a discharge in helium and in hydrogen, by means of a high-frequency azimuthal magnetic field. The natural frequency of the unstable oscillations is 4 kHz. The frequency of the azimuthal magnetic field was varied over the range from 8 to 100 kHz. It was shown that the instability became suppressed, in harmony with the theory expounded by A. A. Ivanov and J. Teichman, when the amplitude of the variable field came to ~1% of the amplitude of the constant longitudinal field.

Suppression of the drift (trapping) instability by means of a high-frequency electric field with a frequency higher than the ion plasma frequency was demonstrated in a report presented by the Japanese scientists Y. Nishida et al. The experiments were carried out using the plasma of a gas discharge struck in helium, at a particle density of $2 \cdot 10^9$ to $5 \cdot 10^{10}$ cm^{-3}.

Sausage type instabilities and helical instability in the hole plasma of indium–antimony semiconductors placed in a magnetic field were suppressed with the aid of an HF field established by quadrupole conductors such as Ioffe rodlets. The results of this work were presented in a paper by A. Anker-Johnson (USA).

The audience also showed keen interest in a report by G. Wolf (West Germany) which made available the results of work on dynamical stabilization of a Rayleigh–Taylor instability in a heavy fluid above a light fluid. High-frequency mechanical oscillations were impressed on the system in a direction parallel to the interface separating the two liquid phases. While these mechanical vibrations were acting, the time over which equilibrium of the heavy fluid over the lighter fluid was maintained was stretched to 10^4 times the length of time in which large-scale instability ensued with the stabilization system deactivated.

The feasibility of stabilizing instabilities by impressing the high-frequency component of a longitudinal magnetic field was studied in experimental papers presented by G. Becker et al. (West Germany) and J. Phillips (USA). The feasibility of stabilizing an instability with the aid of the high-frequency field of a linear quadrupole was also investigated, in the case of a Z-pinch. In both cases particle suppression of the instabilities was achieved.

On the whole, the papers presented at the symposium constitute a valuable contribution to the further development of research on methods for stabilization of plasma by systems using feedback and HF fields. The promising possibilities of these methods were demonstrated in the study of specific instabilities, and avenues open for utilizing these methods in future controlled thermonuclear fusion research were pointed out. The proceedings of the conference are to be published as a separate edition.

LITERATURE CITED

1. V. V. Arsenin and V. A. Chuyanov, Dokl. Akad. Nauk SSSR, 180, 5 (1968).
2. V. V. Arsenin, V. A. Zhil'tsov, and V. A. Chuyanov, Plasma Physics and Controlled Nuclear Fusion Research, Vol. 2, IAEA, Vienna (1969), p. 515.
3. A. I. Morozov and L. S. Solov'ev, Zh. Tekh. Fiz., 34, 1566 (1964).
4. S. M. Osovets, Plasma Physics and Controlled Thermonuclear Fusion Studies, Vol. 4, Izd-vo AN SSSR, Moscow (1958), p. 3.

JUNE 1970 ZAKOPANE SYMPOSIUM ON NONDESTRUCTIVE MATERIALS TESTING EQUIPMENT AND TECHNIQUES USING NUCLEAR RADIATIONS

A. Maiorov

A symposium on nondestructive testing equipment and techniques using nuclear radiations was held at Zakopane (Poland) in June, 1970. Participating in this symposium were specialists from member-nations of COMECON, and 25 reports were presented and discussed.

Z. Pawlowski (Poland) delivered a review report, which pointed out that impressive advances may be expected in the area of automation of radiographic, radiometric, and radio spectroscopic inspection work. Attention was centered on the need to develop a method for determining the critical dimensions of flaws in a variety of structural elements, and studying the effect of critical flaw dimension on the strength of the structure inspected.

E. Becker (East Germany), presenting a historical survey of the development of radiography over the past half-decade, voiced the suggestion that it will be difficult to expect any radical improvements in this method in the immediate future. L. Brunarski et al. (Poland) and A. N. Maiorov (USSR) devoted their reports to optimization of radiographic conditions, which stimulated deep interest in those attending the symposium, who acknowledged the need to develop a unified procedure and unified recommendations in this area of work.

In a joint report by Polish and USSR specialists, L. Brunarski, L. M. Serebrennikov, et al. expounded the fundamentals of supervision of the use of radiographic quality control work applied to concrete and reinforced concrete structures. A list was drawn up of the equipment needed in the radiographic inspection of concrete, the general technical conditions to be observed in testing work, procedures for measuring the thickness of concrete, the diameter of reinforcing rods and wires and the depth to which they are laid in the concrete, detection of internal voids, and basic points in safety practice in the testing of structural members.

V. G. Firstov et al. (USSR) reviewed the present level of work in the area of xeroradiography, and cited data on the PKR-1, ERGA-S, EGU-6m, KS-1 xeroradiographic machines manufactured in the Soviet Union. The characteristics of similar machines manufactured in the USA, Britain, and Japan were surveyed at the same time. E. Gusew (Poland) reported on xeroradiographic equipment manufactured by the Lodz xerography factory. It was reported that the Pyloris (KS-2 and KS-4) xeroradiographic machines developed by the Electrical Engineering Institute, with their stagewise methods of image development, are being used in industrial inspection work in the Polish Peoples Republic. Even today, the level attained in the development of techniques has opened the way clear for the use of xeroradiography in nondestructive testing work.

Z. Godlewski and B. Kaminski (Poland) reported results of work done at the Electrical Engineering Institute; there radiometric flaw detection instruments have been developed for the inspection of active specimens, tungsten nozzles, refractory materials, and carbon blocks. The sources used in these instruments are Co^{60}, Cs^{137}, Ir^{192}, Tm^{170}, and Am^{241}. Information was cited on the development of radiometric flaw detection instruments in East Germany for inspection of steel plate, and for inspection of tubes and tanks in Japan, as well as instruments for inspection of rolled goods at metallurgical plants in France and in West Germany, and joint development of radiometric flaw detection instrumentation for inspection of steel blooms by Czechoslovak and Polish industry.

Translated from Atomnaya Énergiya, Vol. 29, No. 6, pp. 473-474, December, 1970.

A report by V. G. Firstov et al. analyzed the feasibility of applying radiometric flaw detection techniques to nondestructive testing and inspection of blooms in the rolling process, to centrifugally cast tubing in mass production, and to unreinforced welded seams. Spectrometric, spectrometric-count, and collimation-spectrometric procedures in radiometric flaw detection work were discussed, and a procedure was worked out for calculating sensitivity and productivity in inspection work, illustrated by graphs of the dependence of inspection productivity on the minimum dimensions of flaws to be discerned and on the dimensions of the collimation hole.

Despite the successes attained in experimental and theoretical research on methods of radiometric flaw detection, to date we still lack quantity-produced equipment to carry out this work on a routine scale in industry, and this is accounted for by the lack of highly efficient radiation detectors, a lack of high-speed electronic equipment featuring small instrument fluctuations and excellent sensitivity to insignificant changes in the signal arriving for processing, and a lack of low-energy sharply focused sources of high specific activity which might contribute to improved resolution and greater productivity at the same time.

Visual methods of nondestructive testing and inspection were discussed at the symposium in reports delivered by J. Ginsztler, "Visual methods of inspection in industrial radiography," and J. Sorm (CSSR), "Application of an image brightness intensifier in inspection of castings." The Czechoslovak "Tesla" firm has now achieved industrial-scale production of the 03QA41, 040QA41, and 05QA41 type electronic image converter tubes with tube dimensions ranging from 175 to 289 mm, which can be used profitably in visual monitoring and inspection arrangements. The observed trend of development of visual techniques shows that further improvements in radioscopy (radiographic flaw detection work) will be impossible either in the field of new developments or in the area of incorporating existing advanced equipment in regular inspection practice, without first developing the instruments and equipment needed to eliminate the subjective fact in assessments of flaws, and thereby opening the way to proceed ahead to automatic computing of all the related data. To a lesser extent this will obtain to its application in the location and classification of flaws in parts.

A report by A. Jedziewski (Poland) provided a description of the Polish IP-8, IP-25, CP-1, and CP-10 type hose-attachment γ-ray flaw detection instruments with pneumatic feed of IR^{192} and Co^{60} radiation sources to the irradiation target up to distances of 30 m. These sets use lead shielding. At the present time, a modified variant of these γ-ray flaw detection instruments using uranium shielding is under development. These sets are intended mainly for use in production shops where assembly and rigging of outsize equipment and structures are handled. Four types of Polish flaw-detection equipment were demonstrated at an exhibit set up at the symposium; also demonstrated were two negative viewers for decoding radiographic images with photographic density up to three and up to five. The first type of negative viewer has a rectangular light field controlled by adjusting blinds, and a photocell for excluding light, while the second type of negative viewer has a diaphragm-controlled circular field.

R. Dubenski (CSSR), in his report "Stereoscopic viewer for x-ray plates," discussed a stereoscope for simultaneous viewing of two radiographic images made by the method of lead markers. The prerequisite for working with the stereoscope is unimpaired vision and space perception ability on the part of the operator. The report also provides a description of a stereoscope relying on the principle of polarization of light; the operator dons polarized eyeglasses, and the radiographic images are projected onto a screen with a metallized silver coating. In addition, a stereoscopic negative viewer in which a mirror system is used to combine and transpose the images is described. These instruments were developed at the Higher Technical School in Prague, and are used to pinpoint the location of flaws in radiographed products.

V. N. Khoroshev et al. (USSR) provided information on completed development work on γ-ray nondestructive testing instruments in the COMECON normal classification RID-11, RID-21, RID-22, and (RID-32), on sets of equipment for irradiation of piping and tanks of large diameter (the Gazprom, Trassa, and Neva sets), specialized equipment for frontal transmission (the Stapel'-5 and Stapel'-20), and hose-attachment automated γ-ray nondestructive testing instruments (the Labirint and the Kama).

A report by W. Listwan and M. Dobrowolsk (Poland) presented results of joint research and development work of Polish and Czechoslovak specialists on radiometric equipment for inspecting communications cables and piping while these are in service. The method is based on the introduction of radioactive tracers with a short half-life into the piping, through which various gases of petrochemicals, etc., are pumped, the concentrations of these tracers in the medium surrounding the piping and subsequent detection of the affected portion of piping by means of a radiometric instrument inserted into the piping and moving through the

interior of the piping under the pressure of the gas or liquid being pumped through. The method has been tested and has been accepted on an experimental production basis in the Czechoslovak and Polish sections of the Druzhba international pipeline, as well as on other gas pipelines.

A report by N. D. Tyufyakov et al. (USSR) cited results of research work on neutron radiography, going in particular into a detailed discussion of neutron sources, the dependences of slow-neutron beam characteristics on beam shaping conditions, and production of beams with optimized properties; the paper also covers determinations of neutron scattering factors, inspection sensitivity, nomograms of exposures for use with detectors of neutron images that have been developed, and goes into a discussion of the range of applicability and convenience of the method. A. Petrov (Bulgaria) cited information on the joint development, in the USSR and Bulgaria, of lightweight transportable flaw-detection laboratories designed for mounting on the UAZ microbus, and the medium weight type laboratory designed for mounting on a large panel truck, and equipped with a set of varied flaw detection equipment.

Several of the reports were devoted to the present utilization, and outlook for future utilization, of radioisotope, x-ray, and betatron nondestructive testing equipment and techniques in construction, boiler manufacture, aviation, foundry work, and in other branches of industry in the member-nations of the Council for Mutual Economic Aid (COMECON).

THE SATURN-1 PLASMA MACHINE

V. A. Suprunenko

The Saturn-1 toroidal triple-loop stellarator for plasma research was commissioned at the Khar'kov Physicotechnical Institute in the first half of 1970. The distinguishing feature of this plasma machine is its capability of operating in two modes: the stellarator mode and the torsatron mode. In the first mode, magnetic surfaces with large and controlled "shear" values (≤ 0.15) and a rotational transform angle of the lines of force ($\leq 1.3\,\pi$) are established in the effective volume of the machine. In the second mode, surfaces with "shear" (~0.1) and with a "magnetic potential well" (~10%) are established. The maximum intensity of the longitudinal magnetic field in the quasistationary mode attains the level of 10 kOe. The inner diameter of the vacuum chamber is ~170 mm.

The first results of research on the magnetic surfaces revealed excellent agreement with theoretically predicted parameters, as clear evidence of the high precision with which the magnetic trap was fabricated.

Translated from Atomnaya Énergiya, Vol. 29, No. 6, p. 474, December, 1970.

THE ANGLO-SOVIET PLASMA PHYSICS EXPERIMENT

V. V. Sannikov

From February through December 1969, an experiment designed for determining the electron temperature and density of a plasma, and also to determine the radial distribution of the plasma pinch by the method of Thomson scattering of laser emission, has been staged by a team of physicists from Culham Laboratory, including Drs. N. D. Peacock, D. C. Robinson, P. D. Wilcock, and M. D. Forrest, in collaboration with colleagues of the I. V. Kurchatov Institute of Atomic Energy (IAE), at that latter institute. This method, in contrast to those used earlier, made it possible to measure the electron temperature and density of the plasma directly.

British equipment was installed on the Tokamak T-3 plasma machine (large radius 1 m, small radius 25 cm, diaphragm radius 17.5 cm).

With the plasma parameters of this machine $T_e \sim 10^2$ to $2 \cdot 10^3$ eV, $n_e \sim 10^{13}$ to $5 \cdot 10^{13}$ cm^{-3}, the Salpeter coefficient $\alpha = \lambda_0/4\pi\lambda_D \sin\theta/2 \ll 1$, where $\lambda = 6943$ Å; λ_D is the Debye radius; θ is the scattering angle ($\theta = 90°$). The case of scattering on free electrons was realized here. The scattered radiation spectrum is described by a Gaussian curve, with a Maxwellian distribution of electron velocities assumed.

A beam of light with a divergence of 2.5 mrad was directed from a ruby laser operated in the giant pulse mode, with radiation energy 5 J and pulse duration 20 to 30 msec, through the plasma pinch diametrally. Radiation scattered at 90° was recorded from a plasma volume of 1 cm^3 by means of collimating optics and a wide-aperture spectrograph with a ten-channel photoelectric system for recording the spectrum. The spectral width of each channel was 78 Å.

Half the Gaussian curve was taken from the shortward end of the spectrum, from the laser emission line 6943 Å. The spectrum was recorded in a single current pulse simultaneously on all the channels. The intensity of the hydrogen line H_α was measured in one of the channels.

The electron concentration in the plasma was estimated from the ratio of the absolute values of the energy of the scattered light and the energy of laser emission.

A special periscopic viewing system was set up so as to obtain the radial temperature distribution and radial distribution of electron density in the plasma. The distribution of concentration was recorded at the same time by a multichord two-millimeter interferometer. Data on density obtained with the laser and with the microwave interferometer were in close agreement.

The measured electron temperature of the plasma ranged from 100 to 2000 eV, depending on the discharge conditions. The plasma concentration ranged from 10^{13} to $4.5 \cdot 10^{13}$ cm^{-3}, while the current ranged from 40 to 150 kA, and the intensity of the longitudinal magnetic field from 17 to 38 kOe.

It is to be noted that the experimental data points fit closely to the theoretical Gaussian curve, within the limits of error of the measurements. This might mean that a Maxwellian distribution of electron energies prevails in this instance. The electron temperature increases to a maximum in 12 msec, and remains practically constant until the discharge current has died away completely.

The radial temperature distribution and radial electron density distribution are sufficiently flat near the axis of the pinch, and diminish monotonically toward the periphery of the pinch. The temperature increases as the discharge current, roughly in obedience to the law I^2 (dependences were taken at current pulse widths of 35 and 70 msec), and varies inversely with the plasma density.

Translated from Atomnaya Énergiya, Vol. 29, No. 6, p. 475, December, 1970.

The electron temperature of the plasma is virtually independent of the longitudinal magnetic field.

The experiment was performed under conditions featuring high anomalous resistance presented by the plasma. The plasma temperature as calculated on the basis of conductivity in all the sets of conditions investigated is lower than the temperature measured with the laser, and varies slightly over the current pulse. It amounts to 100-200 eV, depending on the operating conditions.

The electron temperature distribution was measured every 4 msec after the onset of current under various sets of conditions, giving some indication of slight "skinning" of the temperature near the edge of the pinch, but no clearcut "skinning" effect was obtained in later experiments, since measurements earlier in time were impossible on account of the high level of the plasma's intrinsic radiation, while measurements taken later than 4 msec yielded a flat distribution near the axis. The rapid levelling off of temperatures is an indication that the electron thermal conductivity of the plasma is well above the classical value.

The particle lifetime found from measurements of the absolute intensity of the H_α line was 15 to 20 msec, and was longer than the energy-derived plasma lifetime of 5 msec.

Data on the radial distribution of the temperature and electron density of the plasma were utilized in computing the transverse energy of the plasma as a function of the time. The transverse component of the energy was determined simultaneously from the diamagnetic effect of the plasma. The energies measured by these two independent techniques were found to be in satisfactorily close agreement.

Note that the data on plasma parameters obtained by the method of laser scattering confirmed the results obtained earlier by Soviet physicists relying on rival methods.

LITERATURE CITED

1. Nature, 224, No. 1, 488-490 (1970).

GKIAÉ – JINR AGREEMENT ON SCIENTIFIC AND TECHNICAL COLLABORATION

V. Biryukov

An agreement on scientific and technical collaboration was signed at Dubna, in June 1970, between the State Committee on the Peaceful Uses of Atomic Energy [GKIAÉ] and the international physics research center of the socialist countries, the Joint Institute for Nuclear Research [JINR]. The purpose of this agreement is to "contribute to the rounded all-sided development of scientific and technical collaboration between member-states of JINR by combining the efforts of JINR scientists and scientists working in GKIAÉ-supervised institutes. . . ." The two parties signatory to the agreement state that they will "jointly develop scientific and technical collaboration in the field of nuclear physics, for the maximum and most efficacious utilization of accelerators, nuclear research reactors, equipment for experimental data processing, and other experimental and research facilities at their disposal, and will also devise new equipment for those purposes. . . ."

Specific efforts will be undertaken and expedited on the basis of bilateral contracts or protocols concluded between JINR and institutes under GKIAÉ, to determine the scope, times, and conditions of this research. The contracting parties, in attainment of mutual agreement, agree to draw upon national or international research organizations and other bodies in carrying out this joint work, and will observe the principles of reciprocity and take into account the interests of the parties involved. Institutes in member-nations of JINR engaged in collaboration with JINR and drawn into the overall scientific plans approved by JINR may also be included in the work carried out jointly by the two signatories.

The agreement lays down the general obligations of the two contracting parties on establishing the prerequisite conditions for work on accelerators and other research facilities: the operation and servicing of the equipment, providing electric power, liquefield gases, tool shops, computer and data processing operations, making available the necessary scientific and technical information for this joint work, and so forth. GKIAÉ will assist JINR and the institutes preparing this joint research in the development and fabrication of experimental equipment needed.

In line with the agreement signed, the contracting parties will sponsor annual meetings of their respective representatives and experts, for discussion of concrete problems in scientific and technical collaboration.

The agreement extends over a five-year period, and will be automatically extended another term of equal length, if neither of the two signatory parties voices an intention of terminating the agreement.

The international juridical document signed at Dubna flows both in spirit and in content from the famous 1959 Moscow agreement on the organization of the Joint Institute for Nuclear Research, and will serve the cause of further development of scientific and technical collaboration between the socialist countries.

Translated from Atomnaya Énergiya, Vol. 29, No. 6, pp. 475-476, December, 1970.

BRIEF COMMUNICATIONS

An All-Union science and engineering seminar was held at the "Atomic Energy" pavilion of the Exposition of Achievements of the National Economy of the USSR in July 1970, on the topic "Methods and equipment for dosimetric monitoring of radioactive radiations and x-rays," with 66 organizations participating. In a review report, V. V. Matveev discussed general topics concerning the development of complex dosimetric and radiometric systems, design of functional modules with unified dimensions, and characteristics of instruments developed at the All-Union Research Institute for Instrument Design.

The participants at the seminar discussed various methods for calibrating dosimeters and radiometers, requirements applicable to dosimetric inspection and checkout systems, design of dosimeters, whole-body spectrometers, etc.

* * *

An All-Republic seminar of workers in chemical plants was held in Kiev in June 1970 on the topic "Radioisotope techniques and instruments in the chemical industry of the Ukraine."

The seminar participants reported that radioisotope techniques and instrumentation have been making their way in recent years in production use at advanced chemical processing plants such as the Severo-Donets Chemical Combine, and the Kaluga Chemical-Metallurgical Combine, where applications of radioisotope instruments are yielding impressive savings and improving working conditions.

* * *

A seminar was held in Moscow in June 1970 to expedite exchanges of experience in the operation of in-plant and base isotope laboratories, and the implementation and acceptance of new methods and radioisotope techniques and equipment in industrial process monitoring. Participating in the seminar were 84 organizations and industrial plants under various ministries and departments, whose representatives reported that the national economy of the country has already been benefiting from applications of radioisotope techniques in terms of impressive savings, and that both base and in-plant isotope laboratories have had a positive effect on the acceptance of atomic science and engineering in industry.

* * *

A science-familiarization excursion organized for the benefit of specialists from developing countries with membership in IAEA and FAO took place from August 6 through August 31, 1970, under the joint auspices of the State Committee on the Peaceful Uses of Atomic Energy of the USSR [GKIAÉ] and the Ministry of Agriculture of the USSR, affording an opportunity for these specialists to be brought up to date on applications of isotopes and radiations in agriculture in various locations throughout the Soviet Union. The group included scientists from Brazil, Chile, Costa Rica, Ghana, India, Iran, Lebanon, Mexico, Pakistan, Philippines, Sierra Leone, Sudan, Thailand, the United Arab Republic, and Yugoslavia, as well as leading staff-members of both IAEA and FAO.

One-day seminars at which lectures were delivered on applications of heavy water in soil and agrochemical research, applications of techniques and equipment for radiation work in agriculture, the study of the transformation and use by plant life of nitrogenous fertilizers through the use of such isotopes as N^{15}, P^{32}, C^{14}, etc., were organized in the course of the trip for the participants.

The program included visits to Moscow-area scientific research institutes such as the V. V. Dokuchaev Soil Science Institute, the isotopes laboratory of the All-Union Scientific Research Institute for Electrification of Agriculture [VNIIESKh], the D. N. Pryanishnikov All-Union Scientific Research Institute for the study of Fertilizers and Agronomical Soil Science, the Institute of Genetics and Plant Selection of the Siberian Division of the USSR Academy of Sciences (in Novosibirsk), the Biology and Soil Science Department of

Translated from Atomnaya Énergiya, Vol. 29, No. 6, p. 476, December, 1970.

Moscow State Unoversity, the V/O Izotop agency exhibit hall, the Exposition of Achievements of the National Economy of the USSR, and the P. Lumumba University.

A discussion of the organization of scientific research work utilizing isotopes in agriculture was held at the V. I. Lenin All-Union Academy of Agricultural Sciences. [VASKhNIL].

* * *

An agreement between Sweden and the Soviet Union covering a thirty-year period of collaboration in the area of peaceful uses of atomic energy was concluded in September 1970. Agreement on signing this convention was reached in the course of a visit to Sweden by the Chairman of the Council of Ministers of the USSR, A. N. Kosygin, in the summer of 1968.

Agreement envisions the possibility of both parties delivering and obtaining equipment, including nuclear reactors and fuels for nuclear reactors, nuclear materials, nuclear raw materials, and special nuclear materials of commercial interest. The Soviet Union will provide services in enriching Swedish-acquired uranium at plants in the USSR. The practical realization of this collaboration will be spelled out in further agreements, protocols, or contracts.

In accordance with the Treaty on nonproliferation of nuclear weapons, Sweden and the Soviet Union have decided to turn to IAEA with a request to carry out the provisions of the Treaty on inspection and control of the utilization of nuclear materials and equipment delivered under the terms of this agreement.

INDEX

SOVIET ATOMIC ENERGY

Volumes 28-29, 1970

SOVIET ATOMIC ENERGY
Volumes 28-29, 1970

(A translation of Atomnaya Énergiya)

L

M

N

O

P

R

S

T

U

V

Y

Z

SOVIET ATOMIC ENERGY
Volumes 28-29, 1970
(A translation of Atomnaya Énergiya)

Volume 28, Number 1 January, 1970

Volume 28, Number 2 February, 1970

ABSTRACTS

LETTERS TO THE EDITOR

Volume 28, Number 3 March, 1970

Volume 28, Number 4 April, 1970

Volume 28, Number 5 May, 1970

Volume 28, Number 6

Volume 29, Number 1 July, 1970

ABSTRACTS

LETTERS TO THE EDITOR

Volume 29, Number 2 August, 1970

Engl./Russ.

Volume 29, Number 3 September, 1970

Volume 29, Number 4 October, 1970

Volume 29, Number 5 November, 1970

Volume 29, Number 6 December, 1970

ALGEBRA AND LOGIC

A cover-to-cover translation of Algebra i logika

A publication of the Institute of Mathematics, Siberian Section of the Academy of Sciences of the USSR Novosibirsk, SSR

Translated from Russian

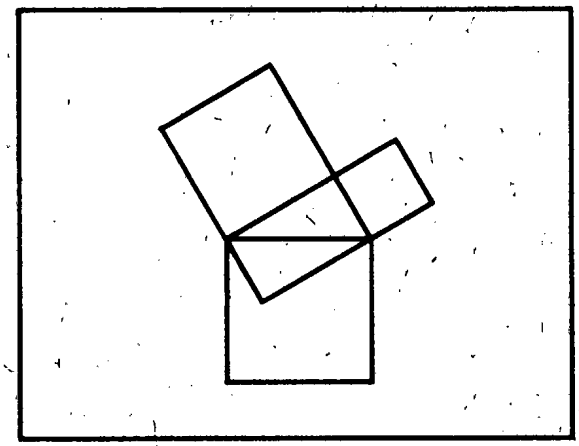

A new Soviet journal which publishes, at bimonthly intervals, results of the latest research in the areas of modern general algebra and of logic considered primarily from an algebraic viewpoint. The algebraic papers, constituting the major part of the contents, are concerned with studies in such fields as ordered, almost torsion-free, nilpotent, and metabelian groups, isomorphism rings, Lie algebras, Frattini subgroups, and clusters of algebras. In the area of logic, the periodical covers such topics as hierarchical sets, logical automata, and recursive functions.

As is the case with all Consultants Bureau journals, *Algebra and Logic* appears in English translation only about six months after publication of the Russian edition. Translation began with the 1968 issues.

Contents of the first issue (Number 1, 1968):

A. A. Akataev and D. M. Smirnov, Lattices of submanifolds of manifolds of algebras • **G. F. Bachurin,** On almost torsion-free nilpotent groups • **L. A. Bokut',** On the extension of ring isomorphisms • **Yu. L. Ershov,** On one hierarchy of sets, I • **V. V. Koz'minykh,** On one-place primitively-recursive functions • **A. I. Kokorin and G. T. Kozlov,** Extended elementary and universal theories of lattice-ordered Abelian groups with a finite number of threads • **Yu. I. Merzlyakov,** On groups almost approximatable by finite *p*-groups • **V. P. Shunkov,** On a periodic group with almost regular involutions.

Contents of the second issue (Number 2, 1968):

V. N. Agafonov, The complexity of computing pseudorandom sequences • **V. M. Kopytov and I. I. Mamaev,** Absolute convexity of certain subgroups of an orderable group • **S. P. Kogalovskii,** On compact classes of algebraic systems • **E. N. Kuz'min,** Algebraic sets in Mal'tsev algebras • **I. A. Lavrov,** The answer to a question by P. R. Young • **L. L. Maksimova,** On the strict implication calculus • **E. A. Polyakov,** Certain aspects of the theory of recursive functions • **V. G. Sokolov,** On the Frattini subgroup • **M. A. Taitslin,** On elementary theories of lattices of ideals in polynomial rings.

Annual subscription (6 issues) **$85.00***
(Add $5.00 for postage outside the U.S.A. and Canada.)

*Your **Continuation Order** authorizes us to ship and bill each volume automatically, immediately upon publication. The **Continuation Order** will remain in effect until cancelled.

PLENUM PUBLISHING CORPORATION
Plenum Press • Consultants Bureau • IFI/Plenum Data Corporation
227 WEST 17th STREET, NEW YORK, N. Y. 10011

In United Kingdom: Plenum Publishing Co. Ltd., Donington House, 30 Norfolk Street, London, W.C. 2.

A New Volume in the Highly Acclaimed Series

MONOGRAPHS IN SEMICONDUCTOR PHYSICS*

Series translated from Russian by **Albin Tybulewicz**
Editor, "Soviet Physics — Semiconductors"

Volume 3: SWITCHING IN SEMICONDUCTOR DIODES

By **Yurii R. Nosov**
A. F. Ioffe Physicotechnical Institute
Leningrad, USSR

Covers the physical basis of the operation of a semiconductor diode under pulse conditions and gives, whenever appropriate, quantitative relationships describing transients in diodes. The volume presents the most general mathematical methods for solving the equations of transient processes, enabling the reader to analyze those pulse conditions not directly referred to in the text. In addition, a model of a planar diode with a semi-infinite base is described in detail. Solid state physicists and electrical engineers will find this work invaluable.

CONTENTS: List of principle symbols • Basic electronics of the switching processes in semiconductor p-n junctions • Switching in a planar diode • Planar diode with a thin base • Transient processes in a diode with a small-area rectifying contact • Effect of an electric field in a diode base on transient processes • Transient processes in diodes during the passage of a forward current pulse • Transient processes in semiconductor diodes and fundamentals of recombination theory • Literature cited • Index.

Approx. 239 pages PP 1969 $19.50

Also available:

Volume 4 SEMICONDUCTING II-VI, IV-VI, AND V-VI COMPOUNDS

By **N. Kh. Abrikosov, V. F. Bankina, L. V. Poretskaya, L. E. Shelimova,** and **E. V. Skudnova**
A. A. Baikov Institute of Metallurgy
Academy of Sciences of the USSR

The first published review of semiconducting chalcogenides of elements in groups II, IV, and V, this monograph presents phase diagrams for binary, ternary, and more complex systems.

234 pages PP 1969 $19.50

Volume 2 LIQUID SEMICONDUCTORS

By **V. M. Glazov, S. N. Chizhevskaya,** and **N. N. Glagoleva**
Baikov Institute of Metallurgy
Academy of Sciences of the USSR, Moscow

The first to deal with semiconductors in the liquid state, this monograph provides a comprehensive review of the electrical conductivity, thermoelectric power, magnetic susceptibility, thermal conductivity, density, and viscosity of elemental and compound semiconductors just below the melting point, at the melting point, and in the liquid state.

362 pages PP 1969 $22.50

Volume 1 HEAVILY DOPED SEMICONDUCTORS

By **V. I. Fistul'**
Institute for Fine Chemical Technology
Academy of Sciences of the USSR, Moscow

Deals with the properties of degenerate materials and their applications, including tunnel diodes, lasers, and Hall probes.

418 pages PP 1969 $25.00

*Place your continuation order today for books in this series. It will ensure the delivery of new volumes **immediately** upon publication; you will be billed later. This arrangement is solely for your convenience and may be cancelled by you at any time.

PLENUM PUBLISHING CORPORATION
Plenum Press • Consultants Bureau • IFI/Plenum Data Corporation
227 WEST 17th STREET, NEW YORK, N. Y. 10011

In United Kingdom: Plenum Publishing Co. Ltd., Donington House, 30 Norfolk Street, London, W.C. 2.